

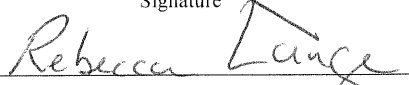


Ada R. Dominguez

On the Behavior of the Geomagnetic Field During the Miocene

submitted in partial fulfillment of the requirements for the degree of
Master of Science in Geology
Department of Earth and Environmental Sciences
The University of Michigan

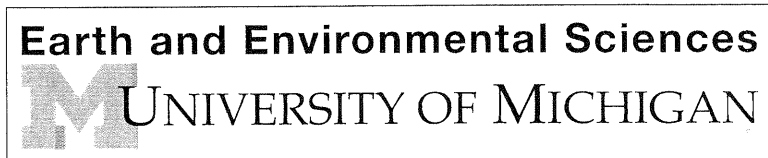
Accepted by:

 Signature	ROB VANDER VOO Name	4/2/2012 Date
 Signature	Rodney C. Ewing Name	4/2/2012 Date
 Department Chair Signature	Rebecca A. Lange Name	4/2/2012 Date

I hereby grant the University of Michigan, its heirs and assigns, the non-exclusive right to reproduce and distribute single copies of my thesis, in whole or in part, in any format. I represent and warrant to the University of Michigan that the thesis is an original work, does not infringe or violate any rights of others, and that I make these grants as the sole owner of the rights to my thesis. I understand that I will not receive royalties for any reproduction of this thesis.

- Permission granted.
 Permission granted to copy after: _____
 Permission declined.


Author Signature



On the Behavior of the Geomagnetic Field During the Miocene

by

Ada R. Dominguez

Thesis manuscript submitted in partial fulfillment

of the requirements for the degree of

Master of Science

Department of Earth and Environmental Sciences

The University of Michigan

May 2012

ACKNOWLEDGEMENTS

My greatest gratitude goes foremost to my advisor, Dr. Rob Van der Voo, for his patience, guidance and undivided attention. I had the privilege to work for him during my undergraduate years and due to that extraordinary experience I made the decision to continue to work with him on further projects. I feel very honored to have the opportunity to work with him and thankful for all the doors he opened for me. I also want to thank Gregory McCracken for his help in the collection of the samples and for keeping me sane through the duration of our fieldwork. Dr. Stephen Reidel has been quite instrumental in this study for his guidance and knowledge of the local geology and for his selfless help; for this I thank him. I am also incredibly grateful to Mike Jackson, Julie Bowles, Peter Solheid, and Joshua Feinberg for their help in the rock magnetic analysis and their insights. I also must thank my peers, Mathew Domeier and Fatim Hankard, who answered my endless questions and shared the good and hard times of academic life with me. I give many thanks to Pavel Doubrovine for his dispersion calculation program, which was quite useful in this study. My deepest gratitude also goes to Andy Biggin for his very helpful advice on improving the foundation of this study and for the resources he provided for further data analysis. Professor Rod Ewing also deserves my appreciation for taking the time from his very busy schedule to revise this manuscript. I also would like to extend my gratitude to the Nez Pierce Tribe for granting us permission to sample in their property. Lastly, I want to thank the four most important people in my life: my parents, my brother and my husband. Thank you for your moral support and words of encouragement.

This project was funded by the National Science Foundation (Grant EAR 0909288), the Turner Research Grant, and the Rackham Graduate Research Grant, all of which made this study possible.

ABSTRACT

This study comprises 118 discrete volcanic flows from the Miocene in the eastern Columbia River Basalt Group (CRBG) with the aim of testing the distributions of geomagnetic field directions as predicted by several geomagnetic field models. This is important because little is known empirically about the behavior of the geomagnetic field prior to the last 5 million years. The results of this study will allow us not only to extend the temporal coverage of the geomagnetic field models, but also point to potential improvements to these models. The rock magnetic analysis of the samples for this collection shows that the primary magnetic directions are uniformly carried by titanomagnetite. Thus, the magnetic behavior of the samples reflects the magnetic field and not aspects of the magnetic mineralogy.

To reduce systematic bias, the sites were analyzed as ungrouped and grouped site directions, where flows with similar directions within the 95% confidence interval were combined. Furthermore, they were analyzed with visual inspection, 45° , and *Vandamme (1994)* cutoff criteria. The overall formation mean of these six scenarios shows that the paleomagnetic directions of the flows are southerly and up and northerly and down. For example, in the case of grouped sites with the Vandamme cutoff, the normal (Dec: 7.1° , Inc: 60.5° , k: 29.4, α_{95} : 4.1°), and reverse (Dec: 177.6° , Inc: -59.6° , k: 15.7, α_{95} : 5.6°) means depict this general behavior. For reference, the local inclination of the geocentric co-axial dipole field is about 64° . Furthermore, deviating directions are also present, possibly due to excursions as part of secular variation, or as intermediate transitions between reversed and normal polarity intervals. No new rock ages were necessary for this study since the CRBG has undergone extensive geochronological analysis with high-quality, reproducible results. Additionally, integrating the Miocene ages of the flows and their corresponding paleomagnetic directions allows us to observe the evolution of the paleosecular variation (PSV) through the Neogene,

because it can be compared with the published characteristics of the geomagnetic field in the last 5 million years. Our elongation results coincide with those predicted from the TK03.GAD (*Tauxe & Kent, 2004*) model, but not the CJ98.GAD (*Constable & Johnson, 1998*) model. However, when comparing our dispersion results, we find that they do not conform to the TK03.GAD, CJ98.GAD, and CP88.GAD (*Constable & Parker, 1988*) models, which underpredict the dispersion values. Thus, this suggests that, although the geomagnetic parameters in general agree with these models, they require some refinement to accommodate the differences during the Miocene.

INTRODUCTION

The Earth's magnetic field is not constant, but undergoes rapid changes in intensity and orientation. This shift in orientation is visible through careful observations with a magnetic compass over the course of years or decades. The Earth's rotation axis, marked by its geographic north, is relatively stationary, while the magnetic north pole moves significantly. Consequently, the direction read from a compass usually differs from the true north; this angular difference is known as geomagnetic declination. Navigation logs dating back to the sixteenth century show that the magnetic field parameters change over time and that the magnetic north pole has moved approximately 1500 km in 150 years. In North America, for example, there has been a documented change in the declination of as large as 1° every five years. This temporal change in the location of the magnetic north, along with changes in magnetic inclination and intensity, is included in what is called secular variation.

Throughout geologic history, ancient volcanic flows have recorded the ambient magnetic field in a process where the remanence of the magnetic particles in the lavas aligns to the field and "freezes" this orientation once the flows continue to cool. This mechanism has allowed geologists

to study the behavior and evolution of the Earth's magnetic field and its variation. There is a constant change in the dispersion of the secular variation as a consequence of the Earth's inner core growth while the liquid outer core, responsible for magnetic field, decreases in size. Due to this relation, studying the patterns in the changes of the secular variation can contribute to understanding the Earth's dynamo. Furthermore, studying such variation could help determine if there are long-term contributions from higher order magnetic fields, such as octupoles and quadrupoles, aside from the main dipolar behavior. Observations have shown that during the last 550 million years of Earth's history, its averaged magnetic field has been principally dipolar and co-axial, but in short time intervals these higher-order magnetic fields do exist while varying in intensity.

The study of the behavior of the geomagnetic field is not only useful for understanding the workings of the Earth's deep interior, but can also be applied in other respects. With paleomagnetism, the recorded direction of the magnetic grains in rocks can be used to determine where continents were located spatiotemporally. In order to do this, it is generally assumed that the Earth's magnetic field is on average purely dipolar. However, it is possible that this assumption is not appropriate throughout geologic history or not valid for some periods due to a combination of stochastic behavior of the magnetic field, high contributions of non-dipolar components, and the increase in the size of the inner core. These changes, in turn, may make this purely-dipolar notion invalid, making continental reconstructions that use these models flawed. Therefore, empirically testing the changes in the geomagnetic field not only contributes to its understanding, but also tests the current models of the field, ultimately allowing us to correctly reconstruct the location of drifting continents.

For the last 5 million years, the Earth's magnetic field has been dipolar to the first order. The Paleosecular Variation (PSV) of the field may have had a correlation between increasing geo-

graphic latitude and increasing dispersion of virtual geomagnetic poles (*Merrill et al., 1996*). Virtual geomagnetic poles (VGPs) are calculated from magnetic directions at a site and are components of the total geomagnetic field, but VGPs are calculated by using the dipole formula, despite the fact that the actual geomagnetic field was probably not purely dipolar most of the time. Averaging over long and well-sampled intervals may solve this problem. Therefore, studying the behavior of the geomagnetic field and verifying the validity of field models requires large collections of high-quality samples, which can be difficult to achieve, especially for older periods of geologic history.

In this study, a collection of 118 individual basaltic flows was sampled in the tri-state area of Idaho, Washington, and Oregon of the eastern Columbia River Basalt Province in order to study the behavior of the magnetic field during the Miocene and to compare its observed behavior with that predicted by the TK03.GAD (*Tauxe & Kent, 2004*), CJ98.GAD (*Constable & Johnson, 1998*), and CP88.GAD (*Constable & Parker, 1988*) models and the MM97 (*McElhinny & McFadden, 1997*) and Time-Averaged Field Initiative (TAFI) (*Johnson, et al., 2008*) empirical data. The results of this study will shed light on how the geomagnetic field behaves during the Miocene and provide a test for the validity of these models.

GEOLOGICAL SETTING

The Columbia River basalts, overlying the Columbia Plateau, are located between the Cascade Range and the Rocky Mountains. They were erupted from linear fissures 17-6 Ma, as determined by K-Ar and ^{40}Ar - ^{39}Ar dating methods (*Long et al., 1983; McKee et al, 1977; McKee et al., 1981; Swanson et al., 1979a; Waters, 1961; Watkins & Baksi, 1974*) on dike swarms in the Precambrian craton and Mesozoic accreted terranes in the western continental U.S. (*Tolan et al., 2009*),

covering parts of Washington, Oregon, and Idaho. However, most of the group was erupted in the relatively short time of 1.5 million years between 17 and 15.5 Ma (*Mangan et al., 1986*). They form a thick basaltic sequence, consisting of at least 300 individual tholeiitic flows (*Swanson et al., 1979b; Tolan et al., 1989*). These flood basalts flowed eastward to the Rocky Mountains, forming the Columbia Plateau, where some sections have basaltic layers greater than 3 km thick (*Reidel et al., 1989*). Paleomagnetic studies of this plateau have shown that there is a 16° regional clockwise rotation in western Washington and Oregon since 12 Ma (*Magill et al., 1982; Simpson et al., 1980*) due to tectonic rotation in the western part of the northwest U.S. from dextral shear between the western section of the North American plate and the northward motion of the Pacific plate (*Beck, 1976; Beck, 1980; Sheriff & Bentley, 1980*). The eastern section, however, is relatively stable, apparently having undergone no relative internal rotations, and perhaps a clockwise block rotation of up to 7° for the area as a whole (*Jarboe et al., 2008; Magill et al., 1982*). The boundary between the stable and rotated sections is in the southern Cascades (*Simpson et al., 1980*).

To avoid rotation bias, only the eastern, stable part of the plateau was sampled (**Figure 1**). According to *Swanson et al. (1979b)*, the Columbia Plateau sequence is divided stratigraphically into five subsections (the Imnaha, Grande Ronde, Wanapum, Saddle Mountain, and Picture Gorge Basalts), with the Grande Ronde Basalt group containing 85% of the total volume (*Reidel et al., 1981*), and the Saddle Mountain Basalt comprising less than 1% of the total volume. The area sampled has very distinct exposures of individual flows. Each discrete flow is typically 30 meters thick and has a characteristic arrangement of a vesicular top, underlain by slender columns, undulatory columns, platy joints, and pillowed basalts (*Mangan et al., 1986; Reidel, 1983*) (**Figure 2a**). A saprolite layer of less than approximately 100,000 years in duration is located between the Grande Ronde and Wanapum sections in most places. Furthermore, the majority of the flows are flat-lying (**Figure 2b-**

c), with very few tilted segments. The Imnaha Basalts are at least 425 m thick in some regions and underlie the Grande Ronde Basalts (*Reidel, 1978*). Sediment layers sometimes lie between these basaltic layers, and in some places there are pillowed, hyaloclastic zones. Ridges formed prior to the basaltic flows, and in some areas, the Imnaha Basalt flows, spread over the canyons. On the other hand, the Saddle Mountain Basalt flows were formed as single flows and as dikes (*Reidel, 1978*).

The basalts in this region are mainly composed of low-magnesium tholeiites and basaltic andesites, with 52-58% SiO₂ and an Mg/(Mg+Fe⁺²) ratio of less than 55. The source magma was originally more iron-rich than typical upper mantle compositions (*Takahashi et al., 1998; Wright et al., 1988; Yaxley, 2000*). An eclogite-rich mantle plume source originating from recycled subducted ocean basalt material is consistent with these observations (*Cordrey et al., 1997*).

The source of the Columbia River basalts is still under debate: one group (*Helz, 1973; Helz, 1978; Swanson & Wright, 1981; Wright et al., 1976; Wright & Helz, 1981*) believes that the basalt originates from a primary to almost primary magma. A second group (*McDougall, 1976*) argues that the basalts are due to fractional crystallization of the magma. On the other hand, some believe that there is strong evidence in support for a mantle plume source. For example, some think that the large number of tholeiitic flows from the Steens and Columbia River province were erupted very quickly (*Camp et al., 2003; Hooper et al., 2002*), and that such large volumes of basalts can only be explained by the existence of a mantle plume. Furthermore, some CRB eruptions contain high Helium isotope ratios, which indicate a deep mantle origin for these basalts (*Dodson et al., 1997*). However, there are lines of evidence against the plume origin, namely a disparity between the ages of the Yellowstone hot spot track and the Columbia River Basalt flows. There is also a significant compositional difference between the Columbia River Basalt province and the silicic Yellowstone volcanics.

SAMPLING METHODS

This study includes samples from 118 individual volcanic flows: 36 from the Saddle Mountain, 18 from the Wanapum, and 64 from the Grande Ronde Formation, each being a discrete site, collectively yielding 636 individual samples. As many samples as possible were collected using a portable Pomeroy drill, but in a few sites, hand samples were collected when the drills were dysfunctional or when a property owner's permission was obtained with the condition of only hand-sampling to eliminate wildfire risks. A solar or Brunton compass and inclinometer were used to determine the azimuth and the plunge of the core-samples and a compass was used to measure the strike and dip of the hand samples. Due to the high probability of the outcrops being significantly magnetic, solar compass readings were taken during predominantly favorable weather conditions. The readings of magnetic compass azimuths matched those of the solar compass readings, indicating that the magnetic intensities of the outcrops were not high enough to deviate a magnetic compass and affect orientation measurements. The azimuths of the cores were marked with the arrows pointing in the down direction convention. The hand samples were leveled and cast in plaster of Paris and cored using a drill press at the University of Michigan. Standard 2.5 cm diameter cylindrical specimens were prepared from the collected samples drilled in situ. From the hand samples, subsets of standard-size cores and smaller, 1.25 cm diameter cores were prepared. All samples were subsequently cut to a 2.5 cm thickness with a diamond-tipped saw. Any visible rust stains transferred from the saw were removed using coarse sandpaper. Afterwards, each sample was cleaned with a damp towel and left to dry. Once dry, the samples were labeled with non-magnetic, temperature-resistant paint, and broken specimens were cemented with alumina cement, which does not affect the magnetic readings in the magnetometer.

For each site, the magnetic flux and magnetic susceptibility of the outcrops were measured in situ and recorded (see Appendix). Since only volcanic samples were collected for this study, there was very low risk of inclination shallowing as can be common in sedimentary rocks. In order to reduce the effects of weathering on the collected samples, only the stable, and relatively pristine undulatory columns were sampled. The tops of flow ridges were avoided to reduce the risk of lightning-induced remagnetization. Furthermore, there was very little erosion between the layers due to the rapid accretion of these basaltic flows. When collecting the samples in the field, precautions were taken to avoid sampling the same flow unit more than once. Most of the samples were collected in road-cuts due to difficulty in obtaining permission to sample on private property, which comprised most of the region. However, the roads cut both horizontally and vertically through the units, so the individual units could be easily sampled and tracked.

Because each flow was approximately 30 m thick, with sampling concentrated in the lower undulatory columns, the chance of baked contact from the overlying flow was greatly diminished. Thus, the magnetic information measured from an individual flow most likely pertains to that flow and not the overlying one. Furthermore, the cooling time, t_c , of the flows was calculated according to the formula $t_c = d^2/4\kappa$, where d is the flow's thickness, and κ is its diffusivity (Davies, 2011). Into the interior of a flow, the temperature increases in a parabolic manner, and at the surface of the flow, the temperature of the flow is equivalent to that of its surrounding. Using a standard κ value of 10^{-6} m²/s, and the maximum thickness of individual flows for the Columbia River Basalt Group, a cooling time of approximately 7 years was calculated. This value is negligible and it can therefore be assumed that the magnetic signatures for each flow were recorded soon after emplacement. This calculation does not take into account further complexities, such as fluid flow through a given flow, which would accelerate the cooling rate, and decrease the cooling time.

The magnetic deviation for the sampling sites was calculated with the *National Geophysical Data Center (NGDC)* calculator from the *United States National Oceanic and Atmospheric Administration (NOAA)*, using the latitude 46°N and longitude -117°W during July 2010, when sampling took place. This yielded a declination of 15°11'E (changing by 0°9'W per year), meaning that approximately 15° was added to the azimuth of the sample's field orientation and its declination. **Table 1** lists the magnetic properties determined for each site in ascending order (from 1 to 118), whereas **Table 2** lists the same, but with the sites in stratigraphic order. Because of work interruptions, due to the need for obtaining permissions, and because of the desirability to use a solar compass with the outcrop in a favorable position with respect to sunlight, the site numbers are not sequential stratigraphically.

LABORATORY METHODS

All samples were measured and demagnetized in a magnetically shielded room in the Paleomagnetism, Structure and Tectonics Laboratory (PaSTeL) at the University of Michigan to prevent any accumulation of viscous magnetization in the samples. There, the natural remanent magnetization (NRM) of the rocks was measured using a three-axis 2G superconducting magnetometer. Most specimens were thermally demagnetized using an ASC TD-48 demagnetizer located in a shielded room with a residual field of less than 200 nT. Alternating Field demagnetization was carried out on some pilot samples and was attempted for some samples whose components were not successfully isolated with thermal demagnetization. Results of the demagnetization treatments have been graphed in orthogonal vector endpoint diagrams (*Zijderveld, 1967*) and in stereographic projections. For calculations of the magnetization directions, principal component analysis (PCA) (*Kirschvink, 1980*) was used on linear segments of the Zijderveld diagrams; in cases where stable endpoints were not obtained, as identified by trajectories along great circle paths, a combined analy-

sis of remagnetization circles and stable-endpoint observations (*McFadden & McElhinny, 1988*) was used. The paleomagnetic measurements were analyzed with the use of the Paleomac software (*Cogné, 2003*).

In order to image the most likely carriers of the magnetization of the samples, a Hitachi scanning electron microscope (SEM) fitted with an energy-dispersive analysis system (EDS) was used to qualitatively assess the compositions of opaque grains and determine whether the magnetization is carried by grains that are likely to be primary. The magnetic properties of the samples were measured at the Institute for Rock Magnetism of the University of Minnesota. Remanence acquisition curves, hysteresis loops and First-Order Reversal Curves (FORC) were measured with applied fields using the Princeton Measurements micro-Vibrating Sample Magnetometers (VSM) in high (~300-1025K; 0-1.7T), low (10-473K; 0-1.7T), and room temperature (~300K; 0-1.4T) conditions. The magnetic remanence was measured using two Quantum Design Magnetic Properties Measurement Systems (MPMS) (Old Blue: 2-320K, 0-5T DC, 0-0.3 mT AC; Big Red: 2-400K, 0-5T DC, 0-0.3 mT AC). Lastly, a Mössbauer Spectrometer was used at ambient temperature to determine the relative amount of magnetic components in representative samples.

DIRECTIONAL ANALYSIS

The analyzed samples primarily show univectorial decay to the origin (**Figure 3**). A quantitative look at the moment diagrams indicate an unblocking temperature point of 580°C (**Figure 4**), suggesting magnetite as the main carrier for the higher unblocking-temperature fraction of the natural remanent magnetization. Some samples show a sharp decrease in the magnetic intensity between 100 and 300°C, probably indicating a low-temperature component (perhaps an iron-sulfide, high Ti-magnetite, or goethite) (**Figure 5**). Some samples' moments indicate the existence of hematite (**Fig-**

ure 6), perhaps as a result of oxidation of the original magnetite; however, their high-temperature directions are the same as those of the magnetite components; thus they were most likely due to weathering of the magnetite during or soon after the emplacement of the corresponding flow. Site mean directions will be discussed at a later section.

SCANNING ELECTRON MICROSCOPY ANALYSIS

In order to determine whether magnetic direction patterns were influenced by the mineralogy of the basalts, selected samples were subjected to a sequence of Scanning Electron Microscope (SEM) and Electron Dispersal Spectroscopy (EDS) analyses. Three samples were selected depending on the behavior of their directions and magnetic moment (CR280, CR208, and CR379). Sample CR280 appears to contain a low-titanium magnetite, with an unblocking temperature of $\sim 550^{\circ}\text{C}$, accompanied by a low temperature component (unblocking temperature between 200 and 300°C) perhaps suggesting the presence of a titano-magnetite component (**Figure 7a-b**). The titano-magnetite and low-titanium magnetite components have nearly the same directions, which might indicate that their magnetizations are of nearly the same age. It is also possible that a present day field direction is visible between 0 and 200°C and is unrecognizably included in a composite remanence removed between 200 and 300°C . Sample CR280 contained a silicate matrix with titano-magnetite present along with acicular and blocky feldspar crystals. The minerals in the sample were very pristine and no exsolution or dissolution was visible; only some minor fractures were present. No other magnetic mineral could be detected, thus the lower-temperature component was interpreted as being caused by either a viscous Present-Day Field component in multi-domain magnetite or by titano-magnetite.

The Zijderveld and intensity diagrams for sample CR208 show different behaviors depending on the demagnetization step (**Figure 8a-b**). From 150 - 450°C , there is an unblocking behavior that

could be indicative of titanomagnetite, while another drop in intensity occurs between 450 and 550°C, possibly due to the presence of low titanium magnetite. The titanomagnetite and low titanium magnetite components have different inclinations, which might indicate that they are of different ages. The SEM and EDS analysis revealed a silicate matrix with feldspar crystals, and very pristine low-Ti magnetite grains with no visible weathering or exsolution. This, in fact, corroborates the intensity diagram for this specimen, which showed the presence of Ti-poor magnetite, and likely a larger amount of titanomagnetite.

Sample CR379 revealed three magnetic components: a low temperature component (unblocking temperature of 250°C), a magnetite component (550°C), and a hematite component (625°C) (**Figure 9**). The SEM and EDS analysis for this sample showed Ti-magnetite, where some grains were pristine, and others were exsolved along the magnetite cleavage planes that were titanium-rich and titanium-poor (**Figure 10**). The depressed unblocking temperatures at about 250°C and 520°C for this sample (**Figure 9b**) might be due to the low-Ti titanomagnetite, and exsolved magnetite, respectively, as indicated in **Figure 10c**. The matrix was silica-rich, most likely feldspar. There were also some acicular and blocky apatite crystals. No hematite was visible, most likely because it might be a very minor phase, as indicated by its thermal demagnetization (**Figure 9b**).

ROCK MAGNETIC ANALYSIS

Since the purpose of this study is to determine the behavior of the geomagnetic field, it is crucial to determine whether the directional analysis of the collected samples is affected by the magnetic mineralogy and/or the ability of the rocks to accurately record the geomagnetic field. If the characteristic remanent magnetization (ChRM) is carried by a likely primary mineral, such as titanomagnetite, and if there are no anisotropy or structural aspects affecting remanence directions, then

the magnetic behavior of the samples can be safely attributed to the characteristics of the magnetic field and not due to their magnetic mineralogy.

1. Magnetic Susceptibility Dependence on Temperature

Thermomagnetic runs, based on the susceptibility dependence on temperature, $\kappa(T)$, were performed for several representative samples for this collection. The purpose of this analysis is to contribute to the list of diagnostics to characterize the remanence carriers, and to determine if magnetochemical changes occurred in the magnetic minerals as a function of temperature. This is reflected by the ability of grains of a particular sample to maintain, lose, or gain magnetization. In this procedure, the temperature was increased from ambient conditions ($\sim 25^\circ\text{C}$) to 800°C in increasing increments while continuously measuring the magnetic moment, and then allowed to cool back to room temperature. When the magnetic mineralogy of the grains remains unaltered, the heating and cooling curves look similar, and the grains are said to have a reversible behavior, implying that the magnetic minerals are stable. On the other hand, if there is a marked difference between the heating and cooling curves, then the magnetic grains have undergone magnetochemical changes, such as oxidation, reduction, and/or annealing. Where they are observed to have irreversible behavior, this indicates that the magnetic minerals are unstable to varying degrees. Furthermore, the decays in magnetic intensity at given unblocking temperatures can aid in the identification of the magnetic grains present, complementing the behavior seen in intensity diagrams.

Samples CR320 and CR447 are representative of the behavior of all others analyzed with this procedure. Sample CR320 showed a relatively clear reversible behavior between the heating and cooling curves, with a slight lag due to thermal inertia (**Figure 11**). The heating curve showed a dip in the magnetic moment around 575°C , due to the presence of mag-

netite. As it cooled, the magnetic behavior remains almost the same, with a slight decrease in the unblocking temperature and magnetic moment. Sample CR447 indicated a difference in behavior, where there was not only a greater separation in the magnetic moment between the heating and cooling curves, but the unblocking temperatures between the heating and cooling curves were significantly different and could not be attributed to thermal inertia. For instance, the unblocking temperature for the heating curve was approximately 150°C, whereas for the cooling curve, it ranged between 300 and 500°C (**Figure 12**). Thus, this sample was considered irreversible, and the cooling curve indicated that the remanence carrier in this sample might have become annealed or oxidized.

2. Hysteresis Properties

The response of a rock's magnetic grains to a variable laboratory magnetic field can yield revealing information about its magnetic mineralogy and domain state, which is represented as a hysteresis loop. For this study's hysteresis analysis, the field was increased in intensity up to a set maximum magnetic field, H_{max} of approximately 1.5 Tesla and then subjected to an antiparallel and growing field to a negative maximum, $-H_{max}$; the process was then reversed and repeated to generate a complete cycle represented by a hysteresis loop. Hysteresis loops show the relationship between the applied magnetic field and the induced magnetization of the sample and reveal the remanence after saturation (M_{rs}), the saturation magnetization (M_s), and coercivity (H_c) (**Figure 13**). The hysteresis analyses of the samples revealed the presence of multi-domain grain sizes (**Figure 13a**) and pseudosingle domain grain sizes (**Figure 13b**) judging by the M_{rs}/M_s ratios of all the samples analyzed with this technique.

3. Day Plots

Given that the primary magnetization carrier in the samples for this study is titanomagnetite, the ratios of the hysteresis parameters indicate the domain state of the grains. In the *Day et al. (1977)* analysis, the Coercivity (H_{cr}/H_c) and Remanence (M_{rs}/M_s) ratios for all hysteresis curves were graphed in a two-axis logarithmic diagram. Single-domain grains have the highest M_{rs}/M_s ratio (greater than 0.5) and the smallest H_{cr}/H_c ratio (less than 2.0), whereas multi-domain grains have a small M_{rs}/M_s ratio (approximately 0.1) and the largest H_{cr}/H_c ratio (greater than 4). The difference in the ratios is because it is energetically easier to translate domain walls in a multi-domain grain than to change the magnetic moment of a single-domain grain. Pseudosingle domain grains show a behavior intermediate between single- and multi-domain grains. Thus, the Day plot should indicate the domain type of the magnetic grains.

The Day plot for samples measured at room temperature (300 K) showed that almost all the samples were borderline multi-to-pseudosingle domain, with M_{rs}/M_s in the range of ~0.08 to 0.4 and H_{rc}/H_c between 1.5 and 5 (**Figure 14**). This indicates that the grain sizes are large enough for the relaxation time of the samples to be long, allowing them to carry a stable magnetization, but not too large for thermoremanent magnetization efficiency to be so high as to allow the grains to easily pick up any viscous magnetization.

4. First Order Reversal Curves

Further analyses of the rock magnetic properties of this collection were performed using First Order Reversal Curve (FORC) diagrams, which are calculated from a compilation of hysteresis curves (*Mayergoyz, 1986*). This was done by saturating a sample with a high positive applied field, which was then decreased and flipped to a reversal field, H_a . A single

reversal curve was then plotted once the applied field was increased from this H_a to the sample's saturation point. This process was then repeated for changing values of this applied field to create a full FORC diagram. The purpose of this method is to determine the interaction of a sample's magnetic grains with applied fields, which can be used to determine the domain state of grains and their magnetic interaction.

For this study, several samples were analyzed using the FORC method at room temperature (300 Kelvin), two of which are shown here as representative of the entire set: CR19 and CR320. Sample CR19 (**Figure 15a**) showed a pseudosingle domain behavior, as can be seen from its concentration towards the origin of the graph and with some vertical spread, but not as much as for a multi-domain grain. However, sample CR320 (**Figure 15b**) showed a classic example of single domain behavior due to the horizontal elongation of the curve contours along the H_a axis that enclose a central peak and have very little vertical spread, indicating a lack of interaction among single-domain particles. Furthermore, these results corroborate those observed with Day plots.

5. Mössbauer Spectroscopy

Mössbauer spectroscopy (*Mössbauer, 1958a; Mössbauer, 1958b*) works by the emission of gamma rays at a specimen, reacting with the specimen's Fe^{2+} and Fe^{3+} electrons, and changing their valence and energy states. These energy state jumps, known as recoil, are then recorded as "excitement peaks," which are characteristic of a magnetic mineral's specific chemical composition. Thus, analyzing the peaks of recoil allows for the determination of a sample's magnetic minerals. Generally, ^{57}Fe is used because its excited state has a half-life of 0.01-1000 nanoseconds. The disadvantage with this technique is that it is very slow and can take up to 4 days to generate a single spectroscopic analysis.

Sample CR431B was analyzed by this method to determine its magnetic mineral composition (**Figure 16**). According to its intensity diagrams, this sample carries low-Ti magnetite (unblocking temperature of 580°C), with a lower-temperature component, possibly high-Ti magnetite, at around 350°C. The Mössbauer results showed a 54% composition of Fe³⁺, and a 46% composition of Fe²⁺. These results indicate the existence of magnetite because it comprises approximately equal amounts of ferrous and ferric iron cations in its structure.

6. Low-Temperature Magnetic Remanence

Magnetic remanence analysis, performed using a Magnetic Properties Measurement System (MPMS), reveals a Verwey transition at approximately 120 Kelvin. This is because during the transition, the anisotropy goes to zero, which causes a rapid drop in magnetic moment. The magnetic remanence curve for sample CR630 shows a representative curve for the samples analyzed using this method (**Figure 17**).

FOLD TEST

Out of the total 118 sampled flows, 15 sites were tilted, thus a fold test was applied (see Appendix for bedding information). The principle behind this technique is that it is necessary to check whether a given site was folded or tilted prior, during, or after the magnetization acquisition by its corresponding magnetic minerals. This idea, first championed by *Graham (1949)*, states that if a region was magnetized prior to folding, the magnetic directions will then become more clustered upon restoration to horizontal; the opposite is true for post-folding magnetization.

In this collection, the fold test was carried out in order to determine if the magnetization was acquired, pre-, syn-, or post-deformation. When comparing the site directions prior to correction,

there is significant inherent scatter, and the site mean directions do not coincide with the northerly and down and southerly and up directions expected for the Miocene (**Figure 18a**). In fact, some directions are easterly and down while others are westerly and up. However, after the tilt-correction, the sites tend to cluster more, and the site means are more similar to those expected for this study (**Figure 18b**). It is apparent that there are some directions that are still quite scattered, namely those pertaining to reverse polarity intervals. Nonetheless, such deviations are also seen in site means for the undeformed beds. Additionally, there are some directions that appear to be quite shallow; these are, in fact, transitional directions, also visible in flows that have not experienced deformation. The fold test is positive at the 95% confidence level with a K -ratio of 2.06 (k_2/k_1 , **Table 3**) using the method of *McElhinny (1964)*.

RELIABILITY CRITERIA

The sampling quality is important to obtain reliable results. This can be checked by using criteria suggested by *Van der Voo (1990)*. The ages of the basalts from the Columbia River Province have been extensively studied and the magnetization of the rocks is of the same age as that of the rock age, as was determined from a very fast cooling time of approximately 7 years (see Sampling section for more details), complying with criterion 1. The majority of site means have an α_{95} of less than 16, also meeting criterion 2 (**Table 1**). The samples were demagnetized using both thermal and Alternating Field, and most samples have univectorial decay with few samples showing more than one vector, covering criterion 3. Stereonet and orthogonal vector diagrams (*Zijderveld, 1967*) were used along with Principal Component Analysis to isolate the vectors of magnetic components (*Kirschvink, 1980*), and demagnetization intervals for both thermal and alternating field treatments are small enough to detect all possible vector components by any magnetic carrier.

Criterion 4 requires that field tests (fold, conglomerate, and contact) be performed on the samples, if possible. The conglomerate test has not proven possible, and the contact test is not possible because, as previously stated, the sampled sections of each flow were buffered by their scoriaceous tops from the overlying flows. Furthermore, the scoriaceous tops of the flows are quite friable and weathered, and it would be very difficult to get any useful results from them. The fold test, as explained in the previous section, was positive. Therefore, criterion 4 is probably met. Criterion 5, which requires structural control, is likely met. The area sampled is believed to be far enough east to prevent significant tectonic rotation (*Jarboe et al., 2008; Magill et al., 1982*). The majority of flows are approximately horizontal (**see Figure 2c**), whereas some folding and tilting is visible in places, but has been corrected for. Both normal and reverse polarities are present in this collection, meeting criterion 6. Furthermore, considering how young these rocks are and only fresh samples were collected, remagnetization is unlikely.

MAGNETOSTRATIGRAPHY

The sites were ordered stratigraphically by using a combination of topographic and geologic maps. Subsequently, the polarity intervals were compared with previously published work (*Baksi, 1988; Berggren et al., 1985; Choiniere & Swanson, 1979; Harland et al., 1982; Hooper et al., 1989; Reidel et al., 2003; Wells et al., 1989*). The site-mean directions were then plotted in stratigraphic order, increasing in age towards the bottom of the column, and ranging from slightly over 6 Ma to 15.6 Ma (**Figure 19a-b**). The magnetic declination for this study's site-means with their corresponding site numbers can be seen in **Table 19a**, and magnetostratigraphically ordered site means can be referenced in **Table 2**. A linear regression analysis was done to determine any possible temporal dependence for declination, which would indicate any possible rotation of the area sampled (i.e. Apparent Polar Wander). The analysis indicates that there is a very small counterclockwise rotation of

0.11° per million years, with a correlation coefficient, R , of 0.038, indicating a very weak time-declination relationship. Thus, the sampled region has experienced little to no rotation.

Figure 19b depicts the inclination changes with time, and **Figure 19c** shows the 6 reversal sequences sampled. The normal polarity reversal given by site 24 was determined to be an outlier, and its interval was not considered reliable (half-bar in magnetostratigraphic column). The flows from this study are sequential, and were matched to the temporally-ordered stratigraphic columns from previous works that had obtained ages for their flows (*Baksi, 1988; Berggren et al., 1985; Harland et al., 1982; Reidel et al., 2003*) (**Figure 19d-g**). The column from *Reidel et al. (2003)* (**Figure 19d**) was used most commonly because it is the most recent and complete. The boundaries of the Saddle Mountain, Wanapum, and Grande Ronde members were determined in the field with the help of lithologic and magnetic polarity maps, and then by comparing our directions with those of these previous studies.

DETERMINATION OF CUTOFF AND GROUPING

To reduce systematic bias in the data analysis, the site directions were analyzed using both grouped and ungrouped site means. Ungrouped sites means were calculated for individual sites without combining those with similar directions. On the other hand, grouped site means were calculated for sites that were stratigraphically contiguous in order to reduce redundancy bias. This was done by first calculating the Non-Random Ordering (*NRO*) factor (*Biggin et al., 2008a*) for each reversal that had five or more flows. An *NRO* factor of 0.95 or higher indicates that data are not randomly oriented with 95% confidence and must therefore be combined (**see Table 2**). The combined site mean of the sites for the applicable reversal intervals was then calculated by plotting the site directions in stereographic projections and grouped only when the directions were within each other's

cone of confidence, or α_{95} . If the α_{95} of two or more consecutive flows contained each others' directions, then the directions were not distinct at the 5% significance level. Thirty-three sites were grouped into thirteen groups (GP1 to GP13), and their site means and VGPs were calculated (**Table 4**). For most grouped sites, only two flows were combined. Thus, their α_{95} and k parameters are unimportant, but still indicate the similarity in their directions.

Both grouped and ungrouped site means were further analyzed using a (i) “visual inspection cutoff,” where outlier sites were determined using visual inspection in stereographic projection, (ii) a “45° cutoff,” in which outliers were determined to be those whose Virtual Geomagnetic Poles (VGPs) were not contained within 45° from the mean pole, and (iii) “Vandamme cutoff”. In the latter scenario, outliers were determined for sites whose VGPs were eliminated through applications of iterative *Vandamme (1994)* criteria. For this cutoff type, the cutoff angle, A , was calculated using the angular standard deviation, ASD , of the distribution of the VGPs by the following equation:

$$A(^{\circ}) = 1.8 \cdot ASD(^{\circ}) + 5^{\circ}$$

For the “grouped with Vandamme cutoff” scenario the cutoff angle was determined to be 45.16°, whereas for the “ungrouped with Vandamme cutoff” case, the cutoff angle was 43.96°. Furthermore, the same sites were eliminated using the 45° and Vandamme cutoffs, thus the elongation, dispersion, site means, and secular variations for the surviving sites were the same.

PALEOMAGNETIC SITE MEANS

Site means were calculated and graphed for each of the scenarios mentioned above (**Figure 20a-d**). For grouped and ungrouped sites with a visual inspection cutoff, the same 11 sites were deemed outliers while for the grouped and ungrouped sites with 45° and Vandamme cutoffs, the same 10 outliers were determined (**Table 5**). The mean direction of all these six scenarios was calcu-

lated, which gave a normal polarity direction with declination of 6.8° and inclination of 63.8° , and a reverse direction with declination of 178.8° , and inclination of -60.3° (**Table 6**). The stereographic projection corresponding to this analysis can be seen in **Figure 21**. Furthermore, the paleomagnetic site means are quite similar to those calculated from previous studies (**Table 7**). Some results from previous work differ slightly from those of this study because they comprised samples from the western section of the CRBG.

Because there was a large dispersion in the site directions for this collection, the 45° and Vandamme cutoffs were more forgiving when selecting outliers than through visual inspection, especially for the reverse polarity directions. There is a significant difference between the dispersion of normal polarity and reverse polarity directions, where the latter tend to be more scattered. The differences between the normal and reverse polarity dispersions can be seen quantitatively (**Table 6**) by comparing their corresponding k -values. For normal polarity directions, the k -values are higher (about 30° on average) than for the reverse polarity directions (averaging about 16°). This discrepancy is addressed later.

GEOMAGNETIC ANALYSIS AND COMPARISON WITH CURRENT MODELS AND DATA

1. Models and Data from Previous Geomagnetic Studies

The ultimate purpose of this study is to compare the geomagnetic field parameters calculated from our results with models of the geomagnetic field. As was previously stated, the validity and accuracy of the current models of the behavior of the magnetic field have been tested with empirical data for the most recent 5 million years of geomagnetic history. However, it is imperative to check the geomagnetic parameters for the rest of geologic history since there are few studies dealing with Mesozoic or Precambrian rocks (*e.g.*: *Bazhenov et*

al., 2012 (in review); Biggin *et al.*, 2008b; Haldan *et al.*, 2009; Heunemann *et al.*, 2004; Swanson-Hysell *et al.*, 2009; Tauxe & Kodama, 2009). Furthermore, the results of this study are also compared to data compiled from other studies of the geomagnetic field for the last 5 million years. This was done in order to determine if there is a difference in the behavior of the magnetic field between the two time intervals.

The TK03.GAD (Tauxe & Kent, 2004) model is one of the most recent, which predicts circularly symmetric VGP distributions, suggesting that their corresponding site directions are elongated, especially in lower latitudes, and that this elongation occurs in a North-South direction while smoothly-varying with latitude or inclination. Most importantly, the model can be employed to correct for inclination shallowing bias, which is common in sedimentary rocks and plagues many paleomagnetic continental reconstructions. It is also seems to correct for potential non-zero, non-dipole contributions, in particular octupole contributions, which cause deviations from ideal dipolar geomagnetic field records.

Another model that analyzes data for the last 5 million years is CJ98.GAD (Constable & Johnson, 1998), which permits a non-zero average of the non-dipole constituents of the magnetic field. It also allows for VGP scatter at high latitudes by increasing the contribution of anti-symmetric terms of the magnetic field relative to the symmetric terms. When compared to the data of the past 5 million years, it provides a good prediction of the VGP scatter in high latitudes, but underestimates the scatter for low latitudes.

Model CP88.GAD (Constable & Parker, 1988) has a zero mean axial quadrupolar term. Its main advantage is that it can generate distributions of the non-dipole components and is comparable to the current 5 Ma paleomagnetic data and predictions of other geomagnetic models. However, it does not take into consideration the variable dispersion values ob-

served for the VGPs calculated from directions depending on latitude. This model is also more symmetric than the CJ98.GAD model because the former has a smaller anti-symmetric contribution.

The data compilation MM97 (*McElhinny & McFadden, 1997*) consists of the paleosecular variation of recent lavas for the last 5 million years within a certain set of criteria, including the rejection of VGPs more than 45° away from the spin axis to eliminate bias from transitional directions. In this study, its authors also calculated the angular standard deviation of the dispersion, S' (*Cox, 1969*), which will be discussed next.

Lastly, the most recent and complete compilation of high-quality data for the last 5 million years was done in the Time-Averaged Field Initiative, or TAFI (*Johnson et al., 2008*), in which paleomagnetic directional data were sampled in 17 different locations around the globe. This impressive collection spanned sampling latitudes between 78°S and 53°N and has enough data to study the secular variation.

2. Dispersion

An important parameter analyzed in geomagnetic field studies is the dispersion of the Virtual Geomagnetic Poles (VGPs), which can be used as an indicator of the stability of the geodynamo during a given polarity interval. The dispersion, S or S' , is calculated by the following formula (*Cox, 1969*):

$$S^2 = (N - 1)^{-1} \sum_{i=1}^N (\Delta_i)^2$$

where N is the number of observations, and Δ is the angle between the i^{th} VGP and the spin axis. Dispersions of the normal and reverse polarity sites were also calculated using all different cutoff and grouping scenarios. The details of the dispersion calculations can be found

in **Tables 8 to 19**. The average dispersion for all scenarios was also determined to have the following values: S' : 21.8208, S_b : 20.6230, and S_w/\sqrt{n} : 7.0887. Furthermore, the mean dispersion, S' , is on average one unit larger than the individual scatter, S_b , for all the scenarios (**Table 20**).

Paleosecular variation may involve a correlation between increasing dispersion of virtual geomagnetic poles (VGPs) with increasing latitude, λ (*Merrill et al., 1996*). VGPs are calculated from magnetic directions at a site and represent spot readings of the total geomagnetic field, but VGPs are calculated by using the dipole formula, even though it is reasonable to assume that the current field was probably not purely dipolar. The dispersions of our study for the reverse and normal polarities for all six scenarios (grouped and ungrouped sites with visual inspection, 45° and Vandamme cutoffs) were plotted against the site latitude along with the TK03.GAD (*Tauxe & Kent, 2004*), CJ98.GAD (*Constable & Johnson, 1999*), and CP88.GAD (*Constable & Parker, 1988*) models and the collected data from the Time-Averaged Field Initiative (TAFI) (*Johnson et al., 2008*) and MM97 (*McElhinny & McFadden, 1997*) (**Figure 22a-e**).

The latitude for this collection is approximately 46°N, which, according to the TK03, CJ98, and CP88 models should have a dispersion, S' , of about 18, 16, and 14°, respectively. However, the S' values obtained for all six of the different scenarios (**Table 20**) are significantly greater than the TAFI and MM97 collected data. Furthermore, none of the dispersion values agree with those determined from the three models tested. Furthermore, our results suggest that the magnetic field's behavior was more stochastic than predicted, as seen from high dispersion values observed in this study.

Comparing the changes in dispersion values with different grouping and cutoff scenarios reveals some interesting results. The overall dispersion value is greater for grouped sites, but they are similar for the cutoff scenarios within their corresponding grouped and ungrouped categories. This means that the type of outlier cutoff did not introduce a significant systematic bias, but there was a slight difference between grouped and ungrouped sites. Furthermore, it is also clear that the reverse polarity dispersion values are consistently higher than the normal polarity dispersion. This phenomenon is also observed in the TAFI (*Johnson et al., 2008*) and MM97 (*McElhinny & McFadden, 1997*) studies. This could be due to a difference in the isolation of the Characteristic Remanent Magnetization (ChRM) in the samples as a function of polarity. But it might also indicate that the geodynamo during the Miocene was more stable in normal polarity intervals than throughout reverse polarity intervals. Of course, this is a purely speculative but interesting idea to investigate.

3. Directional Elongation

A collection of VGPs is typically expected to have circular symmetry about their mean pole (*Tauxe, 2008*), while their corresponding site means are elongated as a function of their inclination (or paleolatitude). The calculations of site mean elongation for the 6 scenarios showed mean values between 1.9 and 2.0, and the mean elongation of all scenarios was determined to be 1.9 (**Table 21**). The elongation values were graphed against the elongation curves for the TK03.GAD (*Tauxe & Kent, 2004*), and CJ98.GAD (*Constable & Johnson, 1998*) models and data from MM97 (*McElhinny & McFadden, 1997*), the Yemeni traps (*Riisager et al., 2005*), Deccan traps (*Vandamme et al., 1991; Vandamme & Courtillot, 1992*), Faroe Island basalts (*Riisager et al., 2002*) and Kerguelen (*Plenier et al., 2002*) (**Figure 23a-d**). The elongation values determined in this study do not contain the CJ98.GAD

curve within their error bars, regardless of the type of scenario; however, they all contain the TK03.GAD curve. Thus, the TK03 model can predict the site mean elongation behavior for the magnetic field, while this is not the case for the CJ98 model.

4. Mean Poles

The poles for the VGPs for all grouping and cutoff scenarios were calculated and can be seen in **Table 22**. The mean pole for all the scenarios was calculated to have a Pole Longitude: 359.8° , Pole Latitude: 88.0° , K: 14246.0, and A_{95} : 0.6° . As can be seen, the K and A_{95} values indicate that the six poles are quite similar to each other. They also all plot close to the geographic North (**Figure 24**).

5. Secular Variation

Secular variation is analyzed in paleomagnetic studies to determine if site means average out the magnetic field for the geologic time interval sampled. But for this study, analyzing secular variation is additionally important due to the implications for the geomagnetic field behavior. Sampling for any given paleomagnetic or geomagnetic study must be large enough to average out the secular variation of the geomagnetic field. This generally takes slightly less than about 100,000 years (*Butler, 1992*) due to the convection of the Earth's liquid outer core, which is responsible for the geomagnetic field (*Bloxham & Gubbins, 1985*), whereas more frequent periodicities are mostly due to electric currents in the ionosphere and magnetosphere (*Merrill et al., 1996*).

Secular variation for this collection was graphed by inverting the reverse polarity VGPs into normal polarity, and sequenced by age to track the progression of the magnetic pole during the 6-15.6 Ma range. Secular variation diagrams were created for each grouping and cutoff scenario (**Figure 25a-d**). The secular variation for the grouped sites with 45° and

Vandamme cutoffs are the same because they have the same outliers (**Figure 20b**). In the case of the ungrouped sites with 45° and Vandamme cutoffs, the same outliers were also eliminated, thus the secular variation is the same for both (**Figure 20d**). In all of these scenarios, it is quite clear that paleosecular variation during the Miocene averages the non-dipole magnetic field, given the coincidence of the mean poles (depicted as red stars) with the rotation axis.

DISCUSSION

The main purpose of this study is to examine the validity of several geomagnetic field models, namely the TK03.GAD (*Tauxe & Kent, 2004*), CJ98.GAD (*Constable & Johnson, 1998*), and CP88.GAD (*Constable & Parker, 1988*) models and their parameters with those determined for this study. This study also compares our empirical results with those of the MM97 (*McElhinny & McFadden, 1997*) and TAFI (*Johnson et al., 2008*) studies. Analyzing the dispersion calculation for all different cutoff and grouping scenarios indicates that the reverse polarity dispersion is significantly greater than that for normal polarity directions; this was also observed in the MM97 and TAFI compilations. This phenomenon is perhaps due to greater inherent instability of the geodynamo during reverse polarity intervals than during normal polarity intervals. Regardless, for all the different cutoff scenarios, the normal and reverse polarity dispersion are both significantly greater than those predicted by the TK03.GAD, CJ98.GAD, and CP88.GAD models, indicating that the dispersion for the Miocene is underpredicted by these current models and that the magnetic field was more stochastic than during the most recent 5 million years of Earth's magnetic history. The mean dispersion value, S' , for the 46°N latitude of our study, with the combined polarities for all cutoff and grouping scenarios is 21.8° , while those predicted by the TK03, CJ98, and CP88 models have dispersion values of about 18° , 16° , and 14° , respectively.

Furthermore, for the site mean elongation calculations, our study yields a mean elongation of 1.9 for all cutoff scenarios. The elongation 95% confidence bars for all cutoff and grouping scenarios contain the TK03.GAD curve, but this is not the case for the CJ98.GAD prediction curve. Hence, this indicates that the TK03 Geomagnetic Axial Dipole model somewhat agrees with our elongation results, while the CJ98 model does not. This being said, further refinement of the TK03.GAD and CJ98.GAD models is probably needed to adjust for this greater elongation.

The secular variation for this study also shows a relatively large dispersion of the magnetic poles, indicating that there may have been a significantly greater dispersion in the Miocene than in the last 5 million years. This greater dispersion could be due to greater contribution of non-dipole fields to the co-axial geocentric dipole (GAD) magnetic field during the Miocene, or perhaps an intrinsic instability of the magnetic field during this time. In any case, this study's empirical parameters all indicate that the magnetic field's behavior only marginally resembles that during the recent 5 Ma of geomagnetic history. Therefore, we suggest that current GAD+non-dipole models should be refined for this time period by adjusting for a greater than predicted dispersion and elongation. Perhaps time-differentiated GAD models might even be necessary to account for a trend in geologic history, since applying an all-encompassing model for the entire geomagnetic history might produce imprecise predictions.

IMPLICATIONS

The interaction of the Earth's liquid outer core with the solid mantle is likely expressed in its geomagnetic field behavior, causing it to vary on a $10\text{-}10^8$ year timescale. Increasing heat flow through the Core-Mantle Boundary (CMB) can cause the geodynamo to become unstable (*Olson et al., 2010*). Thus, the results from this study might give a glimpse into the interaction between the

Earth's outer core and mantle. As was previously noted, the dispersion parameter for this study indicates an increased VGP scatter, which might suggest a greater stochasticity of the geodynamo, perhaps related to an increase in the heat flow through the CMB. The reverse polarity VGPs in this study had a significantly larger dispersion than those for normal polarity, with an average difference of 2.9. Could this mean that there was a greater heat flux during reverse polarities than normal polarities during the Miocene? This study's results point to the need for future studies to understand this phenomenon.

Furthermore, our observations of the geomagnetic parameters during the Miocene indicate that there is some disagreement between our results, and the elongation and dispersion predictions of the models tested in this study. Thus, we recommend that, upon further testing, that these models be refined to conform to these empirical data. Additionally, this study brings into focus the fact that current geomagnetic models may be inaccurate for older geologic periods.

CONCLUSIONS

In this study, 118 sites were collected in the Miocene Columbia River Basalt Group (CRBG) to study the behavior of its magnetic field record, and compare our results to those predicted by the TK03 (*Tauxe & Kent, 2004*), CJ98 (*Constable & Johnson, 1998*), and CP88 (*Constable & Parker, 1988*) models on the behavior of the magnetic field. This is important because these models have been tested with data up to 5 Ma, but their validity has not been tested with older data. Our samples were collected from individual basaltic flows in the eastern section of the CRBG to avoid significant tectonic complications. Furthermore, paleomagnetic analysis reveals that most samples show univectorial decay, and contain titanomagnetite as their magnetic mineral; most of the magnetic grains were also determined to be pseudosingle domain. Both reverse and normal polarity directions

were present, indicating adequate averaging of the magnetic field. Magnetostratigraphic analyses indicate that, for this study, six reversals were sampled altogether for the Saddle Mountain, Wanapum, and Grande Ronde members of the CRBG.

To reduce systematic bias, sites were analyzed as grouped and ungrouped and with a 45° cutoff, Vandamme (1994) cutoff and visual inspection cutoff. The dispersion calculations, S' , for the samples in this collection show average values of dispersion values of 23.4, 20.5 and 21.8° for the reverse polarity, normal polarity, and combined polarity directions, respectively. These values differ significantly from the dispersion values of 18, 16, and 14° predicted by the TK03, CJ98, and CP88 models, respectively, for the corresponding 46°N latitude for this collection. Additionally, the large dispersion might indicate a stochastic behavior of the geodynamo, markedly in the reverse polarity intervals, possibly due to an increased heat flux through the Core-Mantle Boundary. The mean elongation for all grouping and cutoff scenarios for this collection was calculated to be 1.9 for its corresponding 61.2° inclination. Each elongation value contains within its 95% confidence interval the TK03-predicted elongation value of approximately 1.5, but not the for CJ98 curve. These results indicate that, although these geomagnetic models can loosely predict the parameters for the geomagnetic field for this time, they require improvement. Furthermore, these results suggest that it is necessary to test the validity of current geocentric axial dipole models with empirical data from older periods in geologic history.

REFERENCES

- Baksi, A.K., 1988, Estimation of Lava Extrusion and Magma Production Rates for Two Flood Basalt Provinces: *Journal of Geophysical Research*, v. 93, p. 11,809-11,815.
- Bazhenov, M.L., Van der Voo, R., Levashova, N.M., Dominguez, A.R., 2012 (in review), Late Devonian Paleomagnetism of the North Tien Shan, Kyrgyzia: Can Secular Variation Vary on a Short Time Scale?: *Geophysical Journal International*.

- Beck, M.E., Jr., 1976, Discordant paleomagnetic pole position as evidence of regional shear in the Western Cordillera of North America: *American Journal of Science*, v. 276, p. 694-712.
- Beck, M.E., Jr., 1980, Paleomagnetic record of plate-margin tectonic processes along the western edge of North America: *Journal of Geophysical Research*, v. 80, p. 7,115-7,131.
- Beck, M.E., Engebretson, D.C., Plumley, P.W., 1978, Magnetostratigraphy of the Grande Ronde sequence: Western Washington University, RHO-BWI-C-18, 29 p.
- Berggren, W.A., Kent, D.A., Flynn, J.J., Couvering, J.A., 1985, Cenozoic geochronology: *Geological Society of America Bulletin*, v. 96, p. 1,407-1,418.
- Biggin, A.J., van Hinsbergen, D.J.J., Langereis, C.G., Straathof, G.B., Deenen, M.H.L., 2008a, Geomagnetic secular variation in the Cretaceous Normal Superchron and in the Jurassic: *Physics of the Earth and Planetary Interiors*, v. 169, p. 3-19.
- Biggin, A.J., Strik, G.H.M.A., Langereis, C.G., 2008b, Evidence for a very-long-term trend in geomagnetic secular variation: *Nature Geoscience*, v. 1, p. 395-398.
- Bloxham, J., Gubbins, D., 1985, The secular variation of Earth's magnetic field: *Nature*, v. 317, p. 777-781.
- Butler, R.F., 1992, *Paleomagnetism: Magnetic Domains of Geologic Terranes*: Blackwell Science, Oxford, 319 p.
- Camp, V.E., Ross, M.E., Hanson, W.E., 2003, Genesis of flood basalts and Basin and Range volcanic rocks from Steens Mountain to the Malheur River Gorge, Oregon: *Geological Society of America Bulletin*, v. 115, p. 105-128.
- Choiniere, S.R., Swanson, D.A., 1979, Magnetostratigraphy and correlation of Miocene basalts of the northern Oregon and Columbia Plateau, southeast Washington: *American Journal of Science*, v. 279, p. 755-777.
- Coe, R.S., Bogue, S., Myers, C.W., 1978, Paleomagnetism of the Grande Ronde (lower Yakima) Basalt exposed at Sentinel Gap: potential use for stratigraphic correlation: Rockwell Hanford Report, RHOBWI-ST-2, 24 p.
- Cogné, J.P., 2003, PaleoMac: A MacintoshTM application for treating paleomagnetic data and making plate reconstructions: *Geochemistry Geophysics Geosystems*, v. 4, p. 1-8
- Constable, C., Johnson, C., 1999, Anisotropic paleosecular variation models: implications for geomagnetic field observables: *Physics of Earth and Planetary Interiors*, v. 104, p. 35-51.
- Constable, C., Parker, R.L., 1988, Statistics of the geomagnetic secular variation for the past 5 m.y., *Journal of Geophysical Research*, v. 115, p. 11,569-11,581.
- Cordrey, M.J., Davies, G.F., Campbell, I.H., 1997, Genesis of flood basalts from eclogite-bearing mantle plumes: *Journal of Geophysical Research*, v. 102, p. 20,179-20,197.
- Cox, A., 1969, Research note: Confidence limits for the precision parameter, K: *Geophysical Journal of the Royal Astronomical Society*, v. 17, p. 545-549.

- Davies, G., 2011, *Mantle Convection for Geologists*: Cambridge University Press, 240 p.
- Day, R., Fuller, M., Schmidt, V.A., 1977, Hysteresis properties of titanomagnetites: Grain size and composition dependence: *Physics of the Earth and Planetary Interiors*, v. 13, p. 260-267.
- Dodson, A., Kennedy, B.M., DePaolo, D.J., 1997, Helium and neon isotopes in the Imnaha Basalt, Columbia River Basalt group: Evidence for a Yellowstone plume source: *Earth and Planetary Science Letters*, v. 150, p. 443-451.
- Graham, J.W., 1949, The stability and significance of magnetism in sedimentary rocks: *Journal of Geophysical Research*, v. 54, p. 131-167.
- Haldan, M.M., Langereis, C.G., Biggin, A.J., Dekkers, M.J., Evans, M.E., 2009, A comparison of detailed equatorial red bed records of secular variation during the Permo-Carboniferous Reversed Superchron: *Geophysical Journal International*, v. 177, p. 834-848.
- Harland, W.B., Cox, A., Llewellyn, P.G., Pickton, C.A.G., Smith, A.G., Walters, R., 1982, *A Geologic Time Scale*: Cambridge University Press, New York, 131 p.
- Helz, R.T., 1973, Phase relations of basalts in their melting range at $\text{PH}_2\text{O} = 5$ kb as a function of oxygen fugacity: Part I: Mafic phases: *Journal of Petrology*, v. 14, part 2, p. 249-302.
- Helz, R.T., 1978, The petrogenesis of the Ice Harbor Member, Columbia Plateau, Washington: A chemical and experimental study [Ph.D. thesis]: State College, Pennsylvania, The Pennsylvania State University, 284 p.
- Heunemann, C.D., Krasa, D., Soffel, H.C., Gurevitch, E., Bachtadse, V., 2004, Directions and intensities of the Earth's magnetic field during a reversal: results from the Permo-Triassic Siberian Trap Basalts, Russia: *Earth and Planetary Science Letters*, v. 218, p. 197-213.
- Hooper, P.R., 2000, Chemical discrimination of Columbia River basalt flows: *Geochemistry Geophysics Geosystems*, v. 1, p. 1-14.
- Hooper, P.R., Binger, G.B., Lees, K.R., 2002, Ages of the Steens and Columbia River flood basalts and their relationship to the extension-related calc-alkaline volcanism in eastern Oregon: *Geological Society of America Bulletin*, v. 114, p. 43-50.
- Hooper, P.R., Conrey, R. M., 1989, A model for the tectonic setting of the Columbia River Basalt eruptions, *in* Reidel, S.P., Hooper, P.R., editors, *Volcanism and tectonism in the Columbia River flood-basalt province*: Geological Society of America Special Paper v. 239, p. 293-306.
- Hooper, P.R., Steele, W.K., Conrey, R.M., Smith, G.A., Anderson, J.L., Bailey, D.G., Beeson, M.H., Tolan, T.L., Urbanczyk, K.M., 1993, The Prineville basalt, north-central Oregon: *Oregon Geology*, v. 55, p. 3-12.
- Jarboe, N.A., Coe, R.S., Renne, P.R., Glen, J.M.G., Mankinen, E.A., 2008, Quickly erupted volcanic sections of the Steens Basalt, Columbia River Basalt Group: Secular variation, tectonic rotation, and the Steens Mountain reversal: *Geochemistry Geophysics Geosystems*, v. 9, p. 1-24.

- Johnson, C.L., Constable, C.G., Tauxe, L., Barendregt, R., Brown, L.L., Coe, R.S., Layer, P., Mejia, V., Opdyke, N.D., Singer, B.S., H, Staudigel, H., Stone, D.B., 2008, Recent investigations of the 0-5 Ma geomagnetic field recorded by lava flows: *Geochemistry Geophysics Geosystems*, v. 9, p. 1-31.
- Kirschvink, J.L., 1980, The least squares line and plane and the analysis of paleomagnetic data: *Geophysical Journal of the Royal Astronomical Society*, v. 62, p. 699-718.
- Long, P.E., Duncan, R.A., anonymous, 1983, Preview $^{40}\text{Ar}/^{39}\text{Ar}$ ages of Columbia River Basalts from deep boreholes in south-central Washington (abstract): *Earth and Ocean Science Transactions, American Geophysical Union*, v. 64, no. 9, p. 97.
- Magill, J.R., Wells, R.E., Simpson, R.W., Cox, A.V., 1982, Post 12 m.y. rotation of southwest Washington: *Journal of Geophysical Research*, v. 87, p. 3,761-3,776.
- Mangan, M.T., Wright, T.L., Swanson, D.A., Byerly, G.R., 1986, Regional correlation of Grande Ronde Basalt flows, Columbia River Basalt Group, Washington, Oregon, and Idaho: *Geological Society of America Bulletin*, v. 97, p. 1,300-1,318.
- Mayergoyz, I.D., 1986, Mathematical models of hysteresis: *IEEE Transactions on Magnetics*, v. 22, p. 603-608.
- McDougall, I., 1976, Geochemistry and origin of basalt of the Columbia River group, Oregon and Washington: *Geological Society of America Bulletin*, v. 87, p. 777-792.
- McElhinny, M.W., 1964, Statistical Significance of the Fold Test in Palaeomagnetism: *Geophysical Journal of the Royal Astronomical Society*, v. 8, p. 338-340.
- McElhinny, M.W., McFadden, P.L., 1997, Palaeosecular variation over the past 5 Myr based on a new generalized database: *Geophysical Journal International*, v. 131, p. 240-252.
- McFadden, P.L., and M.W. McElhinny, 1988, The combined analysis of remagnetization circles and direct observations in paleomagnetism: *Earth and Planetary Science Letters*, v. 87, p. 161-172.
- McKee, E.H., Hooper, P.R., Kleck, W.D., 1981, Age of Imnaha basalt-Oldest flows of the Columbia River Basalt Group, Northwest United States: *ISO Chron/West*, v. 31, p. 31-33.
- McKee, E.H., Swanson, D.A. and Wright, T.L., 1977, Duration and volume of Columbia River basalt volcanism; Washington, Oregon, and Idaho: *Geological Society of America Abstracts with Programs*, v. 9, p. 463.
- Merrill, R.T., McElhinny, M.W., and McFadden, P.L., 1996. *The magnetic field of the Earth: Paleomagnetism the Core and the Deep Mantle: International Geophysics Series*, Academic Press, San Diego, p. 527.
- Mössbauer, R.L., 1958a, Kernresonanzfluoreszenz von Gammastrahlung in ^{191}Ir : *Zeitschrift für Physik A*, v. 151, p. 124-143.

- Mössbauer, R.L., 1958b, Kernresonanzabsorption von Gammastrahlung in ^{191}Ir : Naturwissenschaften v. 45, p. 538-539.
- Olson, P.L., Coe, R.S., Driscoll, P.E., Glatzmaier, G.A., Roberts, P.H., 2010, Geodynamo Reversal Frequency and Heterogeneous Core-Mantle Boundary Heat Flow: Physics of the Earth and Planetary Interiors, v. 180, p. 66-79.
- Plenier, G., Camps, P., Henry, B., Nicolaysen, K., 2002, Palaeomagnetic study of Oligocene (24-30 Ma) lava flows from the Kerguelen Archipelago (southern Indian Ocean): directional analysis and magnetostratigraphy: Physics of the Earth and Planetary Interiors, v. 133, p. 127-146.
- Reidel, S.P., 1978, Stratigraphy and petrogenesis of the Grande Ronde Basalt in the lower Salmon and adjacent Snake River Canyons [Ph.D. thesis]: Pullman, Washington, Washington State University, 415 p.
- Reidel, S.P., 1983, Stratigraphy and petrogenesis of the Grande Ronde Basalt from the deep canyon country of Washington, Oregon and Idaho: Geological Society of America Bulletin, v. 94, p. 519-542.
- Reidel, S.P., Fetch, K.R., Cross, R.W., 1982, Constraints on tectonic models for the Columbia Plateau from the age and growth rates of Yakima folds (abstract): Earth and Ocean Science Transactions, American Geophysical Union, v. 64, p. 87.
- Reidel, S.P., Hooper, P.R., Webster, G.D., Camp, V.E., 1992, Geologic Map of Southeastern Asotin County, Washington: Washington Division of Geology and Earth Resources, 24 p.
- Reidel, S.P., Long, P.E., Myers, C.W., Mase, J., 1981, New evidence for greater than 3.2 kilometers of Columbia River basalt beneath central Columbia Plateau (abstract): Earth and Ocean Science Transactions, American Geophysical Union, v. 63, p. 173.
- Reidel, S.P., Martin, B.S., Petcovic, H.L., 2003, The Columbia River flood basalts and the Yakima fold belt: *in* Swanson, T.W., ed., Western Cordillera and adjacent areas: Boulder, Colorado: Geological Society of America Field Guide 4, p. 87-105.
- Reidel, S.P., Scott, G.R., Bazard, D.R., Cross, R.W., Dick, B., 1984, Post-12 million year clockwise rotation in the central Columbia Plateau, Washington: Tectonics, v. 3(2), p. 251-273.
- Reidel, S.P., Tolan, T.L., Hooper, P.R., Beeson, M.H., Fecht, K.R., Bentley, R.D., Anderson, J.L., 1989, The Grande Ronde Basalt, Columbia River Basalt Group: Stratigraphic descriptions and correlations in Washington, Oregon, and Idaho, *in* Reidel, S.P., Hooper, P.R., eds., Volcanism and Tectonism in the Columbia River Flood-Basalt Province: Geological Society of America Special Paper, v. 239, p. 21-53.
- Rietman, J.D., 1966, Remanent magnetization of the late Yakima Basalt, Washington State: Ph.D. Dissertation, Stanford University, Stanford, CA, 87 p.
- Riisager, P., Knight, K., Baker, J., Peate, I., Al-Kadasi, M., Al-Subbary, A., Renne, P., 2005, Paleomagnetism and $^{40}\text{Ar}/^{39}\text{Ar}$ geochronology of Yemeni Oligocene volcanics: implications

- for timing and duration of Afro-Arabian traps and geometry of the Oligocene paleomagnetic field: *Earth and Planetary Science Letters*, v. 237, p. 647-672.
- Riisager, P., Riisager, J., Abrahamsen, N., Waagstein, R., 2002, Thellier palaeointensity experiments on Faroes flood basalts: technical aspects and geomagnetic implications: *Physics of the Earth and Planetary Interiors*, v. 131 (2), p. 91-100.
- Sheriff, S.D., 1984, Paleomagnetic evidence for spatially distributed post-Miocene rotation of western Washington and Oregon: *Tectonics*, v. 3, p. 397-408.
- Sheriff, S.D., and Bentley, R.D., 1980, Anomalous paleomagnetic directions from the Miocene Wanapum Basalt, Washington and Oregon (abstract): *Earth and Ocean Science Transactions, American Geophysical Union*, v. 62, p. 949.
- Simpson, R.W., Magill, J.R., Wells, R.E., Cox, A.V., 1980, Post 12 m.y. rotation in southwest Washington (abstract): *Earth and Ocean Science Transactions, American Geophysical Union*, v. 61, p. 1980.
- Swanson, D.A., Wright, T.L., 1981, The regional approach to studying the Columbia River basalt, *in* Subbarao, K.V. and Sukheswala, R.N., edsitors, *Deccan volcanism and related basalt provinces in other parts of the world: Geological Society of India Memoir*, v. 3, p. 58-80.
- Swanson, D.A., Anderson, J.L., Bentley, R.D., Byerly, G.R., Camp, V.E., Gardner, J.N., Wright, T.L., 1979a, Reconnaissance geologic map of the Columbia River Basalt Group in parts of eastern Washington and northern Idaho: U.S. Geological Survey Open-File Report 79-1363, scale 1:250,000, 12 sheets.
- Swanson, D.A., Wright, T.L., Hooper, P.R., and Bentley, R.D., 1979b, Revisions in stratigraphic nomenclature of the Columbia River Basalt Group, U.S.: *Geological Survey Bulletin* 1475-G, 59 p.
- Swanson-Hysell, N.L., Maloof, A.C., Weiss, B.P., Evans, D.A.D., 2009, No asymmetry in geomagnetic reversals recorded by 1.1-billion-year-old Keweenawan basalts: *Nature Geoscience*, v. 2, p. 713-717.
- Takahashi, E., Nakajima, K., Wright, T.L., 1998, Origin of the Columbia River basalts: Melting model of heterogeneous plume head: *Earth and Planetary Science Letters*, v. 162, p. 63-80.
- Tauxe, L., 2008, *Essentials of Rock and Paleomagnetism*: Scripps Institution of Oceanography, 526 p.
- Tauxe, L., 2005, Inclination flattening and the geocentric axial dipole hypothesis: *Earth and Planetary Science Letters*, v. 233, p. 247-261.
- Tauxe, L., Kent, D.V., 2004, A Simplified Statistical Model for the Geomagnetic Field and the Detection of Shallow Bias in Paleomagnetic Inclinations: Was the Ancient Magnetic Field Dipolar?: *Timescales of the Paleomagnetic Field: American Geophysical Union Geophysical Monograph Series*, v. 145, p. 101-115.

- Tauxe, L., Kodama, K.P., 2009, Paleosecular variation models for ancient times: Clues from Keweenawan lava flows: *Physics of the Earth and Planetary Interiors*, v. 177, p. 31-45.
- Tauxe, L., Kodama, K.P., Kent, D.V., 2008. Testing corrections for paleomagnetic inclination error in sedimentary rocks: a comparative approach: *Physics of the Earth and Planetary Interiors*, v. 169, p. 152-165.
- Tolan, T. L, Martin, B.S., Reidel, S.P., Anderson, J.L., Lindsey, K.A., Burt, W., 2009, An Introduction to the stratigraphy, structural geology, and hydrogeology of the Columbia River Flood-Basalt Province: A primer for the GSA Columbia River Basalt trips: *The Geological Society of America Field Guide*, v. 15, p. 599-643.
- Tolan, T.L, Reidel, S.P., Beeson, M.H., Anderson, J.L., Fecht, K.R., and Swanson, D.A., 1989, Revisions to the estimates of the areal extent and volume of the Columbia River Basalt Group, *in* Reidel, S.P., and Hooper, P.R., eds., *Volcanism and Tectonism in the Columbia River Flood-Basalt Province: Geological Society of America Special Paper*, v. 239, p. 1-20.
- Van Alstine, D.R., Gillett, S.L., 1981, Magnetostratigraphy of the Columbia River Basalt, Pasco Basin and Vicinity, Washington: Rockwell Hanford Operations Report, RHO-BWI-C-110, 57 p.
- Vandamme, D., 1994, A new method to determine paleosecular variation: *Physics of the Earth and Planetary Interiors*, v. 85, p. 131-142.
- Vandamme, D., Courtillot, V., Besse, J., Montigny, R., 1991. Palaeomagnetism and age determination of the Deccan traps (India): results of the Napur-Bombay traverse and review of earlier work. *Reviews of Geophysics*, v. 29, p. 159-190.
- Vandamme, D., Courtillot, V., 1992. Paleomagnetic constraints on the structure of the Deccan traps: *Physics of the Earth and Planetary Interiors*, v. 74, p. 241–261.
- Van der Voo, R., 1990, The reliability of paleomagnetic data: *Tectonophysics*, v. 184, p. 1-9.
- Waters, A.C., 1961, Stratigraphic and lithologic variations in the Columbia River basalt: *American Journal of Science*, v. 259, p. 583-611.
- Watkins, N.D., Baksi, A.K., 1974, Magnetostratigraphy and oroclinal folding of the Columbia River, Steens and Owyhee basalts in Oregon, Washington and Idaho: *American Journal of Science*, v. 274, p. 148-149.
- Wells, R.E., Simpson, R.W., Bentley, R.D., Beeson, M.H., Mangan, M.T., Wright, T.L., 1989, Correlation of Miocene flows of the Columbia River Basalt Group from the central Columbia River Plateau to the coast of Oregon and Washington: *Geological Society of America Special Paper*, v. 239, p. 13-129
- Wright, T.L., Helz, R.T., 1981, Generation of tholeiitic basalt: A comparative study of three intraplate provinces, *in* Subbarao, K.V., and Sukheswala, R.N., edsitors, *Deccan volcanism and related basalt provinces in other parts of the world: Geological Society of India Memoir*, v. 3, p. 419-421.

- Wright, T.L., Mangan, M., Swanson, D.A., 1988, Chemical data for flows and feeder dikes of the Yakima Basalt subgroup, Columbia River Basalt Group, Washington, Oregon and Idaho, and their bearing on a petrogenic model: United States Geological Survey Bulletin, v. 1821, 71 p.
- Wright, T.L., Swanson, D.A., Fruchter, J.S., 1976, Petrogenesis of Yakima Basalt in southeastern Washington: Geological Society of America Abstracts with Programs, v. 8, p. 422.
- Yaxley, G.M., 2000, Experimental study of the phase and melting relations of homogeneous basalt + peridotite mixtures and implications for the petrogenesis of flood basalts: Contributions to Mineralogy and Petrology, v. 139, p. 326-338.
- Zijderveld, J.D.A., 1967, A.C. demagnetization of rocks: Methods in Palaeomagnetism, Collinson, D.W., Creer, K.M., Runcorn, S.K. editors, p. 256-286, Elsevier, New York.

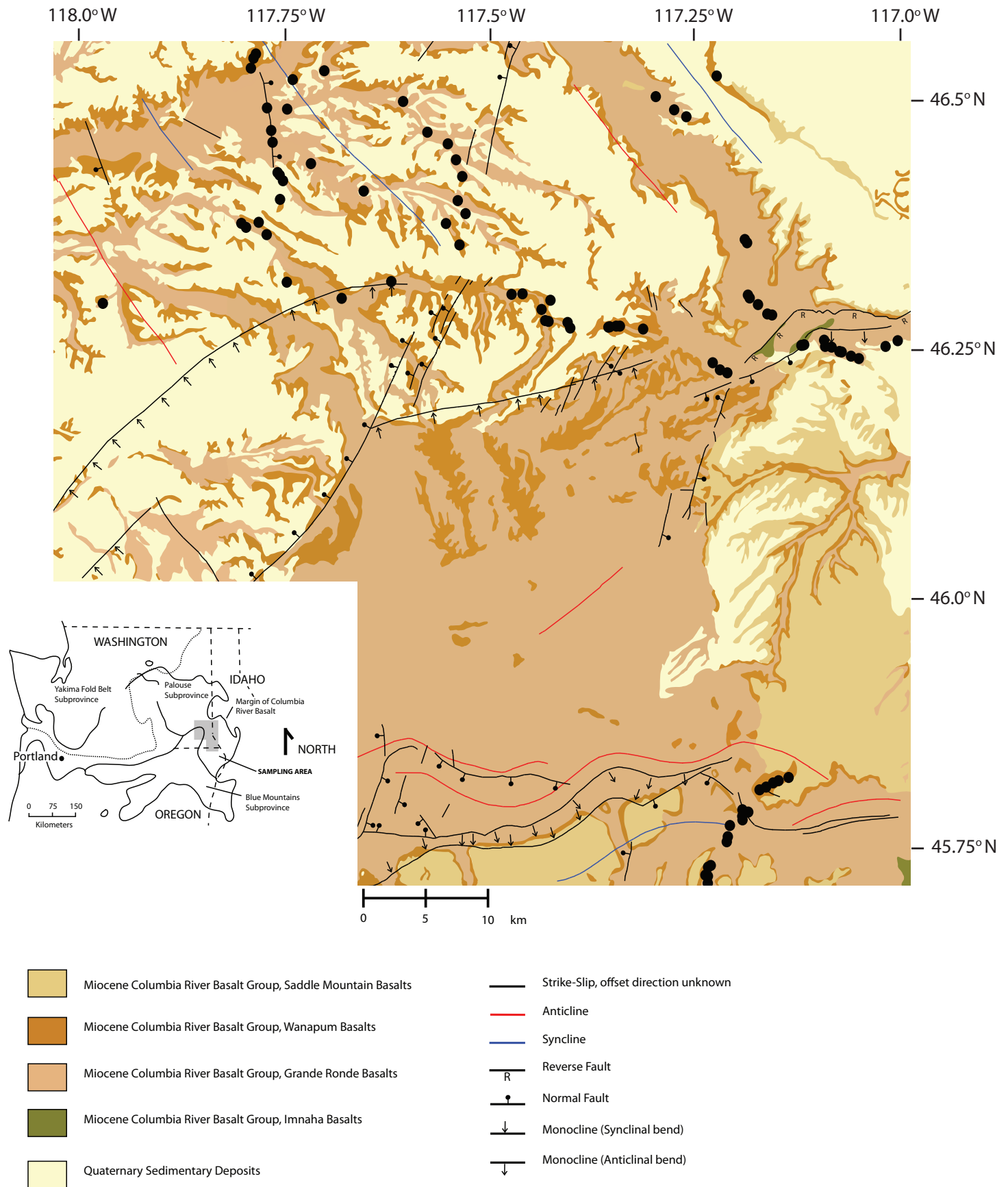


Figure 1: Map of the sampled region, differentiated by basalt stratigraphy. The black circles indicate the sampled sites. The inset on the lower left shows the location of the sampled area (Adapted from Hooper (2000), and the Washington Interactive Geologic Map [<https://fortress.wa.gov/dnr/geology/>]).

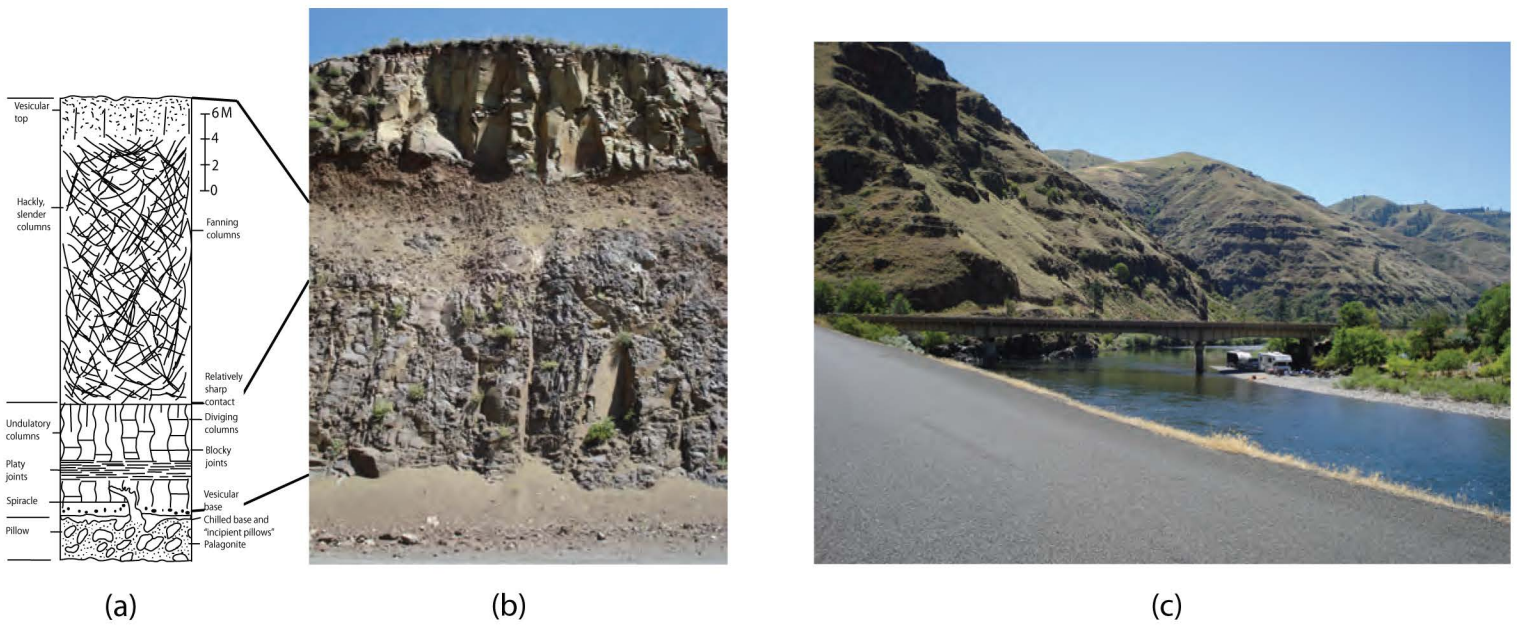
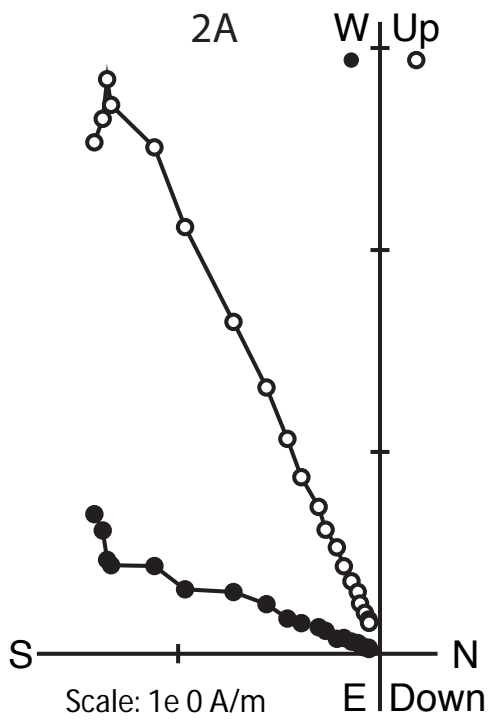
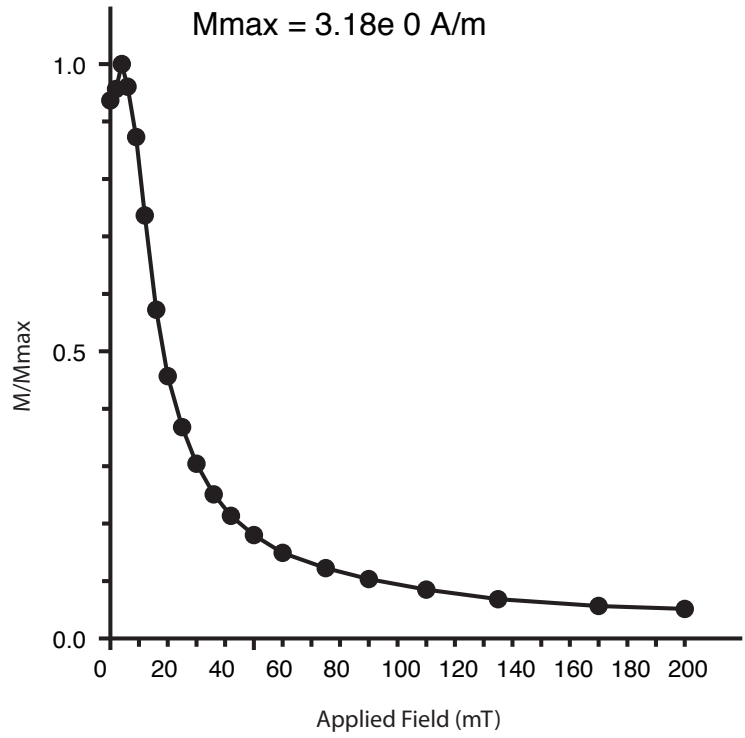


Figure 2: Visual representation of the Columbia River Basalt flows, showing (a) a schematic cross-section of an individual flow, (b) a field photograph of an individual flow showing the characteristics expected for the flows in this region, and (c) horizontal flows near a bridge over the Grande Ronde River.



(a)



(b)

Figure 3: Directional characteristics for sample CR2A, showing its (a) Zijderveld diagram with clear univectorial decay, and its (b) intensity diagram with a smooth demagnetization pattern for an alternating field treatment sequence.

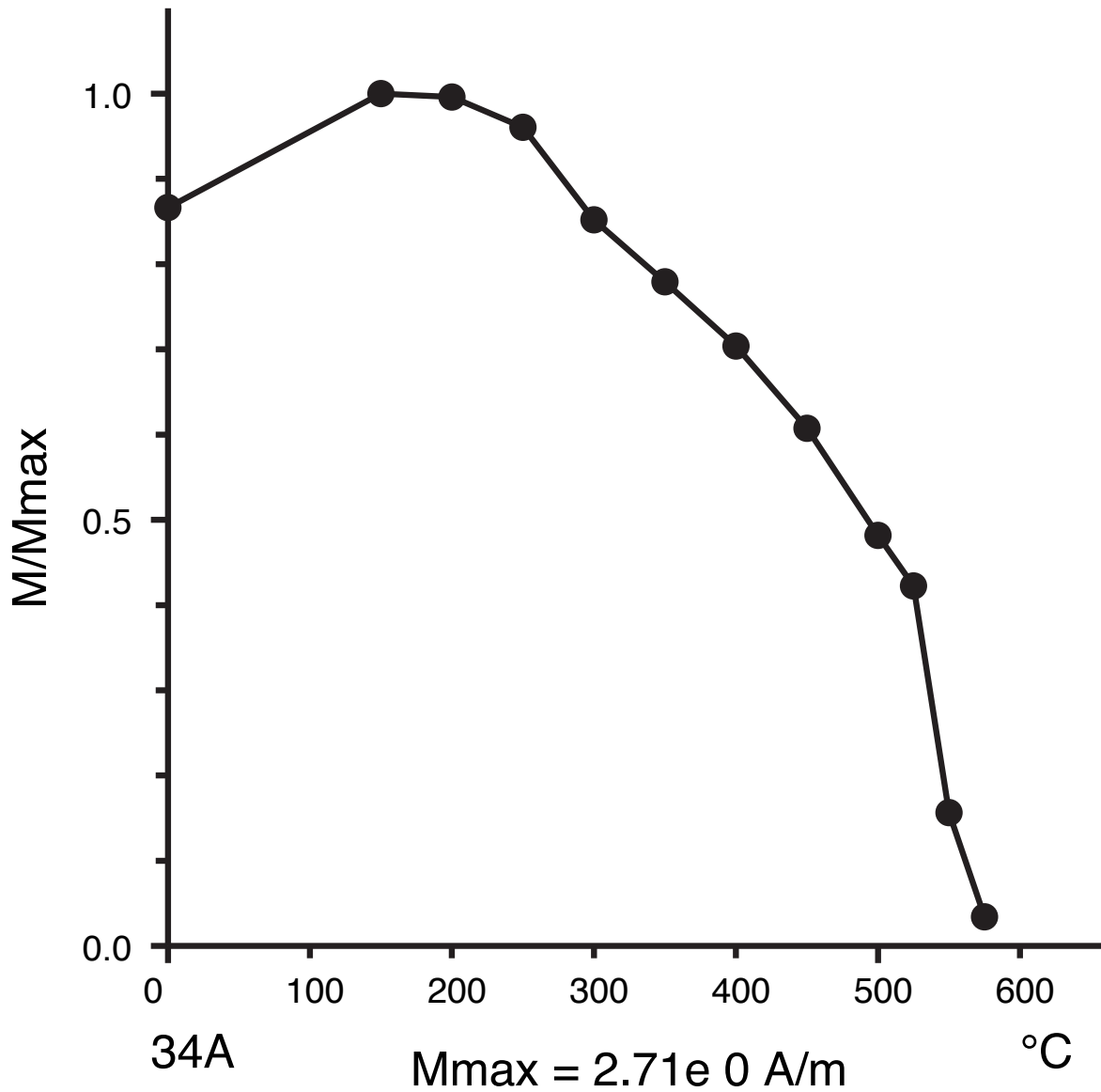
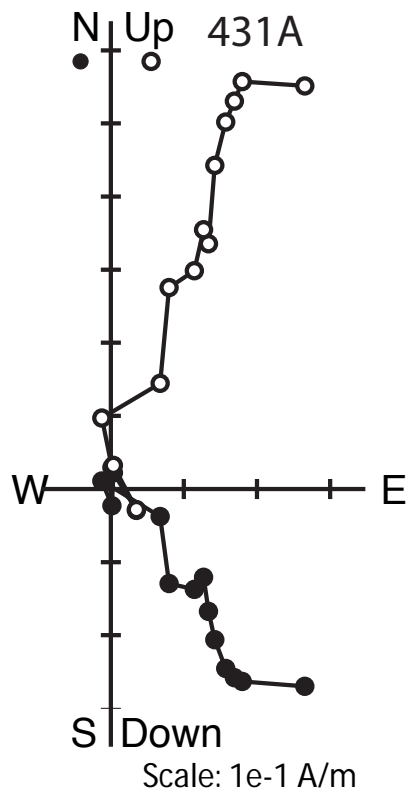
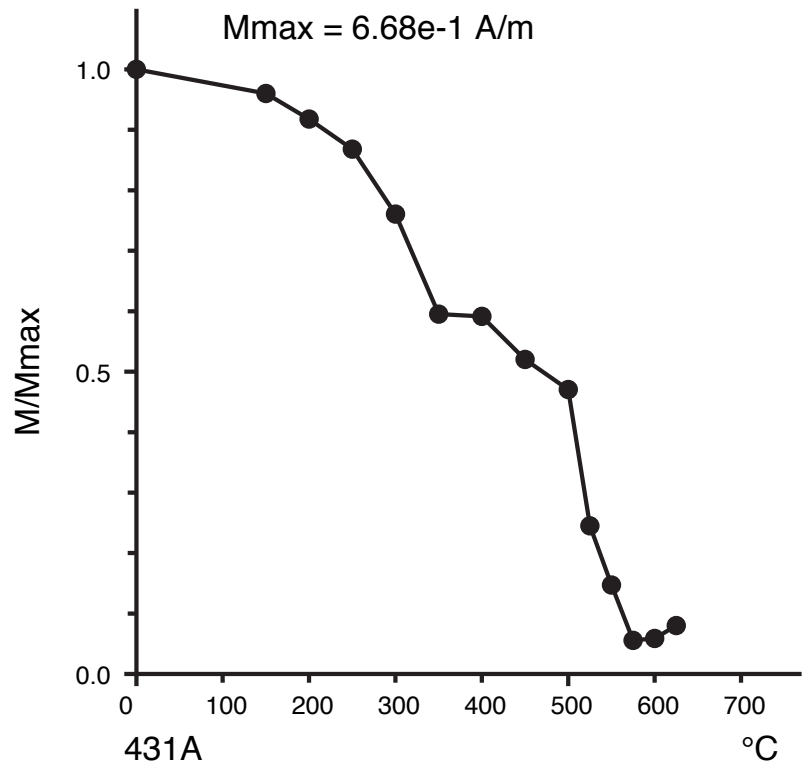


Figure 4: Intensity diagram for sample CR34A, showing decay at a Curie temperature of 580° Celsius, indicating the presence of low-titanium magnetite.

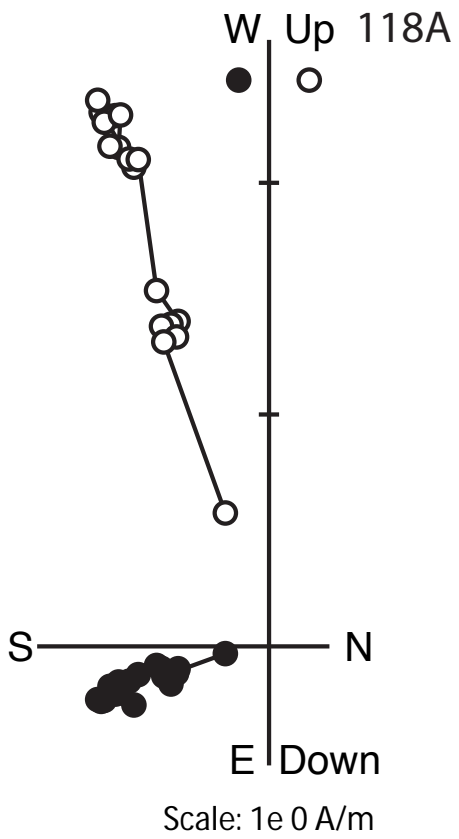


(a)

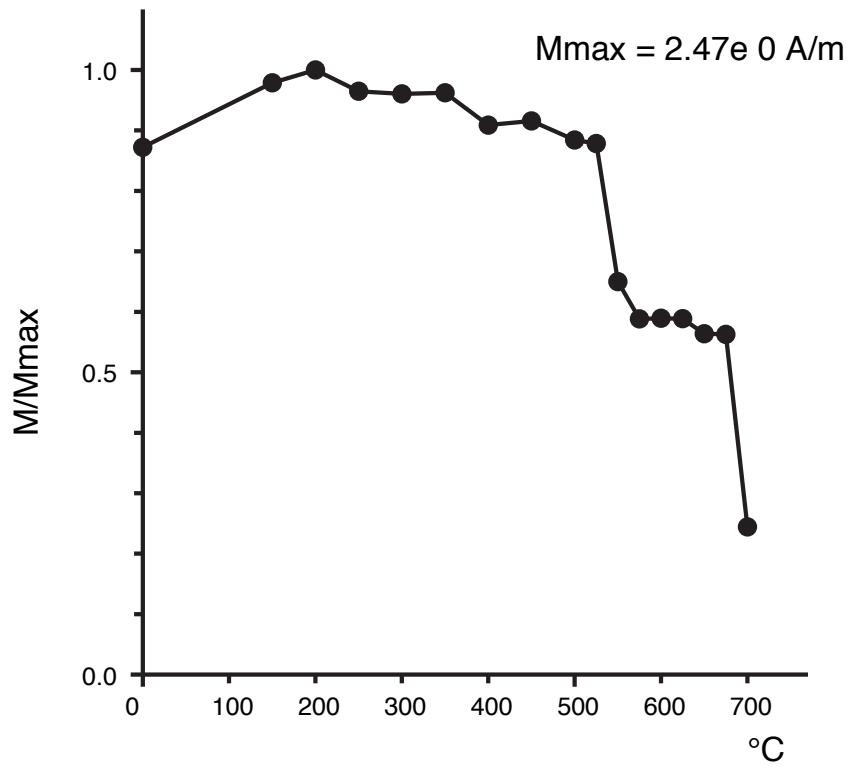


(b)

Figure 5: Demagnetization information for sample CR431A, showing its (a) Zijderveld diagram, indicating a difference in direction between lower- and higher-temperature components, and (b) corresponding intensity diagram, also indicating decay between 100-350° Celsius due to a lower temperature component, and 580° Celsius, suggesting the presence of low-titanium magnetite.

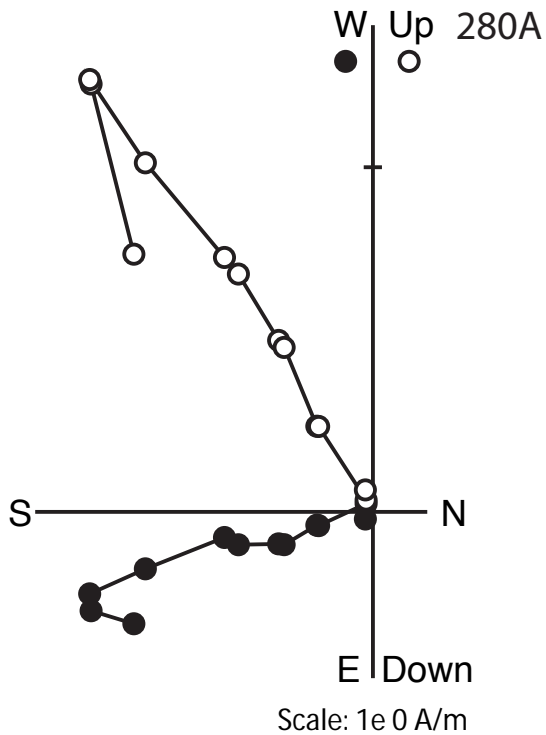


(a)

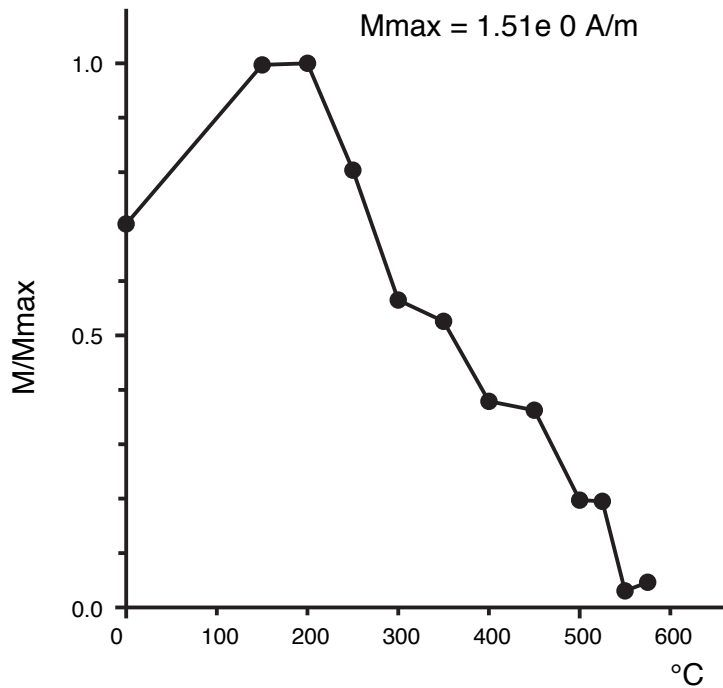


(b)

Figure 6: Demagnetization information for sample CR118A, showing its (a) Zijderveld diagram, indicating a south-southeasterly and up direction, and its (b) intensity diagram, indicating the presence of magnetite as well as uncommon hematite.

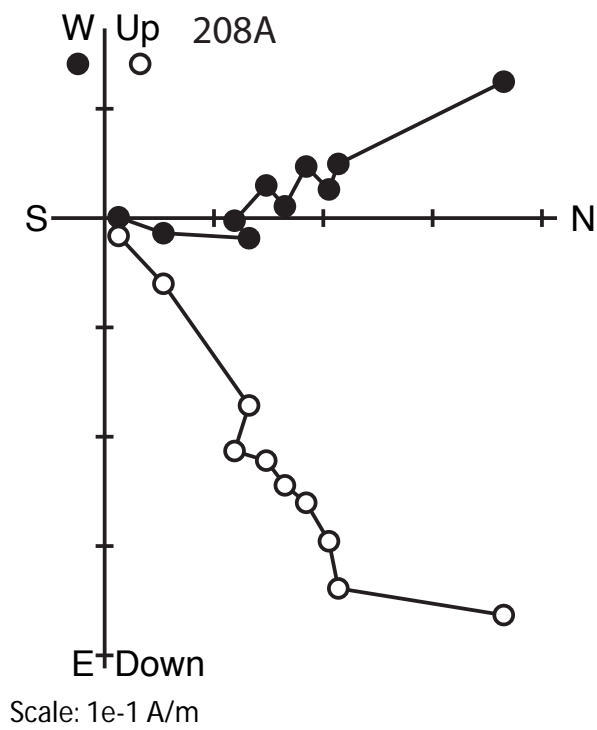


(a)

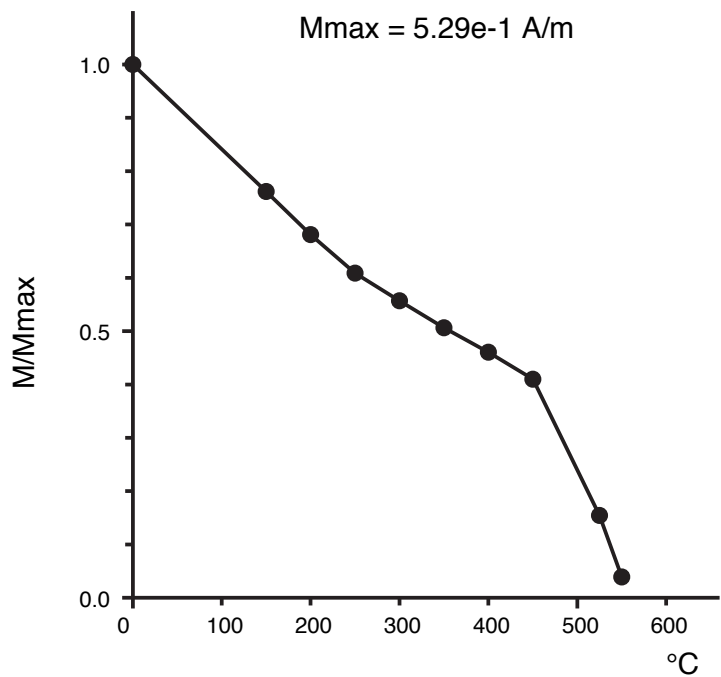


(b)

Figure 7: Demagnetization information for sample CR280A, showing its (a) Zijderveld diagram, indicating an overall southerly and up direction, and its (b) intensity diagram, indicating the presence of magnetite and a lower-temperature component, possibly due to titano-magnetite.

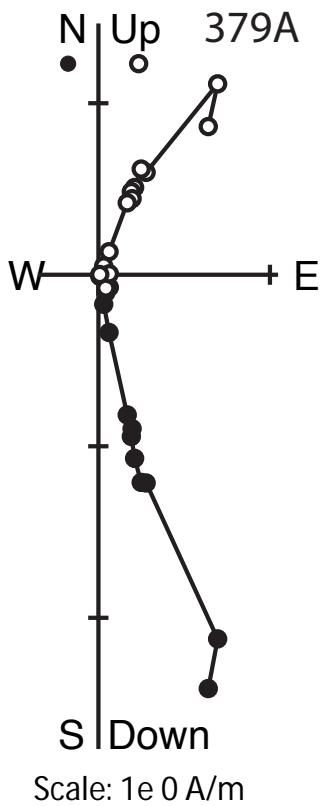


(a)

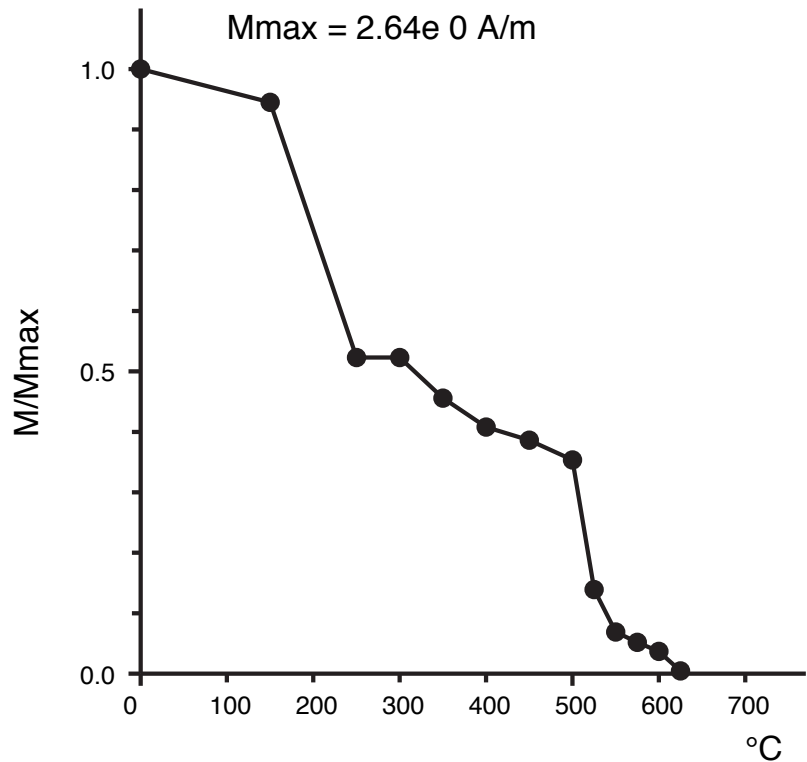


(b)

Figure 8: Demagnetization information for sample CR208A, showing its (a) Zijderveld diagram, indicating an overall northerly and down direction, and its (b) intensity diagram, indicating the presence of magnetite and a less significant lower-temperature component, possibly due to titanomagnetite.

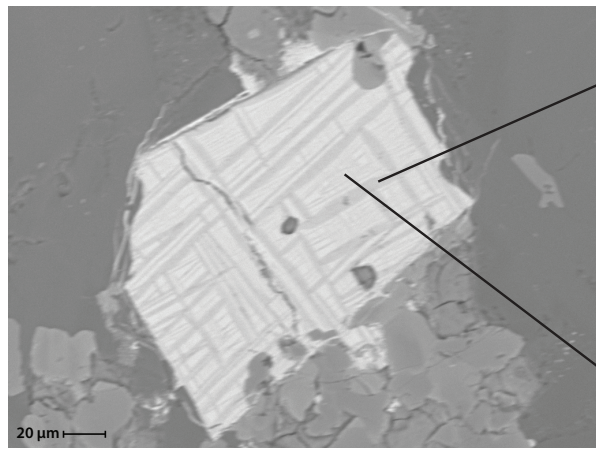


(a)

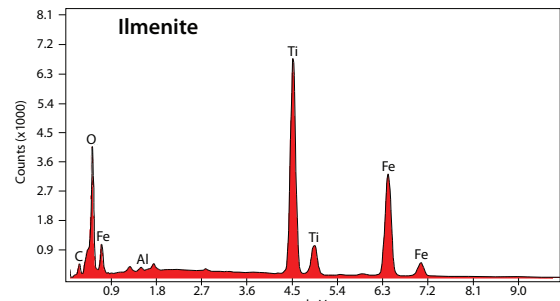


(b)

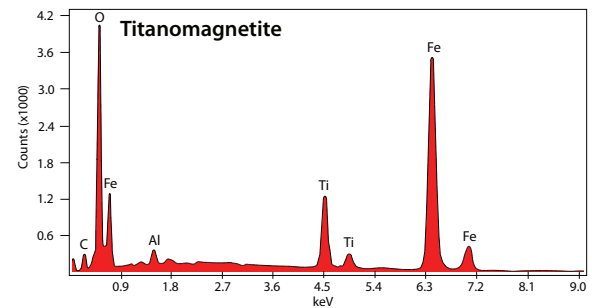
Figure 9: Demagnetization information for sample CR379A, showing its (a) Zijderveld diagram, indicating almost univectorial decay, especially in high temperature, and (b) intensity diagram, showing decay at about 580° Celsius, the unblocking temperature of magnetite, and another small decay above 600° Celsius, possibly indicating the presence of hematite.



(a)



(b)



(c)

Figure 10: Scanning Electron Microscope analysis of sample CR379 (a) with a titanomagnetite grain and its corresponding EDS peaks for the exsolution lamellae. The EDS for the darker lamellae indicates that they are (b) composed of ilmenite, which is not magnetic at room temperature. The lighter lamellae (c) are composed mainly of low-Ti magnetite.

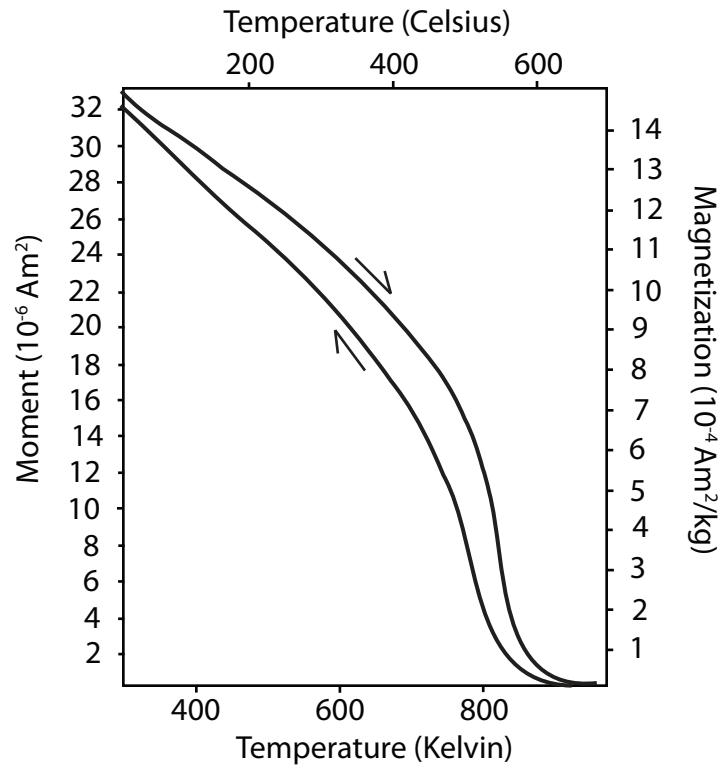


Figure 11: Magnetic susceptibility diagram for sample CR320, indicating the presence of magnetite. The heating and cooling curves are very similar, suggesting that the only magnetic component in this sample is magnetite, and the similarity between the heating and cooling curves represents a reversible, stable behavior.

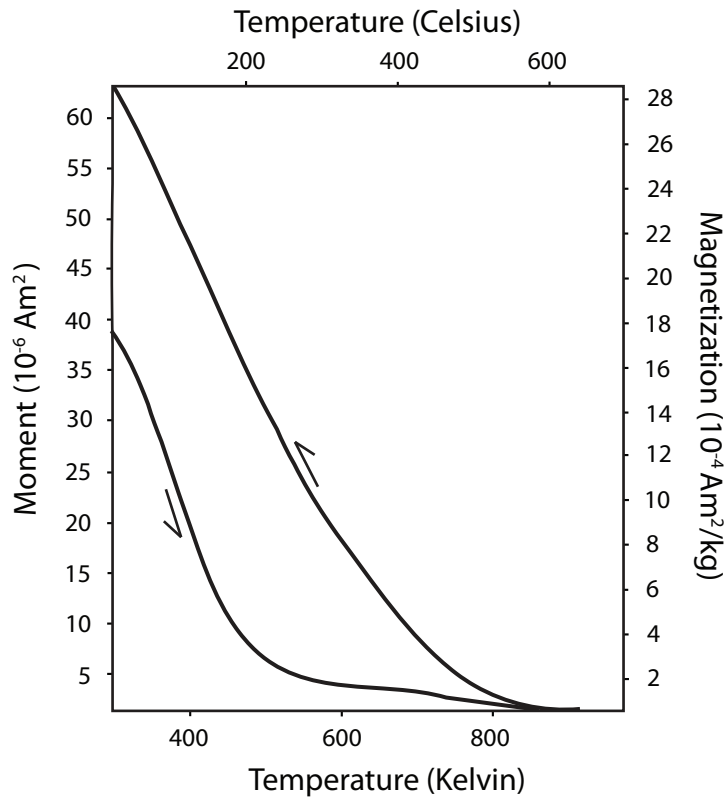


Figure 12: Magnetic susceptibility diagram of sample CR447, showing heating and cooling curves that indicate the presence of a low-temperature component before 200° Celsius and a minor higher temperature component, most likely titano-magnetite. The irreversibility of the curves suggests that the low-temperature component is unstable and easily altered to higher temperature component, possibly magnetite.

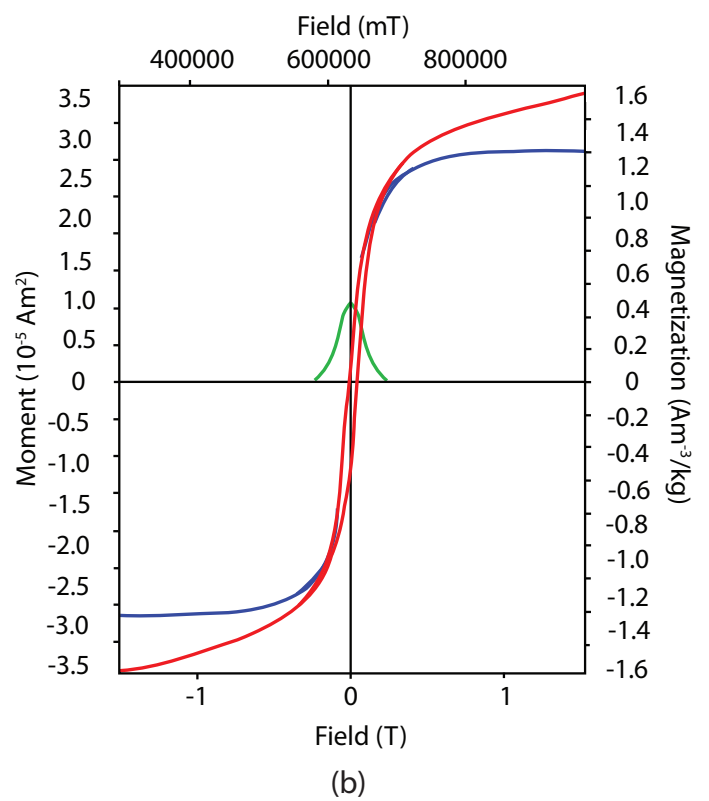
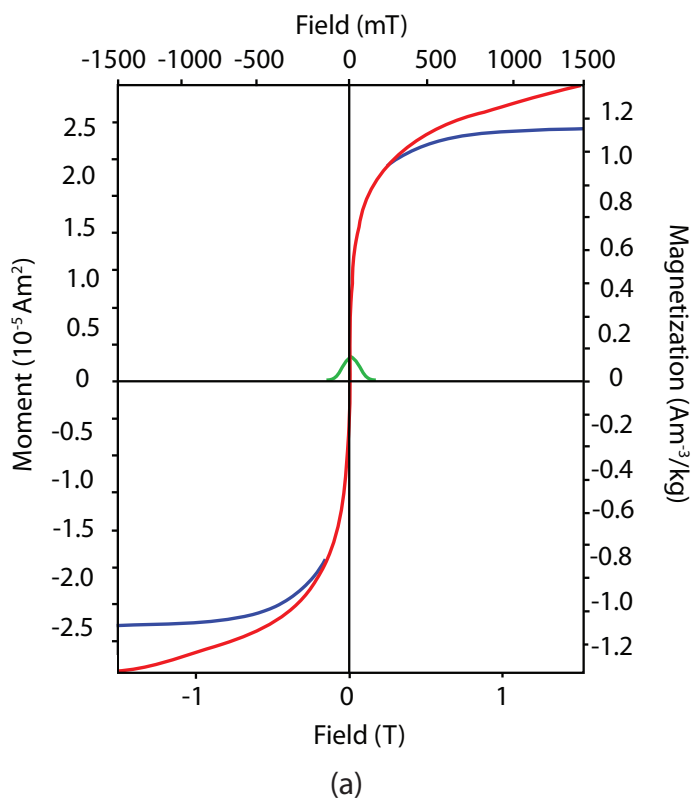


Figure 13: Hysteresis analysis showing (a) the hysteresis loop for sample CR19 at 300 K, showing multidomain behavior, and that of (b) sample CR320 at 300 Kelvin, indicating pseudosingle domain behavior.

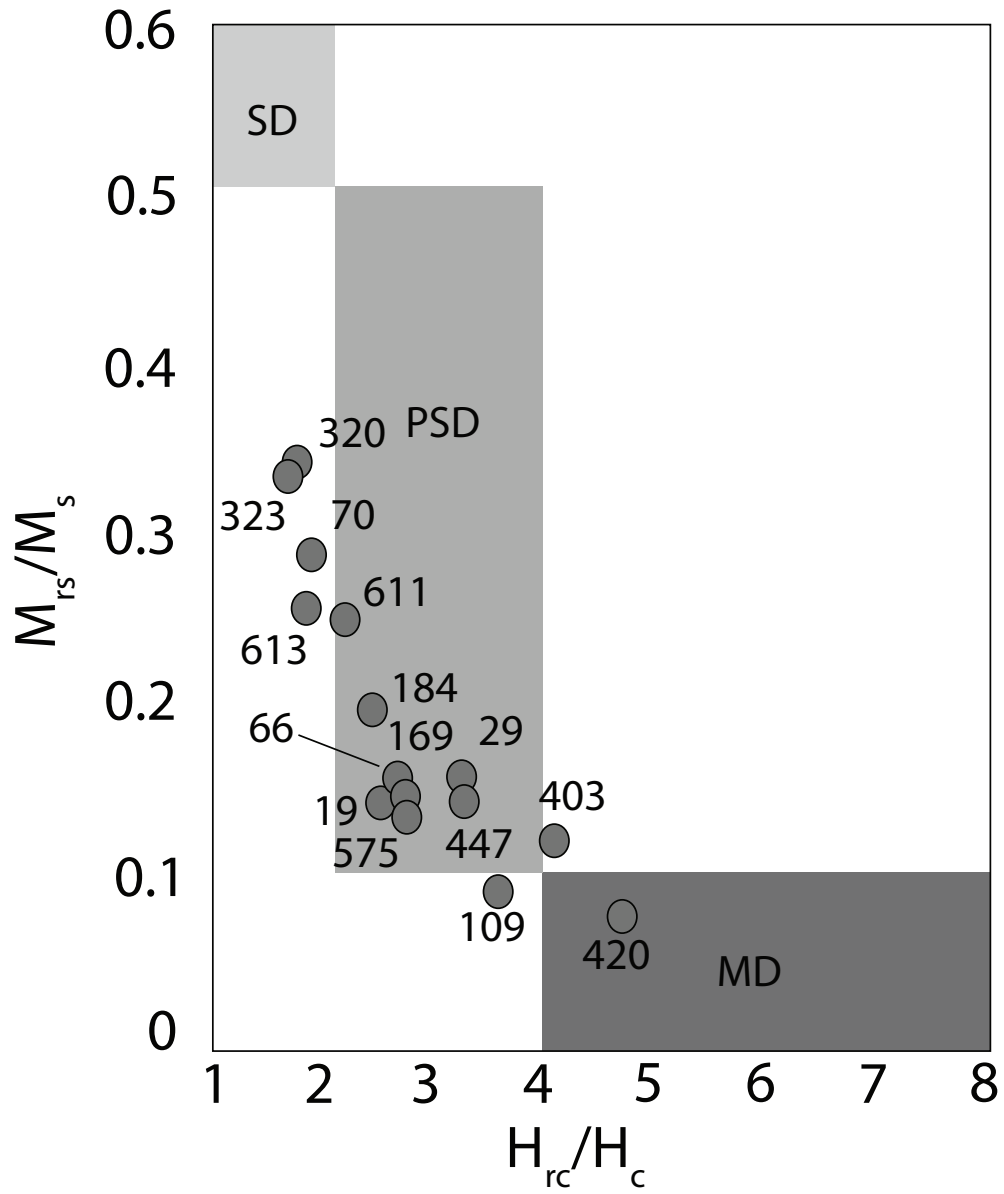


Figure 14: Day plot (*Day et al., 1977*), revealing that the majority of the samples for this study contain pseudosingle domain grains.

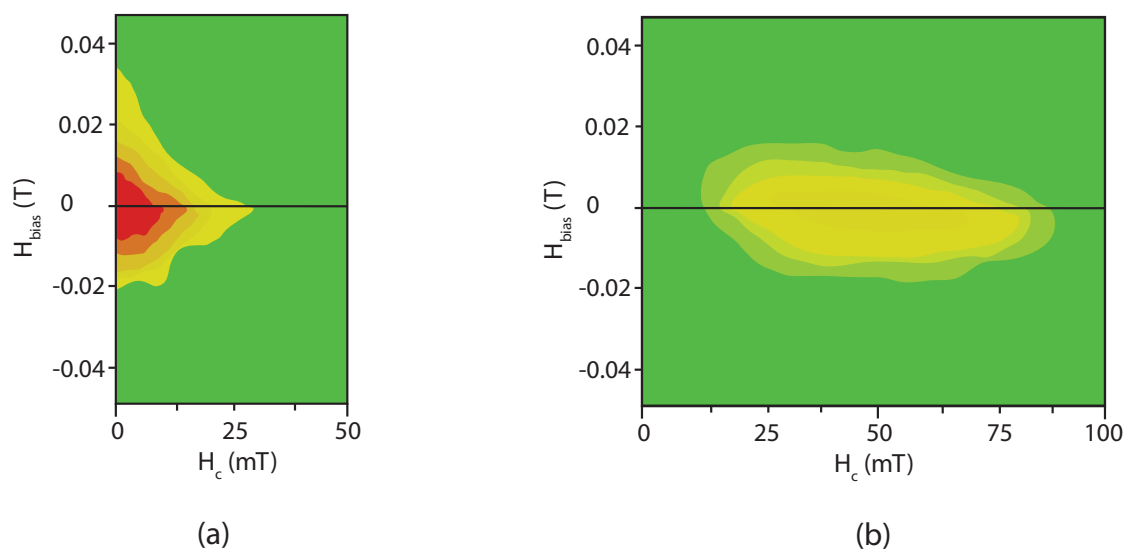


Figure 15: First Order Reversal Curve (FORC) analysis for (a) sample CR19 at 300 Kelvin, indicating pseudosingle domain behavior, and (b) sample CR320 at 300 Kelvin, showing single domain behavior.

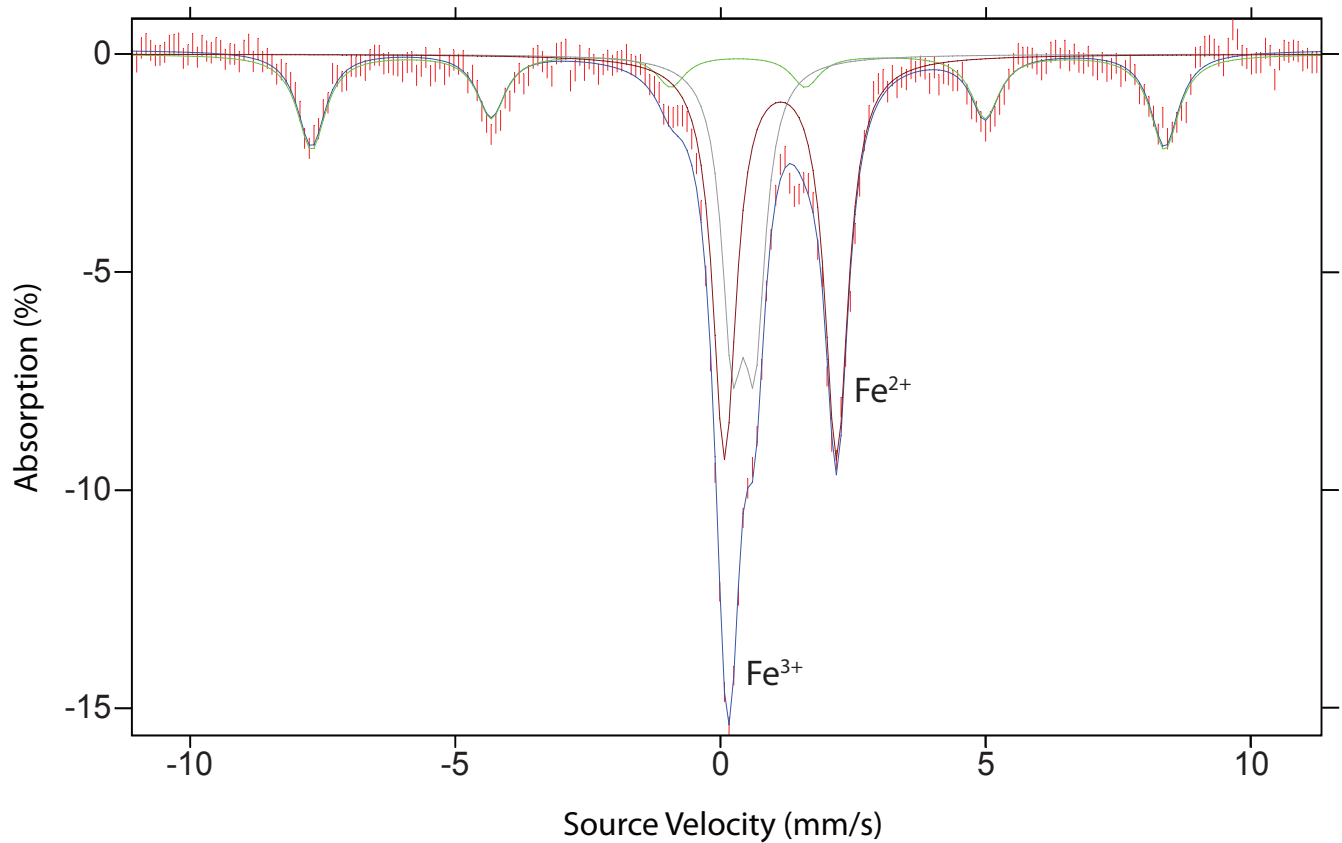


Figure 16: Mössbauer spectroscopy (Mössbauer, 1958a; Mössbauer, 1958b) of sample CR431. The most significant peaks indicate ferrous and ferric iron, both present in magnetite, suggesting that it is the main magnetic mineral in this sample.

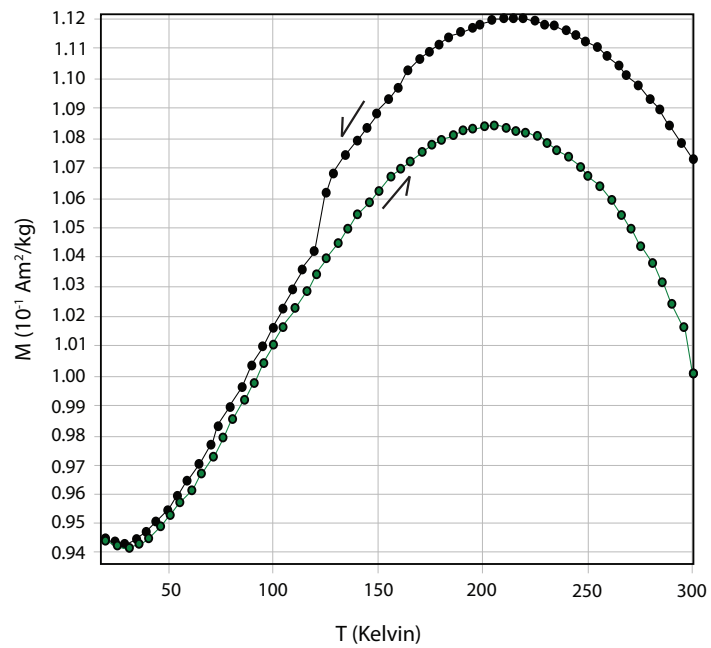


Figure 17: Remanent magnetization intensity upon heating (green curve) and cooling (black curve) of sample CR630, showing a sudden change in remanence at about 125 Kelvin, attributed to the Verwey transition in magnetite.

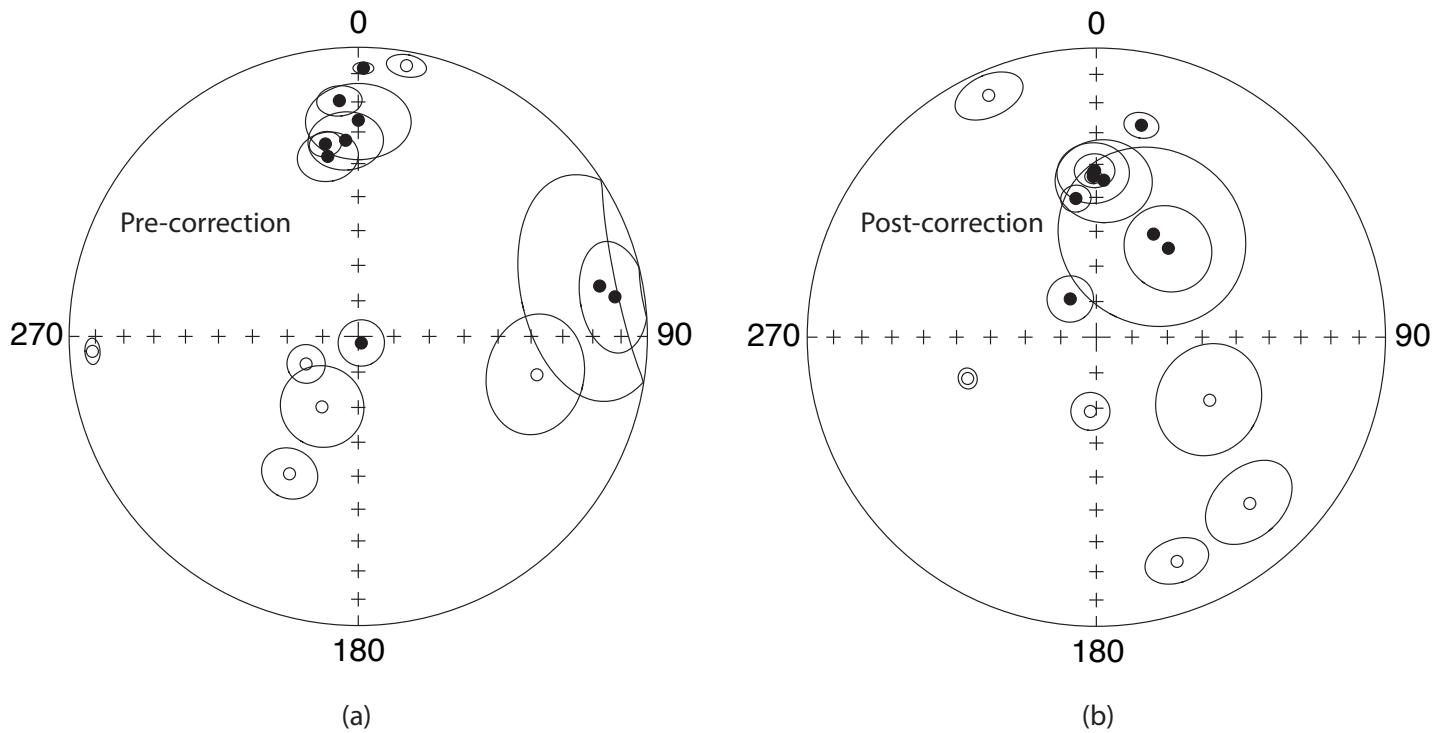


Figure 18: Comparison between directions of tilted sites (a) prior to bedding correction and (b) after bedding correction. The site mean directions after bedding correction are more clustered than those prior to correction, and are more similar to those expected for the Miocene. Despite the large dispersion, the fold test is positive, given that $k_2/k_1=2.06$, which is significant at the 95% confidence level for $N=15$.

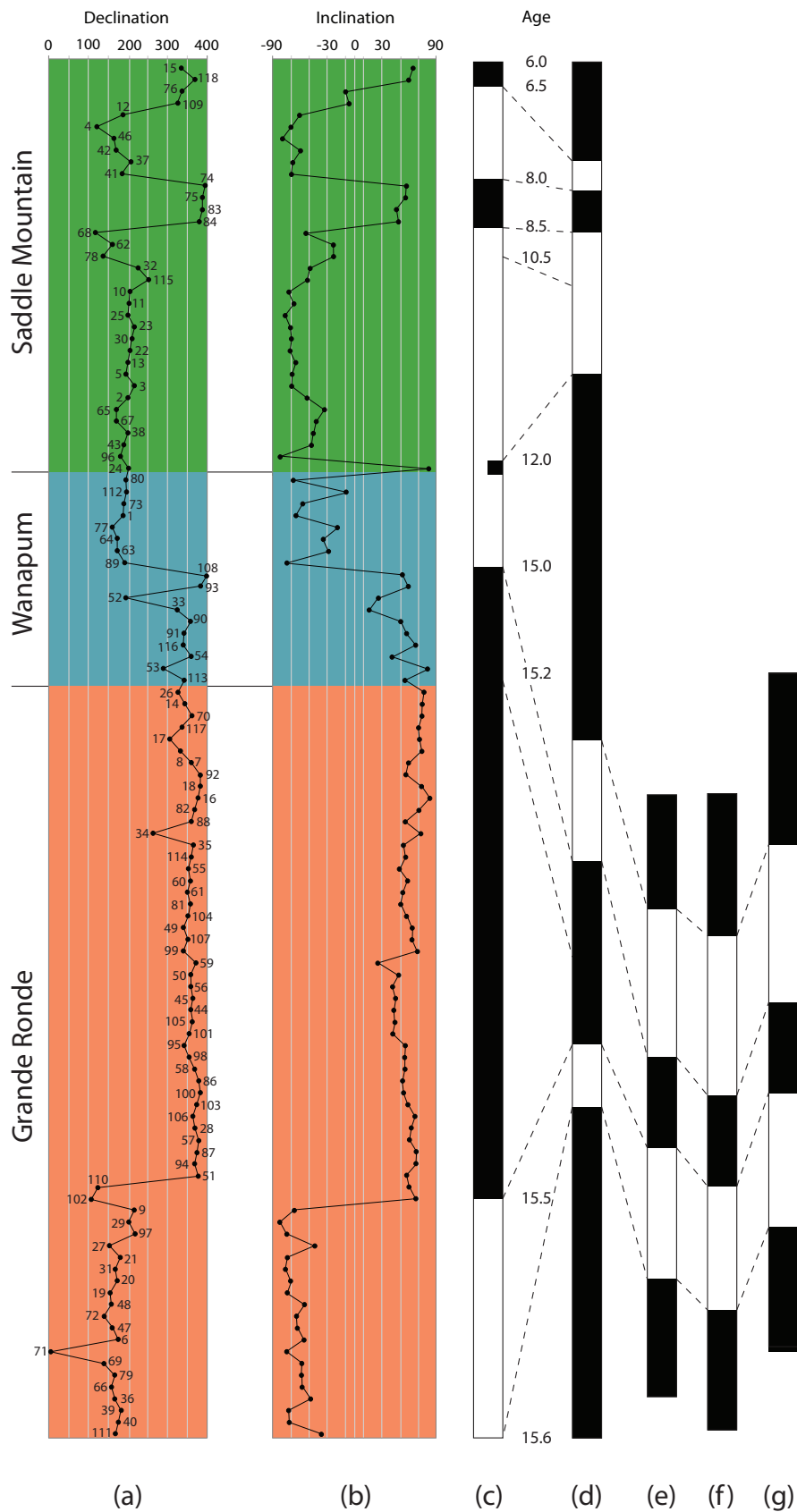


Figure 19: Magnetostratigraphy of the sampled flows for this study showing (a) its declination with corresponding site numbers, and (b) inclination plotted in stratigraphic order of the sites. Site 24 had a steeply down and southwestern direction and was diagnosed as an outlier; its normal polarity is marked as a half-column, indicating its lack of reliability. The polarity of our collection (c) was then compared to the magnetostratigraphic columns from (d) *Reidel et al. (2003)*, (e) *Harland et al. (1982)*, (f) *Berggren et al. (1985)*, and (g) *Baksi (1988)*. The declination and inclination columns are color-coded according to their corresponding formation.

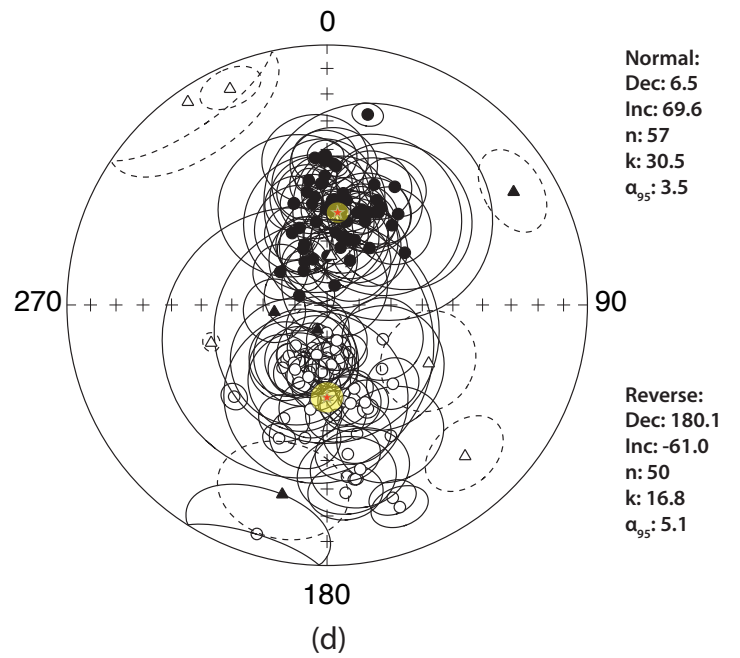
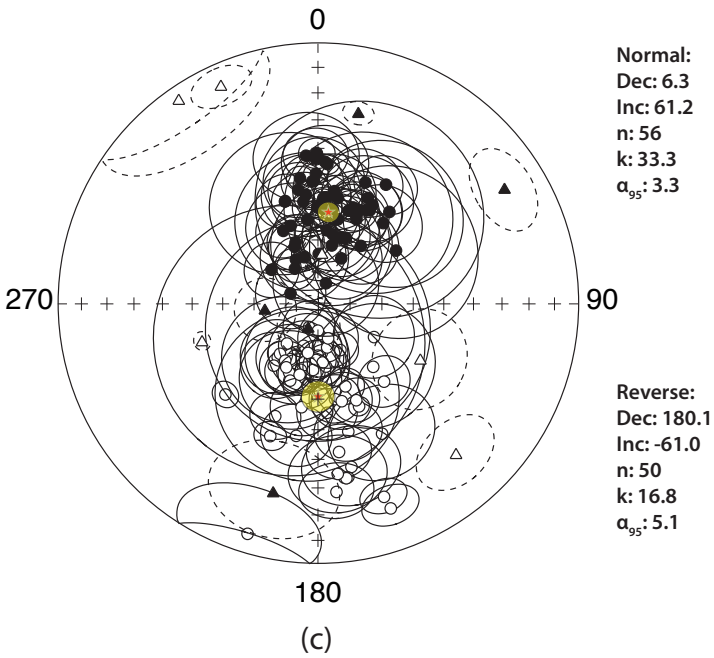
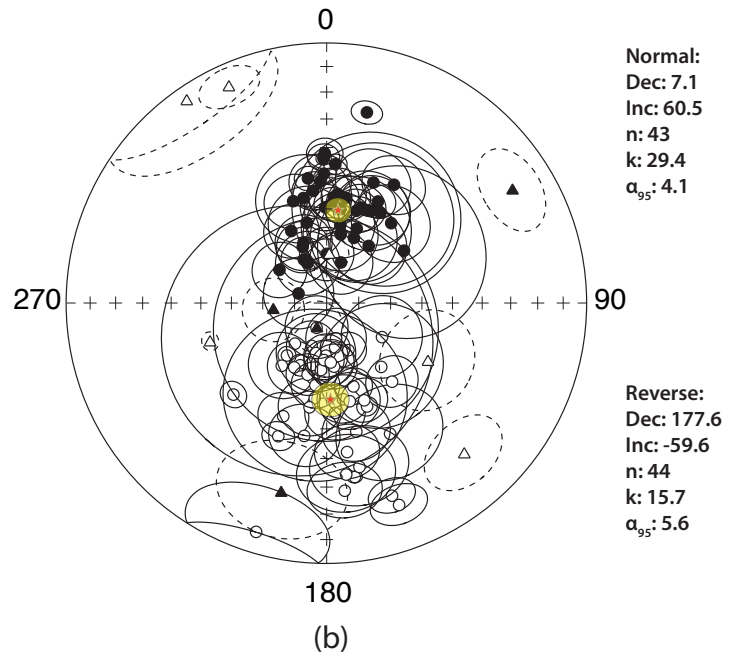
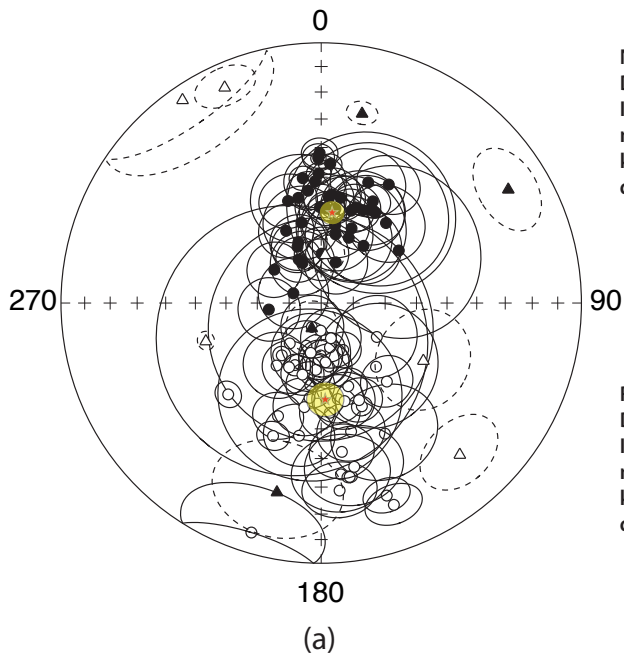


Figure 20: Site means with directions (a) grouped with a visual inspection cutoff, (b) grouped with 45° and Vandamme (1994) cutoffs, (c) ungrouped with a visual inspection cutoff, and (d) ungrouped with 45° and Vandamme cutoffs. Both normal and reverse polarities were recorded in this study; site means are noted at the right of their corresponding figures. Normal and reverse polarity outliers are depicted as closed and open triangles, respectively, with their corresponding cones of confidence, α_{95} , as dashed circles. Red stars and yellow circles indicate their site means and cones of confidence.

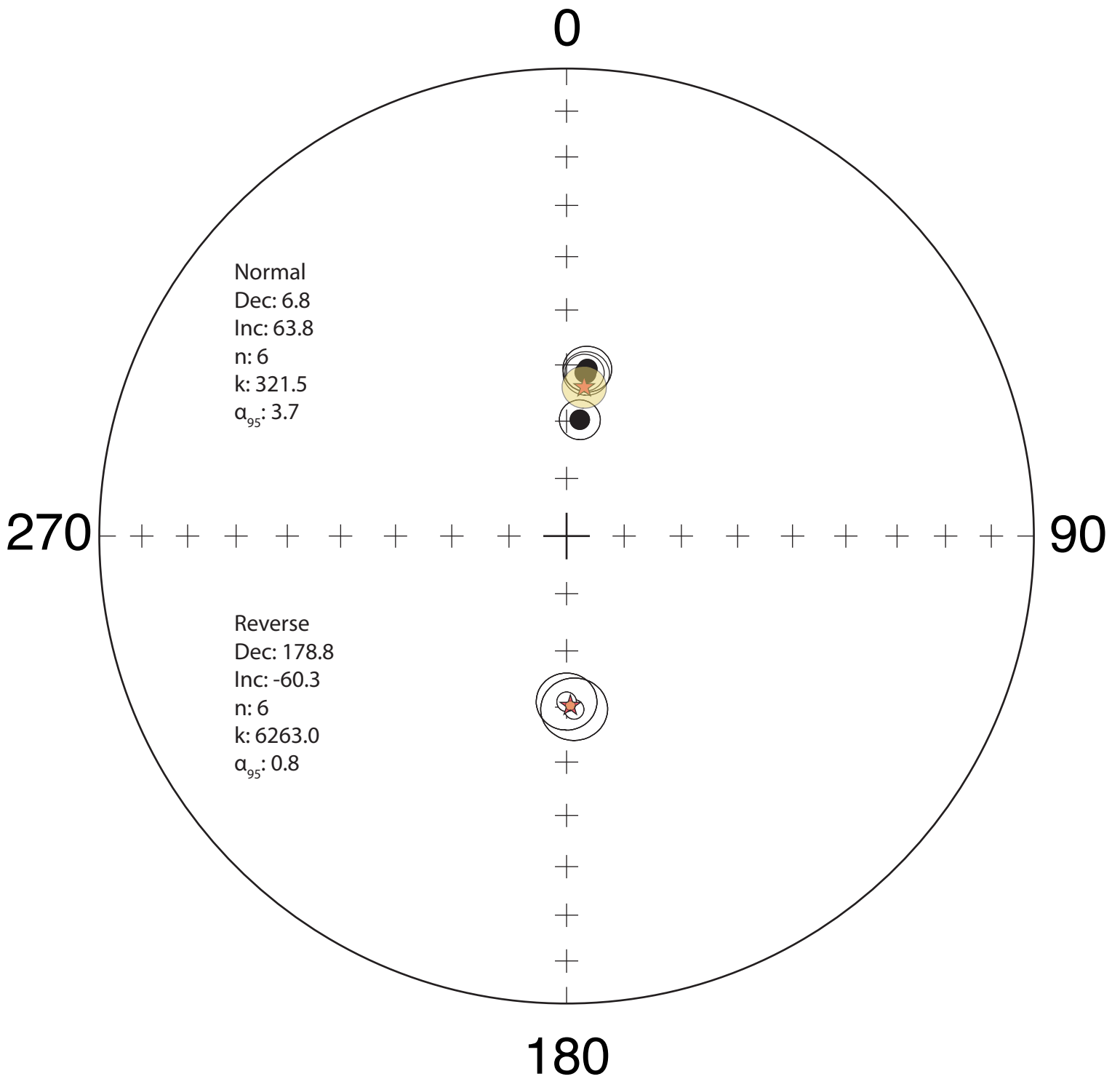
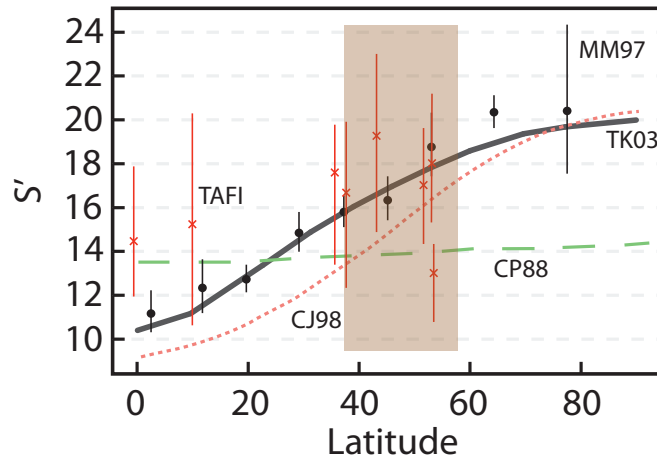
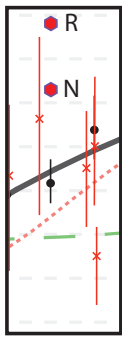


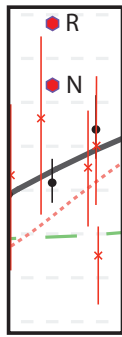
Figure 21: Orthographic projection of mean reverse and normal polarity directions for all six grouping and cutoff scenario site means.



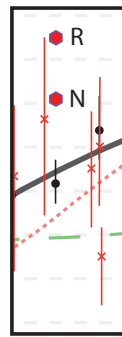
(a)



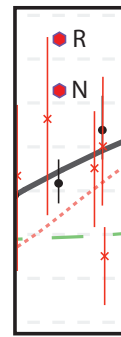
(b)



(c)

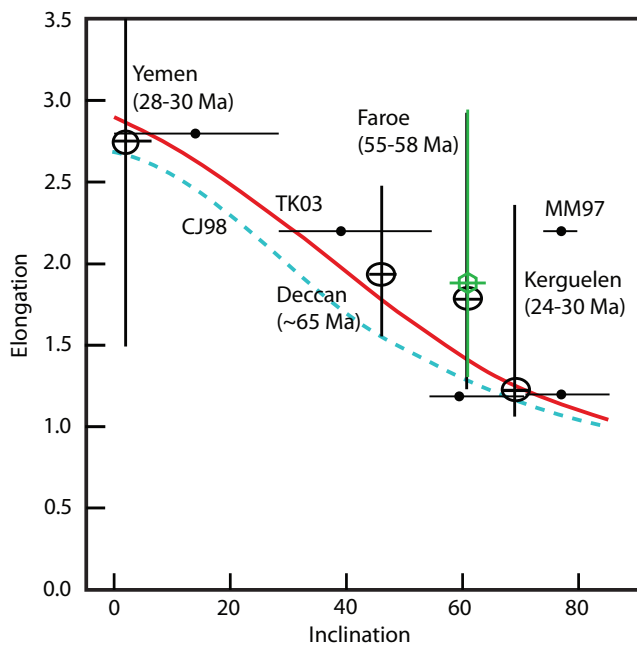


(d)

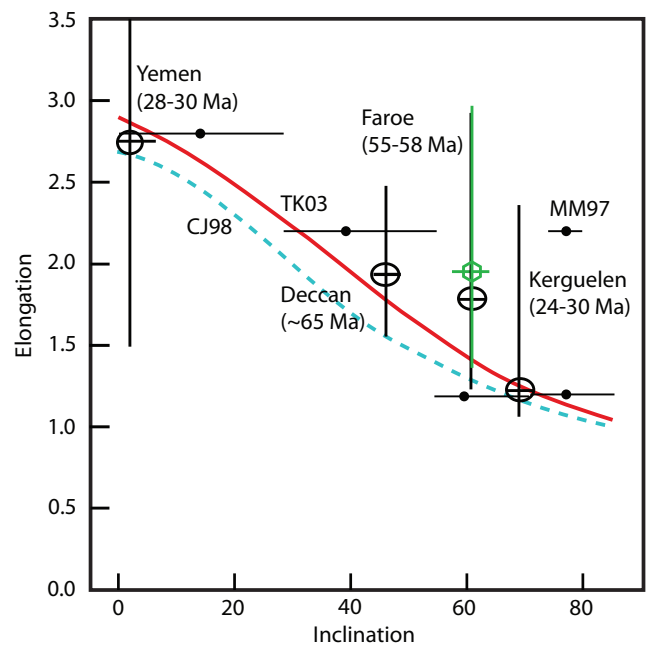


(e)

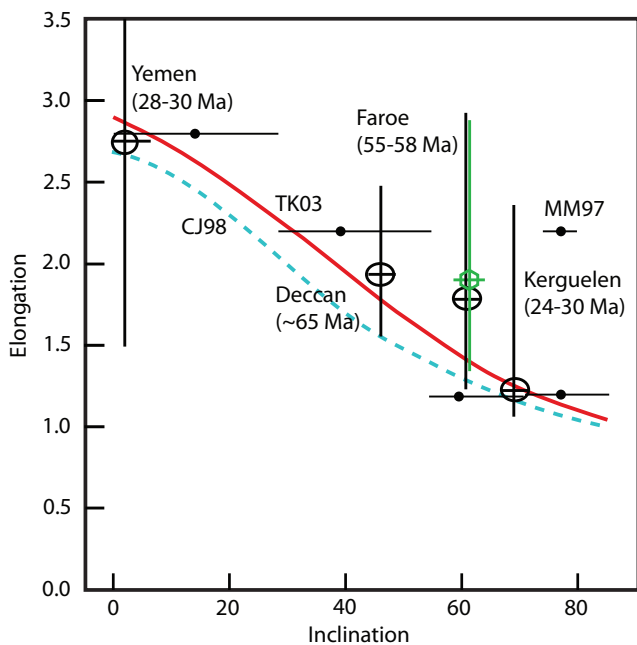
Figure 22: Calculated VGP scatter, S' , as a function of latitude. The solid grey, dotted red, and dashed green curves represent the predicted geomagnetic dispersion behavior according to the TK03 (*Tauxe & Kent, 2004*), CJ98 (*Constable & Parker, 1998*), and CP88 (*Constable & Parker, 1988*) models, respectively. The red crosses and black circles and their corresponding error bars are empirical data collected for the Time-Averaged Field Initiative (TAFI) (*Johnson et al., 2008*) and MM97 (*McElhinny & McFadden, 1997*) studies, respectively. Scatter was determined for the reverse (R) and normal (N) polarity site means for this study, shown as insets marked in maroon box in (a). The scatter was calculated for sites that were (b) grouped with a visual inspection cutoff, (c) grouped with 45° and Vandamme (1994) cutoffs, (d) ungrouped with a visual inspection cutoff, and (e) ungrouped with 45° and Vandamme cutoffs.



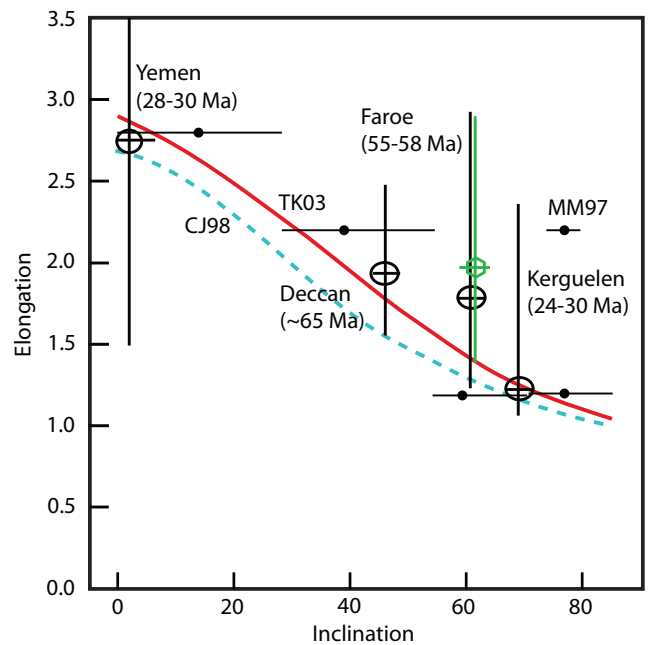
(a)



(b)

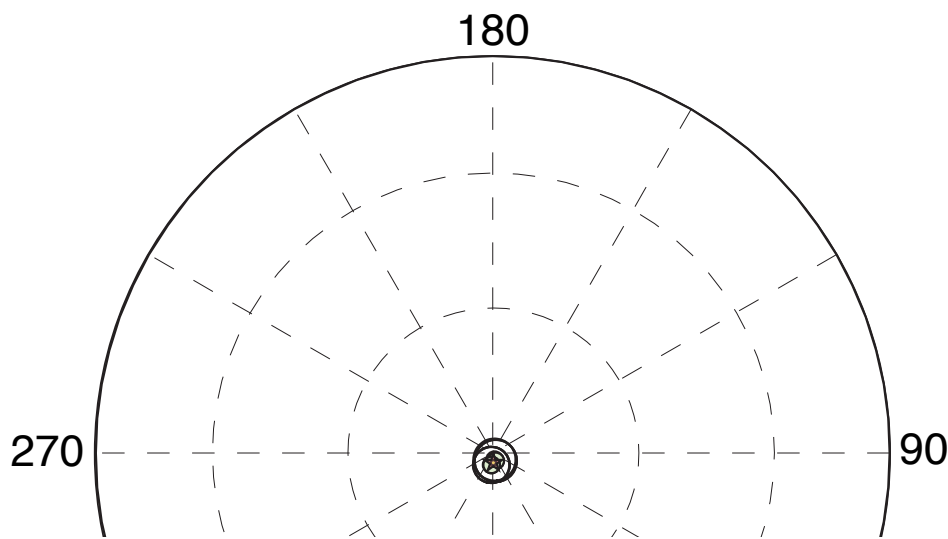


(c)



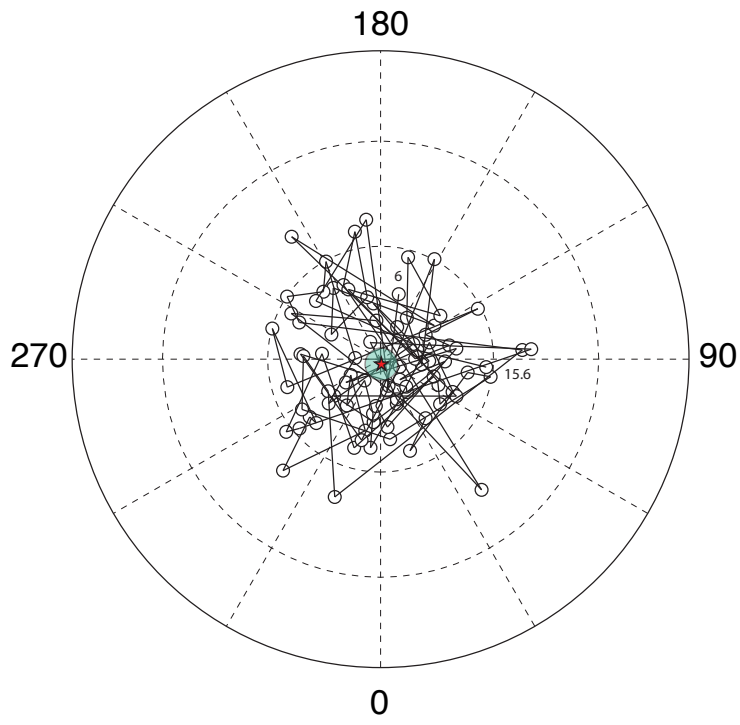
(d)

Figure 23: Diagrams showing the relationship between elongation and magnetic inclination predicted by the TK03.GAD model (Tauxe & Kent, 2004) (red curve) and CJ98.GAD (Constable & Johnson, 1998) (dashed cyan curve). Crossed open circles are data from large igneous provinces: Yemeni traps (Riisager et al., 2005), Deccan traps (Vandamme et al., 1991; Vandamme & Courtillot, 1992), Faroe Island basalts (Riisager et al., 2002), Kerguelen (Plenier et al., 2002), and closed circles with horizontal error bars from the MM97 compilation (McElhinny & McFadden, 1997) (Adapted from Tauxe and Kent, 2004; Tauxe 2005; Tauxe et al., 2008). Green hexagons and error bars indicate the elongation values calculated in this study for the different grouping and cutoff scenarios: (a) grouped sites with a visual inspection cutoff, (b) grouped sites with 45° and Vandamme cutoffs, (c) ungrouped sites with a visual inspection cutoff, and (d) ungrouped sites with 45° and Vandamme cutoffs.

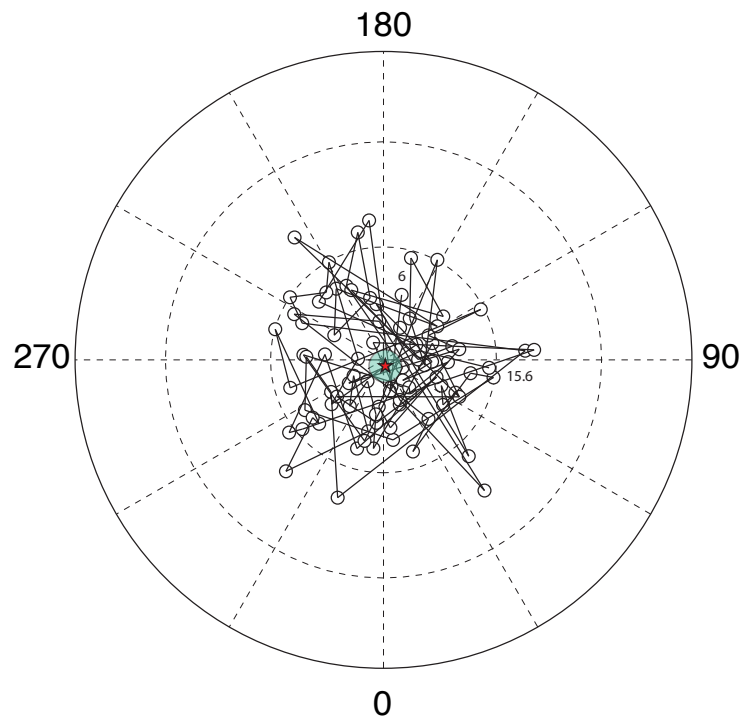


Long: 359.8
 Lat: 88.0
 n: 6
 K: 14246.0
 A_{95} : 0.6
 R: 5.9996
 S: 0.7

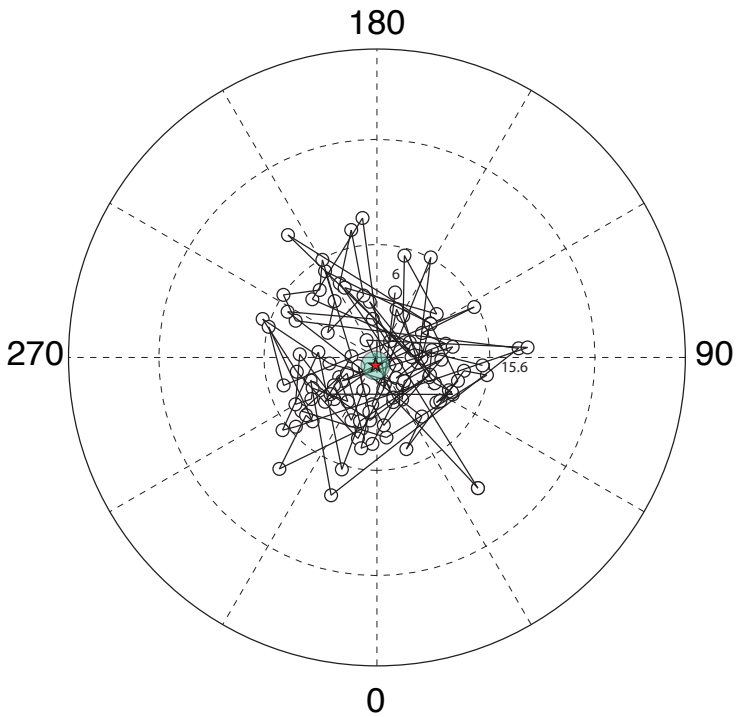
Figure 24: Orthographic projection of mean poles of VGPs calculated from the different grouping and cutoff scenarios; green circles indicate VGPs for the different cutoffs, and their cones of confidence, A_{95} , are shown as black circles. The red star indicates the mean pole, and the transparent yellow circle corresponds to its A_{95} .



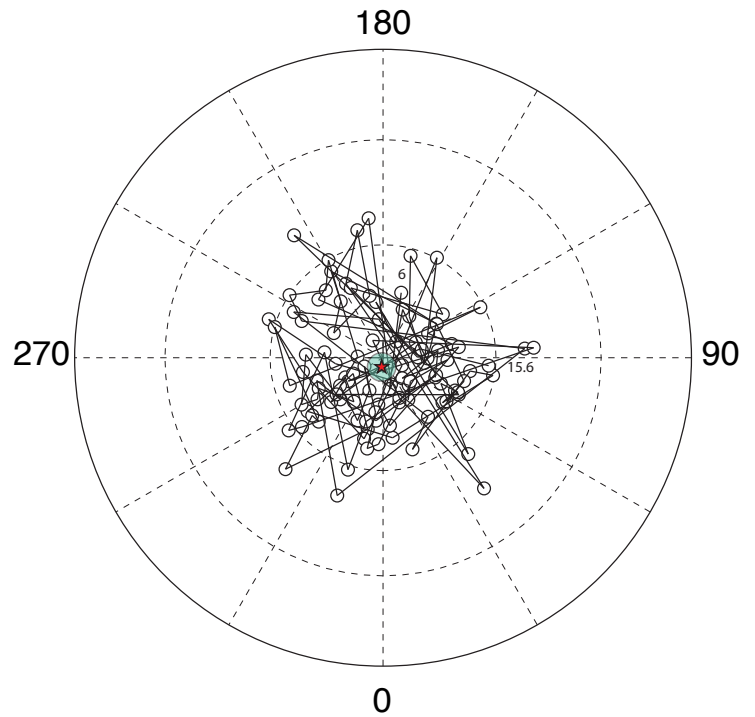
(a)



(b)



(c)



(d)

Figure 25: Mean poles and joined VGPs, indicative of secular variation for sites that were (a) grouped with a visual inspection cutoff, (b) grouped with 45° and Vandamme cutoffs, (c) ungrouped with a visual inspection cutoff, and (d) ungrouped with 45° and Vandamme cutoffs. The numbers indicate the age of the youngest and oldest sites of the collection, in million years, and the red star and cyan circle depict the mean pole and cone of confidence, respectively, for each scenario.

Table 1: General site information, organized by site number, with mean directions, statistical parameters, and VGP directions (*N1*: total number of samples collected; *N2*: number of treated samples; *N3*: number of samples used for analysis).

Site	Sample Range	N1	N2	N3	Dec	Inc	k	α_{95}	GPS Lat.	GPS Long.	VGP Lat.	VGP Long.	dp	dm
1	1-7	7	7	7	187.6	-64.0	67.4	7.4	46.3135	-117.1170	-84.7	30.9	9.4	11.8
2	8-13	6	6	6	200.9	-51.6	78.4	7.6	46.3234	-117.1249	-68.7	186.8	7	10.3
3	14-17	8	7	5	216.9	-68.8	43.5	11.7	46.3242	-117.1097	-65.5	125.4	16.8	19.8
4	18-24	7	7	7	121.4	-69.6	23.1	12.8	46.0538	-117.2318	-52.5	5.9	18.8	21.9
5	25-30	6	6	6	194.8	-68.4	81.0	7.5	46.0473	-117.2379	-78.8	117.5	10.7	12.6
6	31-36	6	6	6	175.5	-55.2	55.9	9.0	46.0504	-117.2385	-79.1	262.6	9.1	12.8
7	37-42	6	6	6	359.3	59.8	79.9	7.5	46.0558	-117.2386	84.6	68.5	8.5	11.3
8	43-48	6	6	6	332.7	74.7	89.2	7.1	46.0426	-117.2532	68.1	206.6	11.7	12.9
9	49-54	6	6	6	215.5	-65.9	42.4	10.4	46.0819	-117.1842	-66.0	134.8	13.9	17
10	55-60	6	6	5	204.7	-71.8	26.0	15.3	46.0792	-117.1960	-71.5	109.0	23.7	26.9
11	61-66	6	6	5	202.9	-66.4	105.3	7.5	46.0775	-117.2031	-74.3	134.3	10.1	12.3
12	67-72	6	5	2	187.0	-59.9	81.8	28.0	46.0736	-117.2106	-82.7	196.6	31.9	42.3
13	73-78	6	6	6	200.0	-64.1	19.1	15.7	46.0714	-117.2177	-76.1	146.5	20	25
14	79-84	6	5	3	342.9	75.0	81.5	13.7	46.0335	-117.2550	71.4	216.9	22.8	25
15	85-90	6	6	6	334.1	64.8	62.7	8.5	46.0299	-117.2560	72.2	164.4	11	13.7
16	91-96	6	6	6	20.7	83.4	17.4	16.5	46.0102	-117.2748	57.9	251.4	31.7	32.4
17	97-102	6	6	6	305.4	72.0	61.2	8.6	46.0031	-117.2804	55.3	191.4	13.4	15.2
18	103-108	6	6	6	27.1	74.3	28.8	12.7	46.0046	-117.2767	68.5	280.1	20.8	23
19	109-114	6	6	6	154.9	-73.8	143.5	5.6	45.9849	-117.2746	-69.7	24.8	9.1	10.1
20	115-120	6	4	4	173.1	-70.0	170.3	7.1	45.9823	-117.2732	-80.9	270.7	10.5	12.2
21	121-126	6	6	6	180.6	-73.6	98.2	6.8	45.9785	-117.2672	-76.5	298.5	11.0	12.2
22	127-132	6	6	5	206.3	-70.5	51.0	10.8	45.9751	-117.2600	-71.2	115.5	16.2	18.7
23	133-138	6	6	6	217.1	-70.1	295.9	3.9	45.9733	-117.2628	-65.1	119.9	5.8	6.7
24	139-144	6	5	5	202.2	82.2	62.5	9.8	45.9729	-117.2733	31.6	236.0	18.6	19.1
25	145-150	6	6	6	199.1	-75.9	75.5	7.8	45.9726	-117.2610	-69.6	87.7	13.2	14.4
26	151-156	6	5	4	325.7	77.0	201.7	6.5	45.9744	-117.2712	63.3	211.0	11.3	12.1
27	157-162	6	5	5	154.0	-43.5	24.4	15.8	45.6356	-117.2687	-60.9	297.4	12.3	19.7
28	163-168	6	5	5	13.0	63.0	84.3	8.4	45.9677	-117.2752	80.7	337.4	10.4	13.2
29	169-174	6	6	6	201.4	-82.0	70.1	8.1	45.9734	-117.2642	-60.1	74.2	15.3	15.7
30	175-180	6	5	3	210.0	-69.2	39.4	19.9	45.9719	-117.2563	-69.5	122.4	28.9	33.9
31	181-186	6	6	5	168.8	-75.9	282.0	4.6	45.9804	-117.2718	-71.5	281.3	7.8	8.5
32	187-192	6	6	6	225.5	-48.5	265.7	4.1	45.9959	-117.2784	-51.1	161.6	3.5	5.4
33	193-198	6	6	6	58.4	16.9	36.3	11.3	46.0025	-117.2783	27.9	350.4	6	11.7
34	199-204	6	6	5	263.7	73.4	61.8	9.8	46.0016	-117.2787	35.4	204.1	15.7	17.6
35	205-210	6	6	6	8.2	54.2	30.1	12.4	46.0093	-117.2768	77.1	31.0	12.2	17.4
36	211-216	6	6	6	166.9	-48.0	45.5	10.0	46.4168	-117.1028	-69.8	278.0	8.5	13.1
37	217-222	6	6	6	206.6	-67.5	66.3	8.3	46.4191	-117.1119	-72.0	130.5	11.5	13.8
38	223-228	6	6	6	199.9	-44.8	199.3	4.8	46.4226	-117.1234	-64.5	197.8	3.8	6.1
39	229-234	6	6	5	182.4	-72.2	153.6	6.2	46.4266	-117.1350	-79.0	303.9	9.7	11.0
40	235-240	6	6	6	175.8	-71.4	87.4	7.2	46.4275	-117.1418	-80.0	283.4	11.0	12.6
41	241-246	6	6	5	184.6	-69.0	202.3	5.4	46.4315	-117.0575	-83.3	87.4	7.8	9.2
42	247-252	6	6	5	170.2	-59.3	96.4	7.8	46.4275	-117.0716	-80.5	294.9	8.8	11.7
43	253-258	6	6	4	189.5	-47.1	78.8	10.4	46.4234	-117.1257	-70.4	217.3	8.7	13.5
44	259-264	6	6	6	358.9	43.7	912.4	2.2	46.4059	-117.2564	69.1	65.5	1.7	2.7
45	265-270	6	6	2	3.7	45.5	5312.0	3.4	46.4084	-117.2637	70.3	52.9	2.7	4.3
46	271-276	6	5	5	164.6	-78.6	67.1	9.4	46.4140	-117.2723	-67.0	48.0	16.8	17.8
47	277-282	6	6	5	162.0	-62.5	177.3	5.8	46.4397	-117.3529	-77.1	327.6	7.1	9.1
48	283-288	6	6	6	158.5	-54.9	475.4	3.1	46.4420	-117.3814	-70.5	306.0	3.1	4.4
49	289-294	6	5	4	340.2	64.2	45.5	13.8	46.4421	-117.3854	76.3	157.8	17.6	22
50	295-300	6	6	5	358.9	48.8	460.2	3.6	46.4416	-117.3922	73.3	66.0	3.1	4.7
51	301-306	6	6	6	24.1	57.9	28.3	12.8	46.4415	-117.3943	70.7	347.9	13.9	18.8
52	307-312	6	6	5	193.4	26.7	19.7	17.7	46.4409	-117.4381	28.3	47.8	10.4	19.2
53	313-318	6	6	6	289.2	80.8	37.8	11.0	46.4454	-117.4420	49.4	216.0	20.4	21.2
54	319-324	6	6	6	359.4	41.9	163.8	5.2	46.4632	-117.4611	67.7	64.0	3.9	6.4
55	325-330	6	5	4	351.6	49.9	517.4	4.0	46.4465	-117.4638	73.0	88.0	3.6	5.3

Site	Sample Range	N1	N2	N3	Dec	Inc	k	$\alpha 95$	GPS Lat.	GPS Long.	VGP Lat.	VGP Long.	dp	dm
56	331-336	6	6	5	358.9	42.5	69.3	9.3	46.4472	-117.4672	68.2	65.3	7.1	11.5
57	337-342	6	6	6	24.4	61.0	51.9	9.4	46.4558	-117.4720	72.1	337.9	11	14.4
58	343-348	6	6	6	10.5	56.2	82.5	7.4	46.4675	-117.4941	77.5	20.0	7.7	10.7
59	349-354	6	6	6	12.0	26.0	254.8	4.2	46.4675	-117.4929	55.7	41.5	2.5	4.5
60	355-360	6	6	6	3.2	60.2	120.6	5.5	46.4677	-117.5059	82.6	43.1	6	8
61	361-366	6	6	5	349.9	53.5	72.5	9.0	46.4777	-117.6455	75.4	97.6	8.7	12.5
62	367-372	6	6	6	161.2	-22.9	115.1	6.3	46.4321	-117.1427	-52.0	273.7	3.6	6.7
63	373-378	6	5	5	174.4	-28.4	58.5	10.1	46.4532	-117.2044	-58.3	127.6	6.1	11.1
64	379-384	6	6	6	173.4	-34.1	24.9	13.7	46.4529	-117.2076	-61.7	130.5	9.0	15.7
65	385-390	6	6	6	170.7	-32.8	1059.0	2.1	46.4611	-117.2189	-60.4	260.9	1.3	2.4
66	391-396	6	6	6	158.7	-57.1	89.9	7.1	46.4670	-117.2301	-72.0	185.8	7.5	10.3
67	397-402	6	6	6	172.1	-41.8	52.4	9.3	46.4666	-117.2295	-66.7	261.3	7	11.4
68	403-408	6	5	3	119.1	-53.0	66.3	15.3	46.4685	-117.2316	-42.8	339.6	14.7	21.2
69	409-414	6	6	5	140.1	-57.7	90.5	8.1	46.5104	-117.2327	-59.8	331.7	8.7	11.9
70	415-420	6	6	6	0.4	74.6	64.1	8.4	46.6264	-117.3385	75.5	243.4	13.9	15.3
71	421-426	6	4	4	4.0	-74.4	236.4	6.0	46.6158	-117.3171	-17.5	60.6	9.9	10.9
72	427-432	6	6	2	139.3	-63.6	164.1	19.6	46.6103	-117.3029	-62.0	344.9	24.6	31.1
73	433-438	6	6	6	189.2	-56.7	51.9	9.4	46.4612	-117.9803	-78.6	202.2	9.9	13.6
74	439-444	6	6	6	39.0	57.5	31.0	12.2	46.4272	-117.1713	60.3	209.2	13.1	17.9
75	445-450	6	6	5	29.0	56.5	9.7	25.9	46.4275	-117.1704	66.6	220.3	27.1	37.4
76	451-456	6	6	6	336.0	-9.3	77.0	7.7	46.4277	-117.1693	-34.6	272.4	3.9	7.8
77	457-460	8	8	7	160.2	-18.7	65.3	7.5	46.4281	-117.1679	-49.5	273.8	4.1	7.8
78	461-464	8	5	4	137.3	-22.8	64.1	11.6	46.4287	-117.1660	-40.2	303.1	6.5	12.3
79	465-468	8	6	5	166.6	-58.2	70.0	9.2	46.5130	-117.2352	-77.6	174.2	10.0	13.6
80	469-472	8	7	7	194.7	-66.8	85.8	6.6	46.6424	-117.2686	-79.8	6.2	9.0	10.9
81	473-476	8	7	7	357.9	51.2	17.2	15.0	46.5217	-117.8140	75.3	69.3	13.8	20.3
82	477-480	8	3	3	13.0	71.5	44.0	18.8	46.5228	-117.8178	77.4	277.2	28.9	33
83	481-484	8	7	7	29.7	46.5	41.2	9.5	46.5176	-117.7944	60.1	236.2	7.8	12.2
84	485-488	8	6	6	21.3	48.8	36.7	11.2	46.5155	-117.7901	66.4	245.7	9.7	14.8
85	489-492	8	2	0	-	-	-	-	46.4643	-117.7034	-	-	-	-
86	493-496	8	7	7	25.2	53.2	19.8	13.9	46.5241	-117.8194	67.1	357.0	13.4	19.3
87	497-500	8	8	8	19.2	68.4	22.0	12.1	46.5232	-117.8173	76.5	303.0	17.2	20.4
88	501-504	8	5	5	4.1	56.5	105.3	7.5	46.5255	-117.8043	80.1	43.0	7.8	10.8
89	505-508	8	5	4	191.9	-74.1	56.6	12.3	46.5255	-117.7985	-74.5	84.7	20.1	22.2
90	509-512	8	8	8	357.1	51.3	36.9	9.2	46.5440	-117.7749	75.3	71.9	8.5	12.5
91	513-516	8	7	7	20.0	57.9	65.7	7.5	46.5591	-117.7715	73.3	353.7	8.1	11
92	517-520	8	4	4	27.2	56.9	69.6	11.1	46.5633	-117.7754	68.0	346.8	11.7	16.1
93	521-524	8	6	6	22.5	59.5	43.6	10.3	46.5652	-117.7775	72.6	345.1	11.6	15.5
94	525-528	8	8	5	11.8	68.0	45.3	11.5	46.5899	-117.7839	81.1	297.9	16.2	19.3
95	529-532	8	8	3	341.8	56.2	29.6	23.1	46.5936	-117.7821	73.3	122.7	24	33.3
96	533-536	8	4	4	181.1	-81.4	7.7	35.5	46.5989	-117.7850	-63.4	62.9	66.5	68.7
97	537-540	8	5	2	217.9	-74.0	35.6	43.2	46.6170	-117.7898	-64.2	106.7	70.4	78
98	541-544	8	5	4	353.5	55.5	48.2	13.4	46.6489	-117.8079	78.3	89.2	13.7	19.1
99	545-548	8	8	5	339.4	69.7	76.2	8.8	46.6563	-117.8055	75.2	187.3	12.9	15.1
100	549-552	8	4	2	28.7	54.6	52.3	35.2	46.6598	-117.8021	65.6	350.1	35.1	49.7
101	553-556	8	7	5	355.2	42.6	26.3	15.2	46.6160	-117.7674	67.7	73.9	11.6	18.8
102	557-560	8	6	6	36.5	67.7	32.7	11.9	46.6275	-117.7207	65.8	309.2	16.6	19.9
103	561-564	8	6	6	18.0	59.4	91.8	7.0	46.6224	-117.6321	75.5	352.1	7.9	10.5
104	565-568	8	6	5	351.6	57.6	64.1	9.6	46.5982	-117.6033	79.6	101.9	10.3	14.1
105	569-572	8	5	5	2.7	44.8	37.8	12.6	46.5888	-117.5794	69.7	55.5	10	15.9
106	573-576	8	8	8	6.7	67.0	31.4	10.0	46.5765	-117.5707	84.6	295.2	13.7	16.6
107	577-580	8	5	2	352.4	63.6	128.5	22.2	46.5628	-117.5628	84.5	140.8	27.9	35.2
108	581-584	8	4	2	37.9	53.4	116.6	23.3	46.5432	-117.5681	58.8	342.6	22.6	32.4
109	585-588	8	5	3	325.8	-5.5	30.6	22.7	46.5377	-117.5602	-32.2	284.0	11.4	22.8
110	589-592	8	4	2	55.9	60.5	89.0	26.8	46.5323	-117.5593	50.3	318.8	31	40.8
111	593-596	8	8	3	168.6	-36.0	80.2	13.9	46.5076	-117.5659	-61.9	265.7	9.4	16.1
112	597-600	8	5	5	197.1	-8.9	19.7	17.7	46.4796	-117.5757	-45.5	217.7	9	17.9
113	601-606	6	6	6	342.0	56.1	58.7	8.8	46.6465	-117.7230	73.3	122.0	9.1	12.7
114	607-612	6	6	6	2.7	56.8	497.9	3.0	46.6396	-117.7605	80.5	49.2	3.2	4.4
115	613-618	6	5	4	252.2	-51.4	1096.0	2.8	46.4774	-117.7675	-34.3	139.8	2.6	3.8

Site	Sample Range	N1	N2	N3	Dec	Inc	k	$\alpha 95$	GPS Lat.	GPS Long.	VGP Lat.	VGP Long.	dp	dm
116	619-624	6	6	6	22.9	67.8	25.9	13.4	46.5724	-117.7384	74.4	308.3	18.8	22.4
117	625-630	6	6	6	337.2	70.9	70.1	8.1	46.5509	-117.6769	73.3	192.2	12.3	14.1
118	631-636	6	6	6	8.6	60.0	199.7	4.8	46.5246	-117.5820	81.6	11.6	5.5	7.3

Table 2: General site information with sites ordered magnetostratigraphically with corresponding basaltic flow members (*NRO Factor*: Non-Random Ordering calculation factor used to determine similarity in directions of contiguous sites; *Combine?*: condition indicating if grouping is possible for a given site; listed as *yes* if site meets all grouping criteria; otherwise, *no*).

Site	Flow Member	Dec	Inc	k	α_{95}	GPS Lat.	GPS Long.	VGP Lat.	VGP Long.	dp	dm	NRO Factor	Combine?
15	Saddle Mountain	334.1	64.8	62.7	8.5	46.0299	-117.2560	72.2	164.4	11.0	13.7	-	no
118	Saddle Mountain	8.6	60.0	199.7	4.8	46.5246	-117.5820	81.6	11.6	5.5	7.3	-	no
76	Saddle Mountain	336.0	-9.3	77.0	7.7	46.4277	-117.1693	-34.6	272.4	3.9	7.8	0.939	no
109	Saddle Mountain	325.8	-5.5	30.6	22.7	46.5377	-117.5602	-32.2	284.0	11.4	22.8	0.939	no
12	Saddle Mountain	187.0	-59.9	81.8	28.0	46.0736	-117.2106	-82.7	196.6	31.9	42.3	0.939	no
4	Saddle Mountain	121.4	-69.6	23.1	12.8	46.0538	-117.2318	-52.5	5.9	18.8	21.9	0.939	no
46	Saddle Mountain	164.6	-78.6	67.1	9.4	46.4140	-117.2723	-67.0	48.0	16.8	17.8	0.939	no
42	Saddle Mountain	170.2	-59.3	96.4	7.8	46.4275	-117.0716	-80.5	294.9	8.8	11.7	0.939	no
37	Saddle Mountain	206.6	-67.5	66.3	8.3	46.4191	-117.1119	-72.0	130.5	11.5	13.8	0.939	no
41	Saddle Mountain	184.6	-69.0	202.3	5.4	46.4315	-117.0575	-83.3	87.4	7.8	9.2	0.939	no
74	Saddle Mountain	39.0	57.5	31.0	12.2	46.4272	-117.1713	60.3	209.2	13.1	17.9	-	no
75	Saddle Mountain	29.0	56.5	9.7	25.9	46.4275	-117.1704	66.6	220.3	27.1	37.4	-	no
83	Saddle Mountain	29.7	46.5	41.2	9.5	46.5176	-117.7944	60.1	236.2	7.8	12.2	-	no
84	Saddle Mountain	21.3	48.8	36.7	11.2	46.5155	-117.7901	66.4	245.7	9.7	14.8	-	no
68	Saddle Mountain	119.1	-53.0	66.3	15.3	46.4685	-117.2316	-42.8	339.6	14.7	21.2	0.999	yes
62	Saddle Mountain	161.2	-22.9	115.1	6.3	46.4321	-117.1427	-52.0	273.7	3.6	6.7	0.999	yes
78	Saddle Mountain	137.3	-22.8	64.1	11.6	46.4287	-117.1660	-40.2	303.1	6.5	12.3	0.999	yes
32	Saddle Mountain	225.5	-48.5	265.7	4.1	45.9959	-117.2784	-51.1	161.6	3.5	5.4	0.999	yes
115	Saddle Mountain	252.2	-51.4	1096.0	2.8	46.4774	-117.7675	-34.3	139.8	2.6	3.8	0.999	yes
10	Saddle Mountain	204.7	-71.8	26.0	15.3	46.0792	-117.1960	-71.5	109.0	23.7	26.9	0.999	yes
11	Saddle Mountain	202.9	-66.4	105.3	7.5	46.0775	-117.2031	-74.3	134.3	10.1	12.3	0.999	yes
25	Saddle Mountain	199.1	-75.9	75.5	7.8	45.9726	-117.2610	-69.6	87.7	13.2	14.4	0.999	yes
23	Saddle Mountain	217.1	-70.1	295.9	3.9	45.9733	-117.2628	-65.1	119.9	5.8	6.7	0.999	yes
30	Saddle Mountain	210.0	-69.2	39.4	19.9	45.9719	-117.2563	-69.5	122.4	28.9	33.9	0.999	yes
22	Saddle Mountain	206.3	-70.5	51.0	10.8	45.9751	-117.2600	-71.2	115.5	16.2	18.7	0.999	yes
13	Saddle Mountain	200.0	-64.1	19.1	15.7	46.0714	-117.2177	-76.1	146.5	20.0	25.0	0.999	yes
5	Saddle Mountain	194.8	-68.4	81.0	7.5	46.0473	-117.2379	-78.8	117.5	10.7	12.6	0.999	yes
3	Saddle Mountain	216.9	-68.8	43.5	11.7	46.3242	-117.1097	-65.5	125.4	16.8	19.8	0.999	yes
2	Saddle Mountain	200.9	-51.6	78.4	7.6	46.3234	-117.1249	-68.7	186.8	7.0	10.3	0.999	yes
65	Saddle Mountain	170.7	-32.8	1059.0	2.1	46.4611	-117.2189	-60.4	260.9	1.3	2.4	0.999	yes
67	Saddle Mountain	172.1	-41.8	52.4	9.3	46.4666	-117.2295	-66.7	261.3	7.0	11.4	0.999	yes
38	Saddle Mountain	199.9	-44.8	199.3	4.8	46.4226	-117.1234	-64.5	197.8	3.8	6.1	0.999	yes
43	Saddle Mountain	189.5	-47.1	78.8	10.4	46.4234	-117.1257	-70.4	217.3	8.7	13.5	0.999	yes
96	Saddle Mountain	181.1	-81.4	7.7	35.5	46.5989	-117.7850	-63.4	62.9	66.5	68.7	0.999	yes
24	Saddle Mountain	202.2	82.2	62.5	9.8	45.9729	-117.2733	31.6	236.0	18.6	19.1	-	no
80	Wanapum	194.7	-66.8	85.8	6.6	46.6424	-117.2686	-79.8	6.2	9.0	10.9	0.4408	no
112	Wanapum	197.1	-8.9	19.7	17.7	46.4796	-117.5757	-45.5	217.7	9.0	17.9	0.4408	no
73	Wanapum	189.2	-56.7	51.9	9.4	46.4612	-117.9803	-78.6	202.2	9.9	13.6	0.4408	no
1	Wanapum	187.6	-64.0	67.4	7.4	46.3135	-117.1170	-84.7	30.9	9.4	11.8	0.4408	no
77	Wanapum	160.2	-18.7	65.3	7.5	46.4281	-117.1679	-49.5	273.8	4.1	7.8	0.4408	no
64	Wanapum	173.4	-34.1	24.9	13.7	46.4529	-117.2076	-61.7	130.5	9.0	15.7	0.4408	no
63	Wanapum	174.4	-28.4	58.5	10.1	46.4532	-117.2044	-58.3	127.6	6.1	11.1	0.4408	no
89	Wanapum	191.9	-74.1	56.6	12.3	46.5255	-117.7985	-74.5	84.7	20.1	22.2	0.4408	no
108	Wanapum	37.9	53.4	116.6	23.3	46.5432	-117.5681	58.8	342.6	22.6	32.4	0.999	yes
93	Wanapum	22.5	59.5	43.6	10.3	46.5652	-117.7775	72.6	345.1	11.6	15.5	0.999	yes
52	Wanapum	193.4	26.7	19.7	17.7	46.4409	-117.4381	28.3	47.8	10.4	19.2	0.999	yes
33	Wanapum	58.4	16.9	36.3	11.3	46.0025	-117.2783	27.9	350.4	6.0	11.7	0.999	yes
90	Wanapum	357.1	51.3	36.9	9.2	46.5440	-117.7749	75.3	71.9	8.5	12.5	0.999	yes
91	Wanapum	20.0	57.9	65.7	7.5	46.5591	-117.7715	73.3	353.7	8.1	11.0	0.999	yes
116	Wanapum	22.9	67.8	25.9	13.4	46.5724	-117.7384	74.4	308.3	18.8	22.4	0.999	yes
54	Wanapum	359.4	41.9	163.8	5.2	46.4632	-117.4611	67.7	64.0	3.9	6.4	0.999	yes
53	Wanapum	289.2	80.8	37.8	11.0	46.4454	-117.4420	49.4	216.0	20.4	21.2	0.999	yes

Site	Flow Member	Dec	Inc	k	$\alpha 95$	GPS Lat.	GPS Long.	VGP Lat.	VGP Long.	dp	dm	NRO Factor	Combine?
113	Wanapum	342.0	56.1	58.7	8.8	46.6465	-117.7230	73.3	122.0	9.1	12.7	0.999	yes
26	Grande Ronde	325.7	77.0	201.7	6.5	45.9744	-117.2712	63.3	211.0	11.3	12.1	0.999	yes
14	Grande Ronde	342.9	75.0	81.5	13.7	46.0335	-117.2550	71.4	216.9	22.8	25.0	0.999	yes
70	Grande Ronde	0.4	74.6	64.1	8.4	46.6264	-117.3385	75.5	243.4	13.9	15.3	0.999	yes
117	Grande Ronde	337.2	70.9	70.1	8.1	46.5509	-117.6769	73.3	192.2	12.3	14.1	0.999	yes
17	Grande Ronde	305.4	72.0	61.2	8.6	46.0031	-117.2804	55.3	191.4	13.4	15.2	0.999	yes
8	Grande Ronde	332.7	74.7	89.2	7.1	46.0426	-117.2532	68.1	206.6	11.7	12.9	0.999	yes
7	Grande Ronde	359.3	59.8	79.9	7.5	46.0558	-117.2386	84.6	68.5	8.5	11.3	0.999	yes
92	Grande Ronde	27.2	56.9	69.6	11.1	46.5633	-117.7754	68.0	346.8	11.7	16.1	0.999	yes
18	Grande Ronde	27.1	74.3	28.8	12.7	46.0046	-117.2767	68.5	280.1	20.8	23.0	0.999	yes
16	Grande Ronde	20.7	83.4	17.4	16.5	46.0102	-117.2748	57.9	251.4	31.7	32.4	0.999	yes
82	Grande Ronde	13.0	71.5	44.0	18.8	46.5228	-117.8178	77.4	277.2	28.9	33.0	0.999	yes
88	Grande Ronde	4.1	56.5	105.3	7.5	46.5255	-117.8043	80.1	43.0	7.8	10.8	0.999	yes
34	Grande Ronde	263.7	73.4	61.8	9.8	46.0016	-117.2787	35.4	204.1	15.7	17.6	0.999	yes
35	Grande Ronde	8.2	54.2	30.1	12.4	46.0093	-117.2768	77.1	31.0	12.2	17.4	0.999	yes
114	Grande Ronde	2.7	56.8	497.9	3.0	46.6396	-117.7605	80.5	49.2	3.2	4.4	0.999	yes
55	Grande Ronde	351.6	49.9	517.4	4.0	46.4465	-117.4638	73.0	88.0	3.6	5.3	0.999	yes
60	Grande Ronde	3.2	60.2	120.6	5.5	46.4677	-117.5059	82.6	43.1	6.0	8.0	0.999	yes
61	Grande Ronde	349.9	53.5	72.5	9.0	46.4777	-117.6455	75.4	97.6	8.7	12.5	0.999	yes
81	Grande Ronde	357.9	51.2	17.2	15.0	46.5217	-117.8140	75.3	69.3	13.8	20.3	0.999	yes
104	Grande Ronde	351.6	57.6	64.1	9.6	46.5982	-117.6033	79.6	101.9	10.3	14.1	0.999	yes
49	Grande Ronde	340.2	64.2	45.5	13.8	46.4421	-117.3854	76.3	157.8	17.6	22.0	0.999	yes
107	Grande Ronde	352.4	63.6	128.5	22.2	46.5628	-117.5628	84.5	140.8	27.9	35.2	0.999	yes
99	Grande Ronde	339.4	69.7	76.2	8.8	46.6563	-117.8055	75.2	187.3	12.9	15.1	0.999	yes
59	Grande Ronde	12.0	26.0	254.8	4.2	46.4675	-117.4929	55.7	41.5	2.5	4.5	0.999	yes
50	Grande Ronde	358.9	48.8	460.2	3.6	46.4416	-117.3922	73.3	66.0	3.1	4.7	0.999	yes
56	Grande Ronde	358.9	42.5	69.3	9.3	46.4472	-117.4672	68.2	65.3	7.1	11.5	0.999	yes
45	Grande Ronde	3.7	45.5	5312.0	3.4	46.4084	-117.2637	70.3	52.9	2.7	4.3	0.999	yes
44	Grande Ronde	358.9	43.7	912.4	2.2	46.4059	-117.2564	69.1	65.5	1.7	2.7	0.999	yes
105	Grande Ronde	2.7	44.8	37.8	12.6	46.5888	-117.5794	69.7	55.5	10.0	15.9	0.999	yes
101	Grande Ronde	355.2	42.6	26.3	15.2	46.6160	-117.7674	67.7	73.9	11.6	18.8	0.999	yes
95	Grande Ronde	341.8	56.2	29.6	23.1	46.5936	-117.7821	73.3	122.7	24.0	33.3	0.999	yes
98	Grande Ronde	353.5	55.5	48.2	13.4	46.6489	-117.8079	78.3	89.2	13.7	19.1	0.999	yes
58	Grande Ronde	10.5	56.2	82.5	7.4	46.4675	-117.4941	77.5	20.0	7.7	10.7	0.999	yes
86	Grande Ronde	25.2	53.2	19.8	13.9	46.5241	-117.8194	67.1	357.0	13.4	19.3	0.999	yes
100	Grande Ronde	28.7	54.6	52.3	35.2	46.6598	-117.8021	65.6	350.1	35.1	49.7	0.999	yes
103	Grande Ronde	18.0	59.4	91.8	7.0	46.6224	-117.6321	75.5	352.1	7.9	10.5	0.999	yes
106	Grande Ronde	6.7	67.0	31.4	10.0	46.5765	-117.5707	84.6	295.2	13.7	16.6	0.999	yes
28	Grande Ronde	13.0	63.0	84.3	8.4	45.9677	-117.2752	80.7	337.4	10.4	13.2	0.999	yes
57	Grande Ronde	24.4	61.0	51.9	9.4	46.4558	-117.4720	72.1	337.9	11.0	14.4	0.999	yes
87	Grande Ronde	19.2	68.4	22.0	12.1	46.5232	-117.8173	76.5	303.0	17.2	20.4	0.999	yes
94	Grande Ronde	11.8	68.0	45.3	11.5	46.5899	-117.7839	81.1	297.9	16.2	19.3	0.999	yes
51	Grande Ronde	24.1	57.9	28.3	12.8	46.4415	-117.3943	70.7	347.9	13.9	18.8	0.999	yes
110	Grande Ronde	55.9	60.5	89.0	26.8	46.5323	-117.5593	50.3	318.8	31.0	40.8	0.999	yes
102	Grande Ronde	36.5	67.7	32.7	11.9	46.6275	-117.7207	65.8	309.2	16.6	19.9	0.999	yes
9	Grande Ronde	215.5	-65.9	42.4	10.4	46.0819	-117.1842	-66.0	134.8	13.9	17.0	0.8726	no
29	Grande Ronde	201.4	-82.0	70.1	8.1	45.9734	-117.2642	-60.1	74.2	15.3	15.7	0.8726	no
97	Grande Ronde	217.9	-74.0	35.6	43.2	46.6170	-117.7898	-64.2	106.7	70.4	78.0	0.8726	no
27	Grande Ronde	154.0	-43.5	24.4	15.8	45.6356	-117.2687	-60.9	297.4	12.3	19.7	0.8726	no
21	Grande Ronde	180.6	-73.6	98.2	6.8	45.9785	-117.2672	-76.5	298.5	11.0	12.2	0.8726	no
31	Grande Ronde	168.8	-75.9	282.0	4.6	45.9804	-117.2718	-71.5	281.3	7.8	8.5	0.8726	no
20	Grande Ronde	173.1	-70.0	170.3	7.1	45.9823	-117.2732	-80.9	270.7	10.5	12.2	0.8726	no
19	Grande Ronde	154.9	-73.8	143.5	5.6	45.9849	-117.2746	-69.7	24.8	9.1	10.1	0.8726	no
48	Grande Ronde	158.5	-54.9	475.4	3.1	46.4420	-117.3814	-70.5	306.0	3.1	4.4	0.8726	no
72	Grande Ronde	139.3	-63.6	164.1	19.6	46.6103	-117.3029	-62.0	344.9	24.6	31.1	0.8726	no
47	Grande Ronde	162.0	-62.5	177.3	5.8	46.4397	-117.3529	-77.1	327.6	7.1	9.1	0.8726	no

Site	Flow Member	Dec	Inc	k	$\alpha 95$	GPS Lat.	GPS Long.	VGP Lat.	VGP Long.	dp	dm	NRO Factor	Combine?
6	Grande Ronde	175.5	-55.2	55.9	9.0	46.0504	-117.2385	-79.1	262.6	9.1	12.8	0.8726	no
71	Grande Ronde	4.0	-74.4	236.4	6.0	46.6158	-117.3171	-17.5	60.6	9.9	10.9	0.8726	no
69	Grande Ronde	140.1	-57.7	90.5	8.1	46.5104	-117.2327	-59.8	331.7	8.7	11.9	0.8726	no
79	Grande Ronde	166.6	-58.2	70.0	9.2	46.5130	-117.2352	-77.6	174.2	10.0	13.6	0.8726	no
66	Grande Ronde	158.7	-57.1	89.9	7.1	46.4670	-117.2301	-72.0	185.8	7.5	10.3	0.8726	no
36	Grande Ronde	166.9	-48.0	45.5	10.0	46.4168	-117.1028	-69.8	278.0	8.5	13.1	0.8726	no
39	Grande Ronde	182.4	-72.2	153.6	6.2	46.4266	-117.1350	-79.0	303.9	9.7	11.0	0.8726	no
40	Grande Ronde	175.8	-71.4	87.4	7.2	46.4275	-117.1418	-80.0	283.4	11.0	12.6	0.8726	no
111	Grande Ronde	168.6	-36.0	80.2	13.9	46.5076	-117.5659	-61.9	265.7	9.4	16.1	0.8726	no

Table 3: Pre- and post-folding correction for tilted beds, yielding a positive fold test (*McElhinny, 1964*). Sites marked with asterisks were inverted to normal polarity.

<i>Pre-tilt</i>					<i>Post-tilt</i>			
Site	Dec	Inc	k	a95	Dec	Inc	k	a95
26	155.3	88	201.7	6.5	325.7	77	201.7	6.5
41*	62.2	73.4	202.3	5.4	4.6	69	202.3	5.4
44	1.1	7.9	912.4	2.2	358.9	43.7	912.4	2.2
54	355.4	19.3	163.8	5.2	359.4	41.9	163.8	5.2
55	350.3	33	517.4	4	351.6	49.9	517.4	4
56	356.3	32.5	69.3	9.3	358.9	42.5	69.3	9.3
59	10.1	-5.5	254.8	4.2	12	26	254.8	4.2
68*	282.1	36.9	66.3	15.3	299.1	53	66.3	15.3
74	81.2	11.1	31	12.2	39	57.5	31	12.2
75	78.2	15.8	9.7	25.9	29	56.5	9.7	25.9
76	350.4	-37	77	7.7	336	-9.3	77	7.7
77*	26.6	45.9	65.3	7.5	340.2	18.7	65.3	7.5
78*	27.3	67.6	64.1	11.6	317.3	22.8	64.1	11.6
105	0	26.2	37.8	12.6	2.7	44.8	37.8	12.6
115*	86.8	8.7	1096	2.8	72.2	51.4	1096	2.8

Mean

Pre-tilt

Dec	Inc	R	k1	a95
18.6	41.3	11.0869	3.6	23.7

Post-tilt

Dec	Inc	R	k2	a95
355.6	47.5	13.0985	7.4	15.1

Table 4: Group-mean directions and corresponding VGP for grouped sites (*Sites*: sites included in their corresponding group).

Group	Sites	Dec	Inc	n	k	a95	GPS Lat	GPS Long	VGP Lat	VGP Long	Dp	Dm
GP1	3, 23	217.0	-69.5	2	7760.0	2.8	46.1488	-117.1863	-65.3	122.6	4.1	4.8
GP2	5, 10, 11, 13, 22, 30	202.9	-68.9	6	569.4	3.4	46.0371	-117.2285	-73.8	121.5	4.9	5.8
GP3	93, 108	30.8	56.7	2	120.8	22.9	46.5542	-117.6728	65.5	343.4	24.1	33.2
GP4	14, 26	334.9	76.2	2	622.2	10.0	46.0039	-117.2631	67.4	213.6	17.1	18.5
GP5	16, 18, 82	19.7	76.5	3	156.0	9.9	46.1489	-117.4564	68.8	266.4	17.0	18.4
GP6	35, 114	5.5	55.5	2	798.5	8.8	46.3244	-117.5187	78.9	38.7	9.0	12.6
GP7	61, 81, 104	353.3	54.2	3	389.5	6.3	46.5325	-117.6876	77.2	87.9	6.2	8.9
GP8	49, 107	346.3	64.0	2	451.7	11.8	46.5024	-117.4741	80.5	152.7	15.0	18.8
GP9	56, 101, 105	358.9	43.3	3	723.0	4.6	46.5507	-117.6047	68.7	65.1	3.6	5.7
GP10	95, 98	347.7	56.0	2	301.8	14.4	46.6212	-117.7950	76.4	108.9	14.9	20.7
GP11	86, 100	26.9	53.9	2	2114.0	5.4	46.5920	-117.8107	66.4	353.5	5.3	7.6
GP12	28, 106	10.1	65.0	2	570.0	10.5	46.2721	-117.4209	83.0	323.0	13.7	16.9
GP13	57, 87	22.1	64.7	2	220.4	16.9	46.4893	-117.6256	74.9	323.9	21.8	27.2

Table 5: List of outliers determined for each grouping and cutoff scenario.

Cutoff Scenario	Determined Outliers
<i>Grouped</i>	
Visual inspection	24, 33, 34, 52, 59, 68, 71, 76, 78, 109, 115
45 degree	24, 33, 34, 52, 68, 71, 76, 78, 109, 115
Vandamme	24, 33, 34, 52, 68, 71, 76, 78, 109, 115
<i>Ungrouped</i>	
Visual inspection	24, 33, 34, 52, 59, 68, 71, 76, 78, 109, 115
45 degree	24, 33, 34, 52, 68, 71, 76, 78, 109, 115
Vandamme	24, 33, 34, 52, 68, 71, 76, 78, 109, 115

Table 6: List of site means of reverse and normal polarity directions for different grouping and cutoff scenarios and their mean.

Normal Polarity

Scenario	Dec	Inc	n	k	a95
Grouped, visual inspection cutoff	6.9	61.3	42	32.8	3.9
Grouped, 45 degree cutoff	7.1	60.5	43	29.4	4.1
Grouped, Vandamme cutoff	7.1	60.5	43	29.4	4.1
Ungrouped, visual inspection cutoff	6.3	61.2	56	33.3	3.3
Ungrouped, 45 degree cutoff	6.5	69.6	57	30.5	3.5
Ungrouped, Vandamme cutoff	6.5	69.6	57	30.5	3.5
Mean	6.8	63.8	6	321.5	3.7

Reverse Polarity

Scenario	Dec	Inc	n	k	a95
Grouped, visual inspection cutoff	177.6	-59.6	44	15.7	5.6
Grouped, 45 degree cutoff	177.6	-59.6	44	15.7	5.6
Grouped, Vandamme cutoff	177.6	-59.6	44	15.7	5.6
Ungrouped, visual inspection cutoff	180.1	-61.0	50	16.8	5.1
Ungrouped, 45 degree cutoff	180.1	-61.0	50	16.8	5.1
Ungrouped, Vandamme cutoff	180.1	-61.0	50	16.8	5.1
Mean	178.8	-60.3	6	6263.0	0.8

Table 7: Compilation of paleomagnetic site means from previous studies on the Columbia River Basalt region. The directions listed here are similar to those determined in this study (*Compiled by Michael G. Sawlan and Jonathan T. Hagstrum*).

Unit	Member	Dec	Inc	k	a95	Reference
Lower Monumental	Saddle Mountain Basalt					
LM 1		341.8	71.2	-	3.5	Choiniere & Swanson, 1979
LM 2		334.6	55.0	-	9.8	Choiniere & Swanson, 1979
Goose Island	Saddle Mountain Basalt					
GI 1		51.3	-19.2	-	11.7	Choiniere & Swanson, 1979
GI 2		33.5	-31.9	-	13.3	Choiniere & Swanson, 1979
Martindale	Saddle Mountain Basalt					
MA 1		185.1	-55.1	-	3.0	Choiniere & Swanson, 1979
MA 2		168.2	-65.0	-	3.3	Choiniere & Swanson, 1979
Basin City	Saddle Mountain Basalt					
BC 1		317.0	54.7	-	4.2	Choiniere & Swanson, 1979
BC 2		319.3	49.5	-	6.3	Choiniere & Swanson, 1979
BC 3		24.0	68.5	-	1.7	Choiniere & Swanson, 1979
Elephant Mountain	Saddle Mountain Basalt					
EM-1		126.6	-15.5	23	14.4	Rietman, 1966
EM-2		123.2	-27.9	22	14.5	Rietman, 1966
EM-3		136.5	-31.0	22	16.9	Rietman, 1966
EM-4		132.5	-37.4	30	14.2	Rietman, 1966
EM-5		115.0	-20.0	-	-	Rietman, 1966
EM-6		135.0	-35.0	-	-	Rietman, 1966
EM 1		6.9	59.6	-	4.2	Choiniere & Swanson, 1979
EM 2		14.2	62.5	-	8.3	Choiniere & Swanson, 1979
EM 3		115.2	-25.6	-	9.3	Choiniere & Swanson, 1979
EM 4		127.9	-39.5	-	9.8	Choiniere & Swanson, 1979
EM2C4		125.6	-38.8	-	5.3	Van Alstine & Gillett, 1981
EM2D2		138.6	-46.9	-	6.1	Van Alstine & Gillett, 1981
EMF2		131.9	-38.5	-	3.9	Van Alstine & Gillett, 1981
EM1D2		137.0	-32.2		12.3	Van Alstine & Gillett, 1981
Pomona	Saddle Mountain Basalt					
PO-1		192.8	-52.7	235	3.6	Rietman, 1966
PO-2		191.9	-52.1	161	4.8	Rietman, 1966
PO-3		191.9	-47.8	209	4.6	Rietman, 1966
PO-4		193.3	-50.1	146	5.6	Rietman, 1966
PO-5*		185.7	-54.4	175	4.6	Rietman, 1966
PO-6		186.2	-51.8	26	13.3	Rietman, 1966
PO-7		192.9	-46.7	39	10.9	Rietman, 1966
PO-8		185.8	-48.4	48	8.1	Rietman, 1966
PO-9*		191.7	-48.8	104	5.5	Rietman, 1966
PO-10		197.7	-51.5	104	7.5	Rietman, 1966
PO-11		182.1	-52.4	250	3.8	Rietman, 1966
PO 1*		187.8	-51.9	1500	1.7	Choiniere & Swanson, 1979
PO 2*		186.3	-53.4	900	2.2	Choiniere & Swanson, 1979
PO 3		203.4	-54.6	1100	2.0	Choiniere & Swanson, 1979
PO 4*		195.4	-50.6	500	2.9	Choiniere & Swanson, 1979
P2C5		205.1	-48.3	-	3.5	Van Alstine & Gillett, 1981
P2D1		180.3	-63.7	-	3.4	Van Alstine & Gillett, 1981
P1D1		194.5	-43.8	-	1.6	Van Alstine & Gillett, 1981
PF2		183.8	-49.2	-	1.9	Van Alstine & Gillett, 1981
PF1		200.3	-56.8	-	3.2	Van Alstine & Gillett, 1981
PO-1		192.8	-52.7	235	3.6	Magill et al., 1982
PO-2		191.9	-52.1	161	4.8	Magill et al., 1982
PO-3		191.9	-47.8	209	4.6	Magill et al., 1982
PO-4		193.3	-50.1	146	5.6	Magill et al., 1982
PO-5		185.7	-54.4	175	4.6	Magill et al., 1982

Unit	Member	Dec	Inc	k	a95	Reference
PO-6		186.2	-51.8	26	13.3	Magill et al., 1982
PO-7		192.9	-46.7	39	10.9	Magill et al., 1982
PO-8		185.8	-48.4	48	8.1	Magill et al., 1982
PO-9		191.7	-48.8	104	5.5	Magill et al., 1982
PO-10		197.7	-51.5	104	7.5	Magill et al., 1982
PO-11		182.1	-52.4	250	3.8	Magill et al., 1982
A		198.0	-52.0	601	2.3	Reidel et al., 1984
C		203.4	-52.0	558	2.4	Reidel et al., 1984
D		187.7	-57.5	17	13.7	Reidel et al., 1984
E		202.4	-52.2	506	2.5	Reidel et al., 1984
F		179.4	-52.0	178	4.5	Reidel et al., 1984
G		186.8	-52.0	201	3.9	Reidel et al., 1984
J		221.9	-51.8	405	2.4	Reidel et al., 1984
K		221.1	-51.3	1320	1.7	Reidel et al., 1984
L*		192.5	-53.7	382	2.5	Reidel et al., 1984
M*		191.0	-49.3	376	2.4	Reidel et al., 1984
N*		195.0	-54.5	415	2.5	Reidel et al., 1984
EPB1*		188.6	-51.5	691	2.1	Reidel et al., 1984
WPB1*		185.2	-54.4	447	2.6	Reidel et al., 1984
A1		210.0	-52.0	258	4.2	Reidel et al., 1984
B1		202.1	-51.9	280	4.0	Reidel et al., 1984
C1		204.0	-52.0	411	2.7	Reidel et al., 1984
D1		196.8	-52.0	666	2.2	Reidel et al., 1984
E1		201.2	-51.3	554	2.4	Reidel et al., 1984
F1		203.0	-52.7	354	3.0	Reidel et al., 1984
G1		198.7	-52.2	1090	1.7	Reidel et al., 1984
H1		198.5	-50.6	1120	1.6	Reidel et al., 1984
I1		204.4	-51.0	2860	1.0	Reidel et al., 1984
J1		202.2	-51.1	100	6.7	Reidel et al., 1984
K1		196.6	-51.0	733	2.1	Reidel et al., 1984
L1		198.3	-50.6	311	3.2	Reidel et al., 1984
N1		193.0	-51.6	506	2.5	Reidel et al., 1984
A2		221.1	-50.8	453	2.6	Reidel et al., 1984
B2		198.0	-52.1	511	2.5	Reidel et al., 1984
D2		200.6	-51.6	192	4.0	Reidel et al., 1984
A3		189.7	-51.4	457	2.6	Reidel et al., 1984
B3		193.5	-50.8	1800	1.3	Reidel et al., 1984
C3		192.3	-50.8	311	3.2	Reidel et al., 1984
BO13		188.4	-45.6	30	12.2	Wells et al., 1989
ML4		182.3	-43.0	34	13.3	Wells et al., 1989
Esquatzel	Saddle Mountain Basalt					
EQ 1		340.8	63.0	-	3.6	Choiniere & Swanson, 1979
EQ 2		308.0	81.7	-	11.4	Choiniere & Swanson, 1979
EC6A		342.9	64.1	-	3.0	Van Alstine & Gillett, 1981
EC6B		339.5	63.9	-	2.0	Van Alstine & Gillett, 1981
EF2		3.6	65.2	-	2.0	Van Alstine & Gillett, 1981
Huntzinger	Saddle Mountain Basalt					
HU-1		305.6	79.1	37	11.2	Rietman, 1966
HU-2		353.5	70.0	353	3.0	Rietman, 1966
A2C1		335.2	67.4	-	2.6	Van Alstine & Gillett, 1981
A?C5		23.7	80.6	-	4.5	Van Alstine & Gillett, 1981
Wilber Creek	Saddle Mountain Basalt					
WC2		345.7	72.1	-	3.4	Van Alstine & Gillett, 1981
Sillusi	Saddle Mountain Basalt					
SE2		321.7	32.2	-	2.6	Van Alstine & Gillett, 1981
Umatilla	Saddle Mountain Basalt					
UM-1		332.8	44.8	174	5.1	Rietman, 1966

Unit	Member	Dec	Inc	k	a95	Reference
UF1		354.6	52.0	-	11.2	Van Alstine & Gillett, 1981
UE1		324.3	31.7	-	3.4	Van Alstine & Gillett, 1981
Priest Rapids	Wanapum Basalt					
PR-1		191.3	-65.9	132	4.2	Rietman, 1966
PR-2		187.9	-65.1	394	2.8	Rietman, 1966
PR-3		196.1	-63.6	111	5.7	Rietman, 1966
PR-4		195.3	-65.5	1142	2.0	Rietman, 1966
PR-5		191.6	-62.8	315	3.1	Rietman, 1966
PR-6		188.0	-64.4	418	3.3	Rietman, 1966
PR-7		181.9	-60.9	297	3.5	Rietman, 1966
PR-8		194.8	-65.0	135	5.8	Rietman, 1966
PRC1		190.5	-64.9		2.8	Van Alstine & Gillett, 1981
Roza	Wanapum Basalt					
RO-1		192.2	8.4	65	6.9	Rietman, 1966
RO-2		183.2	-1.6	135	5.8	Rietman, 1966
RO-3		191.9	-0.3	156	4.4	Rietman, 1966
RO-4		190.9	1.9	52	10.7	Rietman, 1966
RO-5		189.7	-11.6	37	9.2	Rietman, 1966
RO-6		188.8	-6.0	28	11.6	Rietman, 1966
RO-7		185.1	-17.5	83	6.1	Rietman, 1966
RO-8		183.2	-21.2	76	7.8	Rietman, 1966
RO-9		196.2	4.4	70	8.1	Rietman, 1966
RO-10		190.0	-12.0	-	-	Rietman, 1966
RO-11		180.0	-1.0	-	-	Rietman, 1966
RZ 1		214.2	-14.7	-	7.3	Choiniere & Swanson, 1979
RZ 2		184.7	-38.7	-	7.0	Choiniere & Swanson, 1979
Sentinel Gap	Wanapum Basalt					
FS-2		347.5	62.7	409	3.0	Rietman, 1966
SGA3		5.0	62.8	-	2.2	Van Alstine & Gillett, 1981
DC7		356.6	62.5	390	2.8	Wells et al., 1989
Sand Hollow	Wanapum Basalt					
FS-3		358.6	62.4	385	2.8	Rietman, 1966
FS-4		342.2	58.2	120	5.1	Rietman, 1966
FS-12		0.6	60.5	537	2.6	Rietman, 1966
BO12		356.5	58.8	679	2.0	Wells et al., 1989
ML3		0.0	62.5	597	2.3	Wells et al., 1989
Silver Falls	Wanapum Basalt					
SHA1		144.7	39.8	-	3.6	Van Alstine & Gillett, 1981
DC5		353.5	58.0	800	2.0	Wells et al., 1989
Ginkgo	Wanapum Basalt					
FS-1		138.4	46.0	122	5.0	Rietman, 1966
FS-14		146.7	26.4	36	11.3	Rietman, 1966
GA2		146.1	42.1		2.6	Van Alstine & Gillett, 1981
1		135.1	48.3	200	4.9	Sheriff, 1984
2		147.3	42.9	137	4.4	Sheriff, 1984
3		147.0	49.9	155	4.5	Sheriff, 1984
4		145.7	39.0	138	4.7	Sheriff, 1984
5		141.7	39.6	76	6.4	Sheriff, 1984
6		148.3	35.3	94	6.3	Sheriff, 1984
7		148.7	38.9	54	7.6	Sheriff, 1984
8		153.9	43.7	42	8.7	Sheriff, 1984
9		151.3	51.2	77	6.4	Sheriff, 1984
10		155.4	42.7	89	5.9	Sheriff, 1984
11		158.1	42.1	50	8.7	Sheriff, 1984
12		147.5	54.0	106	12.0	Sheriff, 1984
13		146.1	46.1	-	-	Sheriff, 1984
14		186.1	58.1	15	16.4	Sheriff, 1984

Unit	Member	Dec	Inc	k	a95	Reference
15		168.3	51.2	145	10.3	Sheriff, 1984
DC4		140.3	45.0	172	5.9	Wells et al., 1989
BO11		137.9	51.7	31	12.2	Wells et al., 1989
Palouse Falls	Wanapum Basalt					
DC2		69.0	24.1	161	4.4	Wells et al., 1989
DC1		70.2	21.0	419	2.7	Wells et al., 1989
Dodge	Wanapum Basalt					
DJ 1		3.5	62.6	-	1.2	Choiniere & Swanson, 1979
DJ 2		0.9	59.5	-	3.6	Choiniere & Swanson, 1979
Robinette Mountain	Wanapum Basalt					
RM 1		344.2	62.5	-	6.5	Choiniere & Swanson, 1979
Museum	Grande Ronde Basalt					
MP-1		306.2	75.2	143	4.6	Rietman, 1966
MP-2		297.2	73.0	111	5.7	Rietman, 1966
Museum		344.3	75.9	-	1.8	Coe et al., 1978
BO10		327.5	72.8	259	3.8	Wells et al., 1989
Rocky Coulee	Grande Ronde Basalt					
RC-1		2.3	75.7	196	4.0	Rietman, 1966
RC-2		3.6	69.8	188	5.6	Rietman, 1966
RC		332.5	80.4	-	3.9	Coe et al., 1978
11		333.3	84.0	-	9.9	Beck et al., 1978
J		2.6	60.8	-	3.5	Coe et al., 1978
I		0.5	64.7	-	5.6	Coe et al., 1978
G		1.3	56.5	-	2.6	Coe et al., 1978
F		7.1	59.4	-	1.8	Coe et al., 1978
BO9		5.3	58.4	843	2.1	Wells et al., 1989
B08		6.0	54.5	1382	2.5	Wells et al., 1989
10		6.6	57.0	-	4.6	Beck et al., 1978
9		4.3	68.9	-	4.9	Beck et al., 1978
8		7.3	71.5	-	10.5	Beck et al., 1978
McCoy Canyon	Grande Ronde Basalt					
E		355.0	69.0	-	1.7	Coe et al., 1978
7		359.1	64.5	-	3.5	Beck et al., 1978
6		344.7	70.2	-	5.3	Beck et al., 1978
5		355.3	64.7	-	8.5	Beck et al., 1978
CB/GR-5		356.4	64.5	-	3.6	Van Alstine & Gillett, 1981
BO7		354.7	59.8	635	3.6	Wells et al., 1989
BO6		352.5	67.7	1501	1.4	Wells et al., 1989
Winter Water	Grande Ronde Basalt					
CB/GR-6		328.6	25.7	-	5.1	Van Alstine & Gillett, 1981
ML2		336.4	11.8	-	2.7	Wells et al., 1989
PQG 90-1		337.1	12.0	-	3.0	Hooper et al., 1993
Umtanum	Grande Ronde Basalt					
D		349.3	41.8	-	9.0	Coe et al., 1978
C		337.1	36.9	-	9.8	Coe et al., 1978
4		344.2	39.6	-	5.3	Beck et al., 1978
BO5		339.2	40.8	149	5.0	Wells et al., 1989
BO4		338.8	44.0	80	6.8	Wells et al., 1989
Ortley	Grande Ronde Basalt					
CB/GR-7		0.6	61.7	-	5.0	Van Alstine & Gillett, 1981
B		359.4	67.1	-	2.2	Coe et al., 1978
3		355.8	67.2	-	6.8	Beck et al., 1978
BO3		6.7	58.9	27	18.2	Wells et al., 1989
2		17.9	62.8	-	6.7	Beck et al., 1978
1		16.2	63.2	-	6.3	Beck et al., 1978
B02		33.1	64.1	272	4.1	Wells et al., 1989
ML1		41.7	60.8	78	14.0	Wells et al., 1989

Unit	Member	Dec	Inc	k	a95	Reference
BO1		80.2	65.6	58	10.2	Wells et al., 1989
PQG 90-5		62.9	72.1	-	14.5	Hooper et al., 1993
Grouse Creek	Grande Ronde Basalt					
A		267.3	-86.8	-	5.6	Coe et al., 1978

Table 8: Dispersion calculation for normal polarity, grouped sites with a visual inspection cutoff.

Site	Plat	k	K	n	Delta	Sw/sqrt(n)
GP3	47.4904	120.8	55.4	2	23.120	7.694
GP4	46.9524	622.2	289.7	2	22.614	3.365
GP5	47.0917	156.0	72.4	3	19.688	5.498
GP6	44.4393	798.5	399.6	2	11.481	2.865
GP7	47.4683	389.5	178.8	3	14.407	3.498
GP8	47.4444	451.7	207.5	2	11.163	3.976
GP9	47.4889	723.0	331.7	3	22.392	2.568
GP10	47.5538	301.8	138.2	2	15.448	4.872
GP11	47.5242	2114.0	968.9	2	22.476	1.840
GP12	47.2158	570.0	263.5	2	5.283	3.529
GP13	47.4269	220.4	101.3	2	13.368	5.691
7	47.0050	79.9	37.2	6	6.703	5.425
8	46.9914	89.2	41.5	6	22.146	5.134
15	46.9786	62.7	29.2	6	19.232	6.122
17	46.9511	61.2	28.5	6	35.396	6.194
44	47.3542	912.4	420.1	6	22.004	1.613
45	47.3565	5312.0	2445.9	2	20.455	1.158
50	47.3860	460.2	211.7	5	17.830	2.490
51	47.3858	28.3	13.0	6	18.040	9.164
53	47.3884	37.8	17.4	6	40.497	7.930
54	47.4056	163.8	75.3	6	23.360	3.810
55	47.3888	517.4	238.0	4	18.600	2.625
58	47.4089	82.5	37.9	6	12.253	5.369
60	47.4088	120.6	55.4	6	7.988	4.441
70	47.5722	64.1	29.3	6	13.602	6.105
74	47.3780	31.0	14.3	6	29.839	8.755
75	47.3783	9.7	4.5	5	23.191	17.146
83	47.4503	41.2	18.9	7	29.164	7.038
84	47.4483	36.7	16.9	6	22.596	8.055
88	47.4579	105.3	48.3	5	10.433	5.210
90	47.4773	36.9	16.9	8	15.982	6.959
91	47.4924	65.7	30.1	7	15.604	5.577
92	47.4965	69.6	31.9	4	20.706	7.168
94	47.5229	45.3	20.8	5	7.015	7.950
99	47.5886	76.2	34.9	5	15.675	6.135
102	47.5623	32.7	15.0	6	22.327	8.546
103	47.5597	91.8	42.0	6	13.371	5.101
110	47.4718	89.0	40.8	2	37.896	8.962
113	47.5812	58.7	26.9	6	18.590	6.381
116	47.5067	25.9	11.9	6	13.724	9.596
117	47.4870	70.1	32.2	6	17.422	5.831
118	47.4635	199.7	91.7	6	7.948	3.454

S	Sb	Sw/sqrt(n)	VGP Lat	VGP Long	K	A95
20.434	19.384	6.465	88.110	301.761	16.010	5.687

N	Site Lat	Site Long	Paleolat
42	47.534	241.297	48.439

Table 9: Dispersion calculation for reverse polarity, grouped sites with a visual inspection cutoff.

Site	Plat	k	K	n	Delta	Sw/sqrt(n)
GP1	-43.3447	7760.0	4010.9	2	26.123	0.904
GP2	-43.2329	569.4	295.3	6	17.726	1.924
1	-43.5096	67.4	34.7	7	7.863	5.200
2	-43.5194	78.4	40.3	6	19.761	5.208
4	-43.2496	23.1	12.0	7	39.184	8.848
6	-43.2462	55.9	29.0	6	8.367	6.143
9	-43.2778	42.4	22.0	6	24.896	7.057
12	-43.2695	81.8	42.4	2	5.622	8.799
19	-43.1807	143.5	74.5	6	22.637	3.830
20	-43.1781	170.3	88.5	4	6.822	4.306
21	-43.1743	98.2	51.0	6	12.243	4.630
25	-43.1684	75.5	39.2	6	22.930	5.280
27	-42.8314	24.4	12.8	5	27.660	10.122
29	-43.1692	70.1	36.4	6	32.632	5.479
31	-43.1762	282.0	146.5	5	16.476	2.993
32	-43.1917	265.7	138.0	6	38.441	2.815
36	-43.6129	45.5	23.3	6	18.052	6.846
37	-43.6152	66.3	34.0	6	19.135	5.672
38	-43.6186	199.3	102.2	6	23.509	3.271
39	-43.6226	153.6	78.7	5	10.059	4.082
40	-43.6235	87.4	44.8	6	8.170	4.940
41	-43.6277	202.3	103.7	5	9.289	3.558
42	-43.6236	96.4	49.4	5	8.189	5.153
43	-43.6194	78.8	40.4	4	17.054	6.372
46	-43.6098	67.1	34.4	5	25.747	6.175
47	-43.6353	177.3	90.9	5	13.059	3.800
48	-43.6376	475.4	243.6	6	18.508	2.119
62	-43.6281	115.1	59.0	6	35.681	4.305
63	-43.6491	58.5	30.0	5	32.882	6.618
64	-43.6488	24.9	12.8	6	29.367	9.259
65	-43.6570	1059.0	542.3	6	26.986	1.420
66	-43.6628	89.9	46.0	6	16.531	4.874
67	-43.6624	52.4	26.8	6	20.700	6.384
69	-43.7062	90.5	46.3	5	30.378	5.325
72	-43.8060	164.1	83.7	2	28.817	6.262
73	-43.6559	51.9	26.6	6	9.357	6.414
77	-43.6241	65.3	33.5	7	38.181	5.292
79	-43.7088	70.0	35.8	5	11.555	6.055
80	-43.8382	85.8	43.7	7	12.054	4.631
89	-43.7204	56.6	28.9	4	18.095	7.530
96	-43.7938	7.7	3.9	4	29.404	20.437
97	-43.8119	35.6	18.1	2	27.810	13.445
111	-43.7029	80.2	41.0	3	25.587	7.302
112	-43.6748	19.7	10.1	5	41.924	11.408

S	Sb	Sw/sqrt(n)	VGP Lat	VGP Long	K	A95
23.701	22.673	6.904	-87.194	240.471	11.965	6.4946

N	Site Lat	Site Long	Paleolat
44	46.316	242.716	-43.512

Table 10: Dispersion calculation for normal polarity, grouped sites with a 45° cutoff.

Site	Plat	k	K	n	Delta	Sw/sqrt(n)
GP3	46.7134	120.8	56.6	2	22.699	7.611
GP4	46.1771	622.2	296.1	2	23.396	3.328
GP5	46.3156	156.0	74.0	3	20.321	5.438
GP6	44.6646	798.5	397.0	2	10.673	2.875
GP7	46.6912	389.5	182.7	3	13.877	3.460
GP8	46.6681	451.7	212.0	2	11.380	3.934
GP9	46.7121	723.0	339.0	3	21.659	2.540
GP10	46.7763	301.8	141.2	2	15.140	4.820
GP11	46.7466	2114.0	990.1	2	21.933	1.820
GP12	46.4398	570.0	269.3	2	5.116	3.490
GP13	46.6501	220.4	103.5	2	13.213	5.630
7	46.2298	79.9	38.0	6	6.080	5.366
8	46.2161	89.2	42.4	6	22.897	5.078
15	46.2033	62.7	29.8	6	19.606	6.056
17	46.1758	61.2	29.1	6	36.060	6.127
44	46.5789	912.4	429.4	6	21.274	1.596
45	46.5812	5312.0	2499.5	2	19.668	1.146
50	46.6101	460.2	216.4	5	17.111	2.463
51	46.6099	28.3	13.3	6	17.554	9.066
53	46.6123	37.8	17.8	6	41.293	7.844
54	46.6294	163.8	77.0	6	22.620	3.769
55	46.6126	517.4	243.2	4	18.057	2.597
58	46.6326	82.5	38.8	6	11.476	5.311
59	46.6327	254.8	119.7	6	33.854	3.022
60	46.6324	120.6	56.7	6	7.199	4.393
70	46.7965	64.1	30.0	6	14.393	6.039
74	46.6030	31.0	14.6	6	30.608	8.661
75	46.6033	9.7	4.6	5	23.992	16.961
83	46.6728	41.2	19.3	7	29.964	6.962
84	46.6708	36.7	17.2	6	23.368	7.968
88	46.6804	105.3	49.4	5	9.634	5.153
90	46.6998	36.9	17.3	8	15.308	6.884
91	46.7150	65.7	30.8	7	15.044	5.517
92	46.7191	69.6	32.6	4	20.239	7.091
94	46.7454	45.3	21.2	5	7.297	7.864
99	46.8110	76.2	35.6	5	16.276	6.069
102	46.7850	32.7	15.3	6	22.403	8.454
103	46.7828	91.8	43.0	6	12.822	5.046
110	46.6952	89.0	41.7	2	37.829	8.865
113	46.8039	58.7	27.4	6	18.435	6.312
116	46.7294	25.9	12.1	6	13.818	9.492
117	46.7099	70.1	32.9	6	18.068	5.768
118	46.6868	199.7	93.7	6	7.191	3.416

S	Sb	Sw/sqrt(n)	VGP Lat	VGP Long	K	A95
20.8746	19.8899	6.3359	88.111	326.4988	15.3602	5.7438

N	Site Lat	Site Long	Paleolat
43	47.5085	241.3257	47.6336

Table 11: Dispersion calculation for reverse polarity, grouped sites with a 45° cutoff.

Site	Plat	k	K	n	Delta	Sw/sqrt(n)
GP1	-43.3447	7760.0	4010.9	2	26.123	0.904
GP2	-43.2329	569.4	295.3	6	17.726	1.924
1	-43.5096	67.4	34.7	7	7.863	5.200
2	-43.5194	78.4	40.3	6	19.761	5.208
4	-43.2496	23.1	12.0	7	39.184	8.848
6	-43.2462	55.9	29.0	6	8.367	6.143
9	-43.2778	42.4	22.0	6	24.896	7.057
12	-43.2695	81.8	42.4	2	5.622	8.799
19	-43.1807	143.5	74.5	6	22.637	3.830
20	-43.1781	170.3	88.5	4	6.822	4.306
21	-43.1743	98.2	51.0	6	12.243	4.630
25	-43.1684	75.5	39.2	6	22.930	5.280
27	-42.8314	24.4	12.8	5	27.660	10.122
29	-43.1692	70.1	36.4	6	32.632	5.479
31	-43.1762	282.0	146.5	5	16.476	2.993
32	-43.1917	265.7	138.0	6	38.441	2.815
36	-43.6129	45.5	23.3	6	18.052	6.846
37	-43.6152	66.3	34.0	6	19.135	5.672
38	-43.6186	199.3	102.2	6	23.509	3.271
39	-43.6226	153.6	78.7	5	10.059	4.082
40	-43.6235	87.4	44.8	6	8.170	4.940
41	-43.6277	202.3	103.7	5	9.289	3.558
42	-43.6236	96.4	49.4	5	8.189	5.153
43	-43.6194	78.8	40.4	4	17.054	6.372
46	-43.6098	67.1	34.4	5	25.747	6.175
47	-43.6353	177.3	90.9	5	13.059	3.800
48	-43.6376	475.4	243.6	6	18.508	2.119
62	-43.6281	115.1	59.0	6	35.681	4.305
63	-43.6491	58.5	30.0	5	32.882	6.618
64	-43.6488	24.9	12.8	6	29.367	9.259
65	-43.6570	1059.0	542.3	6	26.986	1.420
66	-43.6628	89.9	46.0	6	16.531	4.874
67	-43.6624	52.4	26.8	6	20.700	6.384
69	-43.7062	90.5	46.3	5	30.378	5.325
72	-43.8060	164.1	83.7	2	28.817	6.262
73	-43.6559	51.9	26.6	6	9.357	6.414
77	-43.6241	65.3	33.5	7	38.181	5.292
79	-43.7088	70.0	35.8	5	11.555	6.055
80	-43.8382	85.8	43.7	7	12.054	4.631
89	-43.7204	56.6	28.9	4	18.095	7.530
96	-43.7938	7.7	3.9	4	29.404	20.437
97	-43.8119	35.6	18.1	2	27.810	13.445
111	-43.7029	80.2	41.0	3	25.587	7.302
112	-43.6748	19.7	10.1	5	41.924	11.408

S	Sb	Sw/sqrt(n)	VGP Lat	VGP Long	K	A95
23.7007	22.6729	6.9039	-87.1937	240.4705	11.9649	6.4946
N	Site Lat	Site Long	Paleolat			
44	46.3162	242.7163	-43.5119			

Table 12: Dispersion calculation for normal polarity, grouped sites with a *Vandamme (1994)* cutoff.

Site	Plat	k	K	n	Delta	Sw/sqrt(n)
GP3	46.7134	120.8	56.6	2	22.699	7.611
GP4	46.1771	622.2	296.1	2	23.396	3.328
GP5	46.3156	156.0	74.0	3	20.321	5.438
GP6	44.6646	798.5	397.0	2	10.673	2.875
GP7	46.6912	389.5	182.7	3	13.877	3.460
GP8	46.6681	451.7	212.0	2	11.380	3.934
GP9	46.7121	723.0	339.0	3	21.659	2.540
GP10	46.7763	301.8	141.2	2	15.140	4.820
GP11	46.7466	2114.0	990.1	2	21.933	1.820
GP12	46.4398	570.0	269.3	2	5.116	3.490
GP13	46.6501	220.4	103.5	2	13.213	5.630
7	46.2298	79.9	38.0	6	6.080	5.366
8	46.2161	89.2	42.4	6	22.897	5.078
15	46.2033	62.7	29.8	6	19.606	6.056
17	46.1758	61.2	29.1	6	36.060	6.127
44	46.5789	912.4	429.4	6	21.274	1.596
45	46.5812	5312.0	2499.5	2	19.668	1.146
50	46.6101	460.2	216.4	5	17.111	2.463
51	46.6099	28.3	13.3	6	17.554	9.066
53	46.6123	37.8	17.8	6	41.293	7.844
54	46.6294	163.8	77.0	6	22.620	3.769
55	46.6126	517.4	243.2	4	18.057	2.597
58	46.6326	82.5	38.8	6	11.476	5.311
59	46.6327	254.8	119.7	6	33.854	3.022
60	46.6324	120.6	56.7	6	7.199	4.393
70	46.7965	64.1	30.0	6	14.393	6.039
74	46.6030	31.0	14.6	6	30.608	8.661
75	46.6033	9.7	4.6	5	23.992	16.961
83	46.6728	41.2	19.3	7	29.964	6.962
84	46.6708	36.7	17.2	6	23.368	7.968
88	46.6804	105.3	49.4	5	9.634	5.153
90	46.6998	36.9	17.3	8	15.308	6.884
91	46.7150	65.7	30.8	7	15.044	5.517
92	46.7191	69.6	32.6	4	20.239	7.091
94	46.7454	45.3	21.2	5	7.297	7.864
99	46.8110	76.2	35.6	5	16.276	6.069
102	46.7850	32.7	15.3	6	22.403	8.454
103	46.7828	91.8	43.0	6	12.822	5.046
110	46.6952	89.0	41.7	2	37.829	8.865
113	46.8039	58.7	27.4	6	18.435	6.312
116	46.7294	25.9	12.1	6	13.818	9.492
117	46.7099	70.1	32.9	6	18.068	5.768
118	46.6868	199.7	93.7	6	7.191	3.416

S	Sb	Sw/sqrt(n)	VGP Lat	VGP Long	K	A95
20.8746	19.8899	6.3359	88.111	326.4988	15.3602	5.7438

N	Site Lat	Site Long	Paleolat
43	47.5085	241.3257	47.6336

Table 13: Dispersion calculation for reverse polarity, grouped sites with a *Vandamme (1994)* cutoff.

Site	Plat	k	K	n	Delta	Sw/sqrt(n)
GP1	-43.3447	7760.0	4010.9	2	26.123	0.904
GP2	-43.2329	569.4	295.3	6	17.726	1.924
1	-43.5096	67.4	34.7	7	7.863	5.200
2	-43.5194	78.4	40.3	6	19.761	5.208
4	-43.2496	23.1	12.0	7	39.184	8.848
6	-43.2462	55.9	29.0	6	8.367	6.143
9	-43.2778	42.4	22.0	6	24.896	7.057
12	-43.2695	81.8	42.4	2	5.622	8.799
19	-43.1807	143.5	74.5	6	22.637	3.830
20	-43.1781	170.3	88.5	4	6.822	4.306
21	-43.1743	98.2	51.0	6	12.243	4.630
25	-43.1684	75.5	39.2	6	22.930	5.280
27	-42.8314	24.4	12.8	5	27.660	10.122
29	-43.1692	70.1	36.4	6	32.632	5.479
31	-43.1762	282.0	146.5	5	16.476	2.993
32	-43.1917	265.7	138.0	6	38.441	2.815
36	-43.6129	45.5	23.3	6	18.052	6.846
37	-43.6152	66.3	34.0	6	19.135	5.672
38	-43.6186	199.3	102.2	6	23.509	3.271
39	-43.6226	153.6	78.7	5	10.059	4.082
40	-43.6235	87.4	44.8	6	8.170	4.940
41	-43.6277	202.3	103.7	5	9.289	3.558
42	-43.6236	96.4	49.4	5	8.189	5.153
43	-43.6194	78.8	40.4	4	17.054	6.372
46	-43.6098	67.1	34.4	5	25.747	6.175
47	-43.6353	177.3	90.9	5	13.059	3.800
48	-43.6376	475.4	243.6	6	18.508	2.119
62	-43.6281	115.1	59.0	6	35.681	4.305
63	-43.6491	58.5	30.0	5	32.882	6.618
64	-43.6488	24.9	12.8	6	29.367	9.259
65	-43.6570	1059.0	542.3	6	26.986	1.420
66	-43.6628	89.9	46.0	6	16.531	4.874
67	-43.6624	52.4	26.8	6	20.700	6.384
69	-43.7062	90.5	46.3	5	30.378	5.325
72	-43.8060	164.1	83.7	2	28.817	6.262
73	-43.6559	51.9	26.6	6	9.357	6.414
77	-43.6241	65.3	33.5	7	38.181	5.292
79	-43.7088	70.0	35.8	5	11.555	6.055
80	-43.8382	85.8	43.7	7	12.054	4.631
89	-43.7204	56.6	28.9	4	18.095	7.530
96	-43.7938	7.7	3.9	4	29.404	20.437
97	-43.8119	35.6	18.1	2	27.810	13.445
111	-43.7029	80.2	41.0	3	25.587	7.302
112	-43.6748	19.7	10.1	5	41.924	11.408

S	Sb	Sw/sqrt(n)	VGP Lat	VGP Long	K	A95
23.7007	22.6729	6.9039	-87.1937	240.4705	11.9649	6.4946
N	Site Lat	Site Long	Paleolat			
44	46.3162	242.7163	-43.5119			

Table 14: Dispersion calculation for normal polarity, ungrouped sites with a visual inspection cutoff.

Site	Plat	k	K	n	Delta	Sw/sqrt(n)
7	46.0890	79.9	38.1	6	6.017	5.356
8	46.0753	89.2	42.6	6	23.097	5.068
14	46.0662	81.5	38.9	3	19.506	7.497
15	46.0625	62.7	29.9	6	19.777	6.044
16	46.0422	17.4	8.3	6	31.782	11.469
17	46.0349	61.2	29.2	6	36.260	6.115
18	46.0365	28.8	13.8	6	20.272	8.914
26	46.0066	201.7	96.5	4	27.759	4.124
28	45.9997	84.3	40.3	5	7.289	5.704
35	46.0412	30.1	14.4	6	12.020	8.720
44	46.4380	912.4	431.1	6	21.160	1.593
45	46.4403	5312.0	2509.5	2	19.522	1.143
49	46.4696	45.5	21.5	4	15.715	8.739
50	46.4689	460.2	217.2	5	17.002	2.458
51	46.4687	28.3	13.4	6	17.372	9.048
53	46.4709	37.8	17.8	6	41.484	7.829
54	46.4880	163.8	77.3	6	22.501	3.762
55	46.4712	517.4	244.2	4	18.016	2.592
56	46.4718	69.3	32.7	5	22.049	6.334
57	46.4802	51.9	24.5	6	15.889	6.682
58	46.4911	82.5	38.9	6	11.279	5.301
60	46.4909	120.6	56.9	6	7.053	4.384
61	46.4960	72.5	34.2	5	15.897	6.195
70	46.6553	64.1	30.1	6	14.546	6.028
74	46.4623	31.0	14.6	6	30.806	8.644
75	46.4627	9.7	4.6	5	24.180	16.927
81	46.5340	17.2	8.1	7	15.132	10.754
82	46.5349	44.0	20.7	3	11.510	10.271
83	46.5306	41.2	19.4	7	30.123	6.948
84	46.5286	36.7	17.3	6	23.508	7.952
86	46.5362	19.8	9.3	7	21.099	10.024
87	46.5353	22.0	10.4	8	11.743	8.895
88	46.5381	105.3	49.6	5	9.478	5.143
90	46.5576	36.9	17.4	8	15.219	6.870
91	46.5728	65.7	30.9	7	14.852	5.506
92	46.5769	69.6	32.8	4	20.058	7.077
93	46.5787	43.6	20.5	6	15.443	7.301
94	46.6031	45.3	21.3	5	7.279	7.849
95	46.6069	29.6	13.9	3	18.514	12.535
98	46.6612	48.2	22.6	4	12.789	8.514
99	46.6687	76.2	35.8	5	16.473	6.057
100	46.6723	52.3	24.5	2	22.495	11.561
101	46.6298	26.3	12.4	5	22.842	10.304
102	46.6429	32.7	15.4	6	22.325	8.438
103	46.6409	91.8	43.1	6	12.632	5.036
104	46.6178	64.1	30.1	5	11.832	6.599
105	46.6093	37.8	17.8	5	20.211	8.593
106	46.5973	31.4	14.8	8	3.931	7.452
107	46.5839	128.5	60.5	2	7.506	7.366
108	46.5641	116.6	54.9	2	29.217	7.731
110	46.5536	89.0	41.9	2	37.718	8.847
113	46.6618	58.7	27.6	6	18.503	6.299
114	46.6536	497.9	233.8	6	9.306	2.163
116	46.5873	25.9	12.2	6	13.747	9.473
117	46.5680	70.1	33.0	6	18.269	5.757

Site	Plat	k	K	n	Delta	Sw/sqrt(n)
118	46.5451	199.7	94.1	6	6.991	3.410

S	Sb	Sw/sqrt(n)	VGP Lat	VGP Long	K	A95
20.0808	18.5428	7.7075	87.9716	330.7701	16.5765	4.8126

N	Site Lat	Site Long	Paleolat
56	46.4405	242.4513	46.4622

Table 15: Dispersion calculation for reverse polarity, ungrouped sites with a visual inspection cutoff.

Site	Plat	k	K	n	Delta	Sw/sqrt(n)
1	-44.9170	67.4	33.3	7	7.605	5.308
2	-44.9266	78.4	38.7	6	18.844	5.317
3	-44.9280	43.5	21.5	5	23.405	7.820
4	-44.6537	23.1	11.5	7	39.956	9.033
5	-44.6470	81.0	40.3	6	10.568	5.210
6	-44.6500	55.9	27.8	6	10.580	6.272
9	-44.6834	42.4	21.1	6	22.555	7.205
10	-44.6803	26.0	12.9	5	18.121	10.078
11	-44.6783	105.3	52.3	5	14.323	5.008
12	-44.6742	81.8	40.7	2	4.901	8.983
13	-44.6717	19.1	9.5	6	12.119	10.733
19	-44.5834	143.5	71.5	6	22.645	3.911
20	-44.5808	170.3	84.9	4	9.181	4.396
21	-44.5772	98.2	48.9	6	14.596	4.727
22	-44.5741	51.0	25.4	5	18.144	7.185
23	-44.5722	295.9	147.5	6	24.023	2.723
25	-44.5716	75.5	37.6	6	20.911	5.390
27	-44.2347	24.4	12.3	5	30.057	10.336
29	-44.5722	70.1	34.9	6	30.907	5.594
30	-44.5710	39.4	19.6	3	19.546	10.552
31	-44.5790	282.0	140.5	5	18.860	3.056
32	-44.5942	265.7	132.4	6	36.684	2.874
36	-45.0207	45.5	22.4	6	20.407	6.989
37	-45.0227	66.3	32.6	6	16.746	5.790
38	-45.0258	199.3	98.0	6	23.096	3.340
39	-45.0294	153.6	75.6	5	12.323	4.168
40	-45.0300	87.4	43.0	6	10.578	5.043
41	-45.0370	202.3	99.5	5	7.490	3.632
42	-45.0325	96.4	47.4	5	10.535	5.261
43	-45.0265	78.8	38.8	4	17.534	6.505
46	-45.0120	67.1	33.0	5	24.890	6.304
47	-45.0349	177.3	87.2	5	14.891	3.879
48	-45.0362	475.4	233.8	6	20.816	2.163
62	-45.0346	115.1	56.6	6	37.948	4.395
63	-45.0535	58.5	28.8	5	30.496	6.755
64	-45.0531	24.9	12.2	6	26.996	9.452
65	-45.0609	1059.0	520.4	6	29.028	1.450
66	-45.0664	89.9	44.2	6	15.544	4.975
67	-45.0660	52.4	25.7	6	22.773	6.517
69	-45.1097	90.5	44.4	5	32.245	5.436
72	-45.2070	164.1	80.3	2	30.297	6.391
73	-45.0346	51.9	25.5	6	9.060	6.545
77	-45.0297	65.3	32.1	7	40.447	5.402
79	-45.1122	70.0	34.3	5	10.013	6.181
80	-45.2402	85.8	41.9	7	12.656	4.727
89	-45.1051	56.6	27.8	4	16.177	7.684
96	-45.1789	7.7	3.8	4	28.028	20.855
97	-45.1968	35.6	17.4	2	25.471	13.720
111	-45.0953	80.2	39.4	3	27.737	7.453
112	-45.0670	19.7	9.7	5	42.414	11.643

S	Sb	Sw/sqrt(n)	VGP Lat	VGP Long	K	A95
23.1389	21.948	7.3277	-87.5435	186.4844	12.5457	5.9249

N	Site Lat	Site Long	Paleolat
50	46.2849	242.7238	-44.8829

Table 16: Dispersion calculation for normal polarity, ungrouped sites with a 45° cutoff.

Site	Plat	k	K	n	Delta	Sw/sqrt(n)
7	45.5189	79.9	38.8	6	5.602	5.312
8	45.5052	89.2	43.3	6	23.650	5.027
14	45.4960	81.5	39.6	3	20.086	7.436
15	45.4924	62.7	30.4	6	20.069	5.994
16	45.4720	17.4	8.5	6	32.326	11.376
17	45.4647	61.2	29.7	6	36.749	6.065
18	45.4663	28.8	14.0	6	20.647	8.841
26	45.4364	201.7	98.1	4	28.328	4.090
28	45.4296	84.3	41.0	5	7.060	5.658
35	45.4710	30.1	14.6	6	11.429	8.649
44	45.8678	912.4	438.1	6	20.629	1.580
45	45.8700	5312.0	2550.5	2	18.947	1.134
49	45.8990	45.5	21.8	4	15.952	8.669
50	45.8983	460.2	220.8	5	16.481	2.438
51	45.8981	28.3	13.6	6	17.034	8.975
53	45.9001	37.8	18.1	6	42.068	7.766
54	45.9172	163.8	78.5	6	21.962	3.731
55	45.9004	517.4	248.2	4	17.634	2.571
56	45.9010	69.3	33.2	5	21.516	6.283
57	45.9094	51.9	24.9	6	15.653	6.628
58	45.9202	82.5	39.6	6	10.711	5.258
59	45.9203	254.8	122.2	6	33.085	2.992
60	45.9200	120.6	57.8	6	6.480	4.349
61	45.9246	72.5	34.8	5	15.599	6.145
70	46.0848	64.1	30.6	6	15.129	5.979
74	45.8923	31.0	14.9	6	31.371	8.574
75	45.8927	9.7	4.7	5	24.768	16.791
81	45.9621	17.2	8.2	7	14.634	10.668
82	45.9631	44.0	21.1	3	11.938	10.188
83	45.9588	41.2	19.7	7	30.711	6.892
84	45.9568	36.7	17.6	6	24.077	7.887
86	45.9643	19.8	9.5	7	20.683	9.943
87	45.9635	22.0	10.5	8	11.919	8.823
88	45.9663	105.3	50.4	5	8.894	5.102
90	45.9859	36.9	17.7	8	14.736	6.815
91	46.0011	65.7	31.4	7	14.459	5.461
92	46.0051	69.6	33.3	4	19.732	7.020
93	46.0069	43.6	20.9	6	15.131	7.242
94	46.0314	45.3	21.7	5	7.550	7.785
95	46.0351	29.6	14.1	3	18.432	12.434
98	46.0894	48.2	23.0	4	12.438	8.445
99	46.0968	76.2	36.4	5	16.925	6.008
100	46.1005	52.3	24.9	2	22.140	11.467
101	46.0580	26.3	12.6	5	22.354	10.221
102	46.0713	32.7	15.6	6	22.405	8.370
103	46.0696	91.8	43.8	6	12.250	4.995
104	46.0465	64.1	30.6	5	11.592	6.546
105	46.0381	37.8	18.1	5	19.642	8.523
106	46.0261	31.4	15.0	8	4.311	7.392
107	46.0127	128.5	61.4	2	7.622	7.307
108	45.9930	116.6	55.8	2	28.934	7.668
110	45.9824	89.0	42.6	2	37.681	8.776
113	46.0902	58.7	28.0	6	18.415	6.248
114	46.0819	497.9	237.6	6	8.740	2.145
116	46.0156	25.9	12.4	6	13.854	9.397

Site	Plat	k	K	n	Delta	Sw/sqrt(n)
117	45.9965	70.1	33.5	6	18.751	5.710
118	45.9739	199.7	95.6	6	6.444	3.382

S	Sb	Sw/sqrt(n)	VGP Lat	VGP Long	K	A95
20.3986	18.935	7.5872	87.7313	345.3123	16.0785	4.8471

N	Site Lat	Site Long	Paleolat
57	46.441	242.4522	45.8917

Table 17: Dispersion calculation for reverse polarity, ungrouped sites with a 45° cutoff.

Site	Plat	k	K	n	Delta	Sw/sqrt(n)
1	-44.9170	67.4	33.3	7	7.605	5.308
2	-44.9266	78.4	38.7	6	18.844	5.317
3	-44.9280	43.5	21.5	5	23.405	7.820
4	-44.6537	23.1	11.5	7	39.956	9.033
5	-44.6470	81.0	40.3	6	10.568	5.210
6	-44.6500	55.9	27.8	6	10.580	6.272
9	-44.6834	42.4	21.1	6	22.555	7.205
10	-44.6803	26.0	12.9	5	18.121	10.078
11	-44.6783	105.3	52.3	5	14.323	5.008
12	-44.6742	81.8	40.7	2	4.901	8.983
13	-44.6717	19.1	9.5	6	12.119	10.733
19	-44.5834	143.5	71.5	6	22.645	3.911
20	-44.5808	170.3	84.9	4	9.181	4.396
21	-44.5772	98.2	48.9	6	14.596	4.727
22	-44.5741	51.0	25.4	5	18.144	7.185
23	-44.5722	295.9	147.5	6	24.023	2.723
25	-44.5716	75.5	37.6	6	20.911	5.390
27	-44.2347	24.4	12.3	5	30.057	10.336
29	-44.5722	70.1	34.9	6	30.907	5.594
30	-44.5710	39.4	19.6	3	19.546	10.552
31	-44.5790	282.0	140.5	5	18.860	3.056
32	-44.5942	265.7	132.4	6	36.684	2.874
36	-45.0207	45.5	22.4	6	20.407	6.989
37	-45.0227	66.3	32.6	6	16.746	5.790
38	-45.0258	199.3	98.0	6	23.096	3.340
39	-45.0294	153.6	75.6	5	12.323	4.168
40	-45.0300	87.4	43.0	6	10.578	5.043
41	-45.0370	202.3	99.5	5	7.490	3.632
42	-45.0325	96.4	47.4	5	10.535	5.261
43	-45.0265	78.8	38.8	4	17.534	6.505
46	-45.0120	67.1	33.0	5	24.890	6.304
47	-45.0349	177.3	87.2	5	14.891	3.879
48	-45.0362	475.4	233.8	6	20.816	2.163
62	-45.0346	115.1	56.6	6	37.948	4.395
63	-45.0535	58.5	28.8	5	30.496	6.755
64	-45.0531	24.9	12.2	6	26.996	9.452
65	-45.0609	1059.0	520.4	6	29.028	1.450
66	-45.0664	89.9	44.2	6	15.544	4.975
67	-45.0660	52.4	25.7	6	22.773	6.517
69	-45.1097	90.5	44.4	5	32.245	5.436
72	-45.2070	164.1	80.3	2	30.297	6.391
73	-45.0346	51.9	25.5	6	9.060	6.545
77	-45.0297	65.3	32.1	7	40.447	5.402
79	-45.1122	70.0	34.3	5	10.013	6.181
80	-45.2402	85.8	41.9	7	12.656	4.727
89	-45.1051	56.6	27.8	4	16.177	7.684
96	-45.1789	7.7	3.8	4	28.028	20.855
97	-45.1968	35.6	17.4	2	25.471	13.720
111	-45.0953	80.2	39.4	3	27.737	7.453
112	-45.0670	19.7	9.7	5	42.414	11.643

S	Sb	Sw/sqrt(n)	VGP Lat	VGP Long	K	A95
23.1389	21.948	7.3277	-87.5435	186.4844	12.5457	5.9249

N	Site Lat	Site Long	Paleolat
50	46.2849	242.7238	-44.8829

Table 18: Dispersion calculation for normal polarity, ungrouped sites with a *Vandamme (1994)* cutoff.

Site	Plat	k	K	n	Delta	Sw/sqrt(n)
7	45.5189	79.9	38.8	6	5.602	5.312
8	45.5052	89.2	43.3	6	23.650	5.027
14	45.4960	81.5	39.6	3	20.086	7.436
15	45.4924	62.7	30.4	6	20.069	5.994
16	45.4720	17.4	8.5	6	32.326	11.376
17	45.4647	61.2	29.7	6	36.749	6.065
18	45.4663	28.8	14.0	6	20.647	8.841
26	45.4364	201.7	98.1	4	28.328	4.090
28	45.4296	84.3	41.0	5	7.060	5.658
35	45.4710	30.1	14.6	6	11.429	8.649
44	45.8678	912.4	438.1	6	20.629	1.580
45	45.8700	5312.0	2550.5	2	18.947	1.134
49	45.8990	45.5	21.8	4	15.952	8.669
50	45.8983	460.2	220.8	5	16.481	2.438
51	45.8981	28.3	13.6	6	17.034	8.975
53	45.9001	37.8	18.1	6	42.068	7.766
54	45.9172	163.8	78.5	6	21.962	3.731
55	45.9004	517.4	248.2	4	17.634	2.571
56	45.9010	69.3	33.2	5	21.516	6.283
57	45.9094	51.9	24.9	6	15.653	6.628
58	45.9202	82.5	39.6	6	10.711	5.258
59	45.9203	254.8	122.2	6	33.085	2.992
60	45.9200	120.6	57.8	6	6.480	4.349
61	45.9246	72.5	34.8	5	15.599	6.145
70	46.0848	64.1	30.6	6	15.129	5.979
74	45.8923	31.0	14.9	6	31.371	8.574
75	45.8927	9.7	4.7	5	24.768	16.791
81	45.9621	17.2	8.2	7	14.634	10.668
82	45.9631	44.0	21.1	3	11.938	10.188
83	45.9588	41.2	19.7	7	30.711	6.892
84	45.9568	36.7	17.6	6	24.077	7.887
86	45.9643	19.8	9.5	7	20.683	9.943
87	45.9635	22.0	10.5	8	11.919	8.823
88	45.9663	105.3	50.4	5	8.894	5.102
90	45.9859	36.9	17.7	8	14.736	6.815
91	46.0011	65.7	31.4	7	14.459	5.461
92	46.0051	69.6	33.3	4	19.732	7.020
93	46.0069	43.6	20.9	6	15.131	7.242
94	46.0314	45.3	21.7	5	7.550	7.785
95	46.0351	29.6	14.1	3	18.432	12.434
98	46.0894	48.2	23.0	4	12.438	8.445
99	46.0968	76.2	36.4	5	16.925	6.008
100	46.1005	52.3	24.9	2	22.140	11.467
101	46.0580	26.3	12.6	5	22.354	10.221
102	46.0713	32.7	15.6	6	22.405	8.370
103	46.0696	91.8	43.8	6	12.250	4.995
104	46.0465	64.1	30.6	5	11.592	6.546
105	46.0381	37.8	18.1	5	19.642	8.523
106	46.0261	31.4	15.0	8	4.311	7.392
107	46.0127	128.5	61.4	2	7.622	7.307

Site	Plat	k	K	n	Delta	Sw/sqrt(n)
108	45.9930	116.6	55.8	2	28.934	7.668
110	45.9824	89.0	42.6	2	37.681	8.776
113	46.0902	58.7	28.0	6	18.415	6.248
114	46.0819	497.9	237.6	6	8.740	2.145
116	46.0156	25.9	12.4	6	13.854	9.397
117	45.9965	70.1	33.5	6	18.751	5.710
118	45.9739	199.7	95.6	6	6.444	3.382

S	Sb	Sw/sqrt(n)	VGP Lat	VGP Long	K	A95
20.3986	18.935	7.5872	87.7313	345.3123	16.0785	4.8471

N	Site Lat	Site Long	Paleolat
57	46.441	242.4522	45.8917

Table 19: Dispersion calculation for reverse polarity, ungrouped sites with a *Vandamme (1994)* cutoff.

Site	Plat	k	K	n	Delta	Sw/sqrt(n)
1	-44.9170	67.4	33.3	7	7.605	5.308
2	-44.9266	78.4	38.7	6	18.844	5.317
3	-44.9280	43.5	21.5	5	23.405	7.820
4	-44.6537	23.1	11.5	7	39.956	9.033
5	-44.6470	81.0	40.3	6	10.568	5.210
6	-44.6500	55.9	27.8	6	10.580	6.272
9	-44.6834	42.4	21.1	6	22.555	7.205
10	-44.6803	26.0	12.9	5	18.121	10.078
11	-44.6783	105.3	52.3	5	14.323	5.008
12	-44.6742	81.8	40.7	2	4.901	8.983
13	-44.6717	19.1	9.5	6	12.119	10.733
19	-44.5834	143.5	71.5	6	22.645	3.911
20	-44.5808	170.3	84.9	4	9.181	4.396
21	-44.5772	98.2	48.9	6	14.596	4.727
22	-44.5741	51.0	25.4	5	18.144	7.185
23	-44.5722	295.9	147.5	6	24.023	2.723
25	-44.5716	75.5	37.6	6	20.911	5.390
27	-44.2347	24.4	12.3	5	30.057	10.336
29	-44.5722	70.1	34.9	6	30.907	5.594
30	-44.5710	39.4	19.6	3	19.546	10.552
31	-44.5790	282.0	140.5	5	18.860	3.056
32	-44.5942	265.7	132.4	6	36.684	2.874
36	-45.0207	45.5	22.4	6	20.407	6.989
37	-45.0227	66.3	32.6	6	16.746	5.790
38	-45.0258	199.3	98.0	6	23.096	3.340
39	-45.0294	153.6	75.6	5	12.323	4.168
40	-45.0300	87.4	43.0	6	10.578	5.043
41	-45.0370	202.3	99.5	5	7.490	3.632
42	-45.0325	96.4	47.4	5	10.535	5.261
43	-45.0265	78.8	38.8	4	17.534	6.505
46	-45.0120	67.1	33.0	5	24.890	6.304
47	-45.0349	177.3	87.2	5	14.891	3.879
48	-45.0362	475.4	233.8	6	20.816	2.163
62	-45.0346	115.1	56.6	6	37.948	4.395
63	-45.0535	58.5	28.8	5	30.496	6.755
64	-45.0531	24.9	12.2	6	26.996	9.452
65	-45.0609	1059.0	520.4	6	29.028	1.450
66	-45.0664	89.9	44.2	6	15.544	4.975
67	-45.0660	52.4	25.7	6	22.773	6.517
69	-45.1097	90.5	44.4	5	32.245	5.436
72	-45.2070	164.1	80.3	2	30.297	6.391
73	-45.0346	51.9	25.5	6	9.060	6.545
77	-45.0297	65.3	32.1	7	40.447	5.402
79	-45.1122	70.0	34.3	5	10.013	6.181
80	-45.2402	85.8	41.9	7	12.656	4.727
89	-45.1051	56.6	27.8	4	16.177	7.684
96	-45.1789	7.7	3.8	4	28.028	20.855
97	-45.1968	35.6	17.4	2	25.471	13.720
111	-45.0953	80.2	39.4	3	27.737	7.453
112	-45.0670	19.7	9.7	5	42.414	11.643

S	Sb	Sw/sqrt(n)	VGPLat	VGPLong	K	A95
23.1389	21.948	7.3277	-87.5435	186.4844	12.5457	5.9249

N	Site Lat	Site Long	Paleolat
50	46.2849	242.7238	-44.8829

Table 20: Dispersion values for all grouping and cutoff scenarios and their mean dispersion.

Scenario	S'	Sb	Sw/sqrt(n)
Grouped, visual inspection cutoff (normal)	20.4335	19.3840	6.4646
Grouped, visual inspection cutoff (reverse)	23.7007	22.6729	6.9039
Grouped, visual inspection cutoff (combined)	22.1051	21.0667	6.6894
Grouped, 45 degree cutoff (normal)	20.8746	19.8899	6.3359
Grouped, 45 degree cutoff (reverse)	23.7007	22.6729	6.9039
Grouped, 45 degree cutoff (combined)	22.3039	21.2974	6.6232
Grouped, Vandamme cutoff (normal)	20.8746	19.8899	6.3359
Grouped, Vandamme cutoff (reverse)	23.7007	22.6729	6.9039
Grouped, Vandamme cutoff (combined)	22.3039	21.2974	6.6232
Ungrouped, visual inspection cutoff (normal)	20.0808	18.5428	7.7075
Ungrouped, visual inspection cutoff (reverse)	23.1389	21.9480	7.3277
Ungrouped, visual inspection cutoff (combined)	20.8539	19.3904	7.6649
Ungrouped, 45 degree cutoff (normal)	20.3986	18.9350	7.5872
Ungrouped, 45 degree cutoff (reverse)	23.1389	21.9480	7.3277
Ungrouped, 45 degree cutoff (combined)	21.6791	20.3429	7.4659
Ungrouped, Vandamme cutoff (normal)	20.3986	18.9350	7.5872
Ungrouped, Vandamme cutoff (reverse)	23.1389	21.9480	7.3277
Ungrouped, Vandamme cutoff (combined)	21.6791	20.3429	7.4659
Mean	21.8208	20.6230	7.0887

Table 21: Elongation values for all different cutoff scenarios and their mean elongation.

Scenario	Mean Inc	Mean Elong	Lower Inc	Upper Inc	Lower Elong	Upper Elong	Edec	Einc
Grouped, visual inspection cutoff	61.0	1.9	57.9	63.8	1.3	2.9	352.7	-28.6
Grouped, 45 degree cutoff	60.6	2.0	57.4	63.5	1.4	3.0	355.8	-29.2
Grouped, Vandamme cutoff	60.6	2.0	57.4	63.5	1.4	3.0	355.8	-29.2
Ungrouped, visual inspection cutoff	61.6	1.9	59.0	64.1	1.3	2.9	350.2	-27.8
Ungrouped, 45 degree cutoff	61.3	2.0	58.6	63.8	1.4	2.9	353.1	-28.3
Ungrouped, Vandamme cutoff	61.3	2.0	58.6	63.8	1.4	2.9	353.1	-28.3
Average	61.1	1.9	58.2	63.8	1.4	2.9	356.4	-28.5

Table 22: Mean VGP values for all grouping and cutoff scenarios and their mean pole.

Scenario	Long	Latg	n	K	A95	R	S
Grouped, visual inspection cutoff	9.1	88.6	86	13.7	4.3	79.798	22.1
Grouped, 45 degree cutoff	16.3	88.3	87	13.5	4.3	80.637	22.3
Grouped, Vandamme cutoff	16.3	88.3	87	13.5	4.3	80.637	22.3
Ungrouped, visual inspection cutoff	349.2	87.5	106	14.5	3.7	98.760	21.5
Ungrouped, 45 degree cutoff	351.5	87.5	107	14.4	3.7	99.619	21.6
Ungrouped, Vandamme cutoff	351.5	87.5	107	14.4	3.7	99.619	21.6
Mean pole	359.8	88.0	6	14246.0	0.6	5.9996	0.7

Appendix:

Sampling Localities:

Basic information on sites collected. Most sites are flat-lying, while a few are tilted; their strike and mean measurements are listed using Right-Hand Rule convention. Magnetic properties were measured for each flow, using a Fluxgate Magnetometer (FM, units: μT) and a Kappameter (K, units: SI).

Site 1: Fine-grained basalt, columnar, slightly vesicular. Wanapum Basalt Member.

Samples: CR1-7

Location: N 46.3135°, W 117.1170°

K: 2.56

FM: 17.5

Site 2: Fine-grained basalt, just below stack of vesicular section. Saddle Mountain Basalt Member.

Samples: CR8-13

Location: N 46.3234°, W 117.1249°

K: 3.12

FM: 27.3

Site 3: Fine-grained basalt, slightly vesicular, some oxidation on vesicles. Overlies a red, friable outcrop. Saddle Mountain Basalt Member.

Samples: CR14-17

Location: N 46.3242°, W 117.1097°

K: 10.8

FM: 7.9

Site 4: Fine-grained, massive basalt. Some small vesicles. Saddle Mountain Basalt Member.

Samples: CR18-24

Location: N 46.0538°, W 117.2318°

K: 12.5

FM: 14.5

Site 5: Fine-grained basalt, slightly friable, some flattened vesicles. Saddle Mountain Basalt Member.

Samples: CR25-30

Location: N 46.0473°, W 117.2379°

K: 36.8

FM: 18.9

Site 6: Fine-grained basalt, slight vesicular on top of flow, vesicularity decreases towards bottom of flow. Grande Ronde Basalt Member.

Samples: CR31-36

Location: N 46.0504°, W 117.2385°

K: 24.4

FM: 15.5

Site 7: Fine-grained basalt, some possible limonite and hematite weathering, no vesicularity. Grande Ronde Basalt Member.

Samples: CR37-42

Location: N 46.0558°, W 117.2386°

K: 7.02

FM: 12.5

Site 8: Fine-grained basalt, some limonite. Grande Ronde Basalt Member.

Samples: CR43-48

Location: N 46.0426°, W 117.2532°

K: 5.21

FM: 31.7

Site 9: Fine-grained basalt, some vesicles, somewhat friable. Grande Ronde Basalt Member.

Samples: CR49-54

Location: N 46.0819°, W 117.1842°

K: 5.47

FM: -13.7

Site 10: Massive to friable, very fine-grained basalt. Saddle Mountain Basalt Member.

Samples: CR55-60

Location: N 46.0792°, W 117.1960°

K: 6.3

FM: 23.2

Site 11: Medium-grained basalt, some vesicularity. Saddle Mountain Basalt Member.

Samples: CR61-66

Location: N 46.0775°, W 117.2031°

K: -14.5

FM: 0.7

Site 12: Fine-grained basalt, some globules, outcrop underlies rocks containing flattened vesicles. Saddle Mountain Basalt Member.

Samples: CR67-72

Location: N 46.0736°, W 117.2106°

K: -17.9

FM: 4.41

Site 13: Typical basaltic flow with vesicular top, thin columns in center and thicker columns in top, fine-grained basalt. Thin center columns sampled. Saddle Mountain Basalt Member.

Samples: CR73-78

Location: N 46.0714°, W 117.2177°

K: 27.7

FM: -9.3

Site 14: Fine-grained basalt, some small vesicles. Grande Ronde Basalt Member.

Samples: CR79-84

Location: N 46.0335°, W 117.2550°

K: -1.7

FM: 21.1

Site 15: Fine-grained basalt, some very small vesicles. Saddle Mountain Basalt Member.

Samples: CR85-90

Location: N 46.0299°, W 117.2560°

K: 9.82

FM: 15.2

Site 16: Massive, fine-grained basalt, some vesicles. Grande Ronde Basalt Member.

Samples: CR91-96

Location: N 46.0102°, W 117.2748°

K: 20.1

FM: 13.4

Site 17: Fine-grained basalt, slender columns in top portion and massive in bottom of outcrop. Grande Ronde Basalt Member.

Samples: CR97-102

Location: N 46.0031°, W 117.2804°

K: 31.8

FM: -3.7

Site 18: Fine-grained basalt, friable upper section, massive lower section. No vesicles. Sampled lower section. Grande Ronde Basalt Member.

Samples: CR103-108

Location: N 46.0046°, W 117.2767

K: 36.3

FM: 16.2

Site 19: By Mile 1 of Oregon side bordering Washington. Massive, fine-grained basalt, some small vesicles. Grande Ronde Basalt Member.

Samples: CR109-114

Location: N 45.9849°, W 117.2746°

K: 10.7

FM: 20.6

Site 20: Fine-grained basalt, smooth surface with perhaps erosional vesicles. Site previously drilled. Grande Ronde Basalt Member.

Samples: CR115-120

Location: N 45.9823°, W 117.2732°

K: 27.5

FM: 9.1

Site 21: Fine-grained basalt. Mainly massive outcrop with top section slightly friable. Sampled lower section. Grande Ronde Basalt Member.

Samples: CR121-126

Location: N 45.9785°, W 117.2672°

K: 16.4

FM: 33.3

Site 22: Very fine-grained basalt. Some flattened striations, perhaps originally vesicles. Saddle Mountain Basalt Member.

Samples: CR127-132

Location: N 45.9751°, W 117.2600°

K: 33.2

FM: 41.4

Site 23: Very fine-grained basalt, no visible vesicles. Saddle Mountain Basalt Member.

Samples: CR133-138

Location: N 45.9733°, W 117.2628°

K: 23.5

FM: -2.3

Site 24: Fine- to medium-grained basalt, massive in bottom and less vesicular than top of flow. Sampled bottom section. Saddle Mountain Basalt Member.

Samples: CR139-144

Location: N 45.9729°, W 117.2733°

K: 8.38

FM: 26.8

Site 25: Very fine-grained basalt, slightly friable but sampling is feasible. Saddle Mountain Basalt Member.

Samples: CR145-150

Location: N 45.9726°, W 117.2610°

K: 35.9

FM: -6.7

Site 26: Medium-grained basalt, slightly eroded columns. Grande Ronde Basalt Member.

Samples: CR151-156

Location: N 45.9744°, W 117.2712°

K: 12.2

FM: -27.9

Strike: 057

Dip: 15

Site 27: About Mile 27 or 28 into Oregon on Highway 3. Outcrops not as high-quality as Washington rocks. Very fine-grained basalt. Rocks somewhat friable. Grande Ronde Basalt Member.

Samples: CR157-162

Location: N 45.6356°, W 117.2687°

K: 18.9

FM: -8.5

Site 28: Ultra-fine-grained basalt. Very massive. Grande Ronde Basalt Member.

Samples: CR163-168

Location: N 45.9677°, W 117.2752°

K: 14.4

FM: 31.3

Site 29: Ultra-fine-grained basalt. Slightly friable but still very massive. Grande Ronde Basalt Member.

Samples: CR169-174

Location: N 45.9734°, W 117.2642°

K: 23

FM: -14.3

Site 30: Massive, fine-grained basalt. Previously drilled. Saddle Mountain Basalt Member.

Samples: CR175-180

Location: N 45.9719°, W 117.2563°

K: 23.1

FM: 34.8

Site 31: Fine-grained basalt. Slightly vesicular. Previously drilled. Grande Ronde Basalt Member.

Samples: CR181-186

Location: N 45.9804°, W 117.2718°

K: 9.29

FM: 45.5

Site 32: Slightly weathered, fine-grained basalt. Almost complete flow sequence visible with another flow above it. Very massive. Saddle Mountain Basalt Member.

Samples: CR187-192

Location: N 45.9959°, W 117.2784°

K: 10.4

FM: 18.2

Site 33: Fine-grained basalt, some laminar rocks above massive sections that were sampled. Very little vesicularity. Wanapum Basalt Member.

Samples: CR193-198

Location: N 46.0025°, W 117.2783°

K: 9.66

FM: 11.1

Site 34: Flow stratigraphically below site 33. Fine-grained basalt. Grande Ronde Basalt Member.

Samples: CR199-204

Location: N 46.0016°, W 117.2787°

K: 14.8

FM: 28.4

Site 35: Massive, fine-grained basalt. Slightly vesicular but can be sampled. On Mile 1 marker on Washington side of border with Oregon. Grande Ronde Basalt Member.

Samples: CR205-210

Location: N 46.0093°, W 117.2768°

K: 33.2

FM: 21.6

Site 36: Massive, fine-grained basalt. Can see slender columns and friable vesicular upper section of flow layer. Grande Ronde Basalt Member.

Samples: CR211-216

Location: N 46.4168°, W 117.1028°

K: 9.3

FM: -17.4

Site 37: Flow below site 36. Massive section below slender columns and vesicular rocks. Fine-grained basalt. Saddle Mountain Basalt Member.

Samples: CR217-222

Location: N 46.4191°, W 117.1119°

K: 26.2

FM: -12.1

Site 38: Perfect exposure of columns. More slender columns visible above thicker ones at base of flow. Fine-grained basalt. Saddle Mountain Basalt Member.

Samples: CR223-228

Location: N 46.4226°, W 117.1234°

K: 2.82

FM: 3.5

Site 39: Massive, fine-grained basalt. Non-vesicular. Grande Ronde Basalt Member.

Samples: CR229-234

Location: N 46.4266°, W 117.1350°

K: 8.03

FM: -12.4

Site 40: Massive, slightly vesicular basalt. Fine-grained. Grande Ronde Basalt Member.

Samples: CR235-240

Location: N 46.4275°, W 117.1418°

K: 8.33

FM: -17.8

Site 41: Site located on Wawawai River Road, subparallel to Highway 12, Washington. Fine-grained basalt with some flattened vesicles. Saddle Mountain Basalt Member.

Samples: CR241-246

Location: N 46.4315°, W 117.0575°

K: 42.0

FM: -0.8

Strike: 045

Dip: 19

Site 42: Flow slightly west of site 41, on Wawawai River Road. Fine-grained, slightly vesicular basalt. Some friable, vesicular units overlying massive section sampled. Saddle Mountain Basalt Member.

Samples: CR247-252

Location: N 46.4275°, W 117.0716°

K: 16.1

FM: -33.8

Site 43: Massive, fine-grained basalt. Slender columns visibly overlying sampled thicker columns. Saddle Mountain Basalt Member.

Samples: CR253-258

Location: N 46.4234°, W 117.1257°

K: 24.8

FM: -13.1

Site 44: Fine-grained, massive basalt. Underlies upper, vesicular section of flow. Grande Ronde Basalt Member.

Samples: CR259-264

Location: N 46.4059°, W 117.2564°

K: 12.7

FM: 37.4

Strike: 277

Dip: 36

Site 45: Massive, fine-grained basalt. One flow visible above it. Grande Ronde Basalt Member.

Samples: CR265-270

Location: N 46.4084°, W 117.2637°

K: 27.3

FM: 21.5

Site 46: Massive, fine-grained basalt underlying friable, vesicular rocks. Saddle Mountain Basalt Member.

Samples: CR271-276

Location: N 46.4140, W 117.2723°

K: 15.5

FM: 21.1

Site 47: Massive, fine-grained basalt; slightly vesicular and fractured. Friable rocks overlying outcrop. Grande Ronde Basalt Member.

Samples: CR277-282

Location: N 46.4397°, W 117.3529°

K: 30.3

FM: 19.4

Site 48: Massive, fine-grained basalt underlying vesicular section; some erosional laminar feature on surface. Grande Ronde Basalt Member.

Samples: CR283-288

Location: N 46.4420°, W 117.3814°

K: 13.9

FM: 30.8

Site 49: Massive, fine-grained basalt. Slightly friable. Previously drilled. Grande Ronde Basalt Member.

Samples: CR289-294

Location: N 46.4421°, W 117.3854°

K: 31.4

FM: 21.3

Site 50: Massive, fine-grained basalt with some vesicles. Grande Ronde Basalt Member.

Samples: CR295-300

Location: N 46.4416°, W 117.3922°

K: 3.92

FM: 9.4

Site 51: Massive, slightly friable, fine-grained basalt. Sitting on man-made asphalt shelf. Grande Ronde Basalt Member.

Samples: CR301-306

Location: N 46.4415°, W 117.3943°

K: 3.51

FM: 21.3

Site 52: Massive, fine-grained basalt, somewhat friable. Slender columns visible above outcrop sampled. Wanapum Basalt Member.

Samples: CR307-312

Location: N 46.4409°, W 117.4381°

K: 11.7

FM: 16.9

Site 53: Fine-grained basaltic columns, no vesicles visible. More friable towards top, more massive towards bottom. Wanapum Basalt Member.

Samples: CR313-318

Location: N 46.4454°, W 117.4420°

K: 9.32

FM: 23.9

Site 54: Massive, thick columns of fine-grained basalt underlying friable, vesicular rock. Wanapum Basalt Member.

Samples: CR319-324

Location: N 46.4632°, W 117.4611°

K: 12.9

FM: 24.2

Strike: 251

Dip: 23.5

Site 55: Massive, thick columns of fine-grained basalt; vesicular and friable rocks overlie thick columns. Grande Ronde Basalt Member.

Samples: CR325-330

Location: N 46.4465°, W 117.4638°

K: 1.16

FM: 36.7

Strike: 256

Dip: 17

Site 56: Fine-grained basalt, slightly vesicular toward top and less vesicular towards bottom. Friable rocks above massive ones sampled. Grande Ronde Basalt Member.

Samples: CR331-336

Location: N 46.4472°, W 117.4672°

K: 6.15

FM: 22.8

Strike: 249

Dip: 10.5

Site 57: Very small outcrop of fine-grained basalt. Somewhat vesicular, vesicularity increases upwards through exposure. Outcrops more massive toward bottom of outcrop. Grande Ronde Basalt Member.

Samples: CR337-342

Location: N 46.4558°, W 117.4720°

K: 11.1

FM: 35.5

Site 58: Massive, non-vesicular, fine-grained basalt. Slightly friable; increases in friability towards top of outcrop. Grande Ronde Basalt Member.

Samples: CR343-348

Location: N 46.4675°, W 117.4941°

K: 8.98

FM: 50.4

Site 59: Fine-grained basalt; massive on bottom with no vesicles and friable at top with large amount of vesicles. Grande Ronde Basalt Member.

Samples: CR349-354

Location: N 46.4675°, W 117.4929°

K: 11.6

FM: 30.6

Strike: 263

Dip: 33

Site 60: Somewhat friable, fine-grained basalt. Vesicular upper section, non-vesicular lower section with some lineation. Grande Ronde Basalt Member.

Samples: CR355-360

Location: N 46.4677°, W 46.4677°

K: 12.6

FM: 22.3

Site 61: Site West of Pomeroy; very small exposure but with massive, fine-grained basalt. Sampled near USGS survey marker. Grande Ronde Basalt Member.

Samples: CR361-366

Location: N 46.4777°, W 117.6455°

K: 15.6

FM: 37.8

Site 62: Massive, fine-grained basalt. Saddle Mountain Basalt Member.

Samples: CR367-372

Location: N 46.4321°, W 117.1427°

K: 5.39

FM: -21.2

Site 63: Fine-grained basalt. Massive columns in bottom, slender columns on top. Wanapum Basalt Member.

Samples: CR373-378

Location: N 46.4532°, W 117.2044°

K: 16.5

FM: 11.4

Site 64: Massive, fine-grained basalt. Vesicular on top, more massive at bottom. Wanapum Basalt Member.

Samples: CR379-384

Location: N 46.4529°, W 117.2076°

K: 19.2

FM: 35.4

Site 65: Massive basaltic flow. Fine-grained, non-vesicular. Saddle Mountain Basalt Member.

Samples: CR385-390

Location: N 46.4611°, W 117.2189°

K: 17.2

FM: 30.9

Site 66: Massive, fine-grained basalt. Non-vesicular. Grande Ronde Basalt Member.

Samples: CR391-396

Location: N 46.4670°, W 117.2301°

K: 29.1

FM: 16.9

Site 67: Massive columns of fine-grained basalt. Vesicular in top and non-vesicular in bottom. Saddle Mountain Basalt Member.

Samples: CR397-402

Location: N 46.4666°, W 117.2295°

K: 43.3

FM: 10.6

Site 68: Massive, fine-grained basalt, no vesicles. Flow overlies site 66; witnessing post near it. Saddle Mountain Basalt Member.

Samples: CR403-408

Location: N 46.4685°, W 117.2316°

K: 10.8

FM: 27.2

Strike: 154

Dip: 23

Site 69: Massive, fine-grained, somewhat friable basalt; slightly vesicular; in entrance of Nesqually John Canyon Management Unit. Grande Ronde Basalt Member.

Samples: CR409-414

Location: N 46.5104°, W 117.2327°

K: 6.28

FM: -5.7

Site 70: Site located inside Wawawai County Park, on Wawawai Grade Road. Slightly friable, fine-grained basalt. Grande Ronde Basalt Member.

Samples: CR415-420

Location: N46.6264°, W 117.3385°

K: 49.2

FM: 21.3

Site 71: Massive, fine-grained basalt. Vesicularity increasing towards top of section, no vesicles in bottom. Grande Ronde Basalt Member.

Samples: CR421-426

Location: N 46.6158°, W 117.3171°

K: 11.7

FM: -14.1

Site 72: Suboptimal flow, fine-grained basalt, friable rocks overlying massive section sampled in base. Grande Ronde Basalt Member.

Samples: CR427-432

Location: N 46.6103°, W 117.3029°

K: 16.0

FM: -21.6

Site 73: Outcrop is on a roadcut on Highway 195. Very fresh, fine-grained basalt. Slender columns with thicker columns at sampled base. Wanapum Basalt Member.

Samples: CR433-438

Location: N 46.4612°, W 117.9803°

K: 61.7

FM: -1.9

Site 74: Outcrop on Wawawai River Road. Fine-grained basalt, Slightly vesicular, slightly friable but still massive. Saddle Mountain Basalt Member.

Samples: CR439-444

Location: N 46.4272°, W 117.1713°

K: 5.52

FM: 32.3

Strike: 023

Dip: 67

Site 75: Fine-grained basalt, slightly crumblier than site 74. Barely vesicular. Saddle Mountain Basalt Member.

Samples: CR445-450

Location: N 46.4275°, W 117.1704°

K: 11.9

FM: 42.5

Strike: 023

Dip: 67

Site 76: Massive and slightly friable, fine-grained basalt. Vesicular at top, non-vesicular at bottom. Saddle Mountain Basalt Member.

Samples: CR451-456

Location: N 46.4277°, W 117.1693°

K: 9.67

FM: 19.7

Strike: 023

Dip: 67

Site 77: Non-vesicular, fine-grained basalt. Wanapum Basalt Member.

Samples: CR457-460

Location: N 46.4281°, W 117.1679°

K: 5.44

FM: 25.9

Strike: 023

Dip: 67

Site 78: Fine-grained, slightly friable, vesicular basalt. Saddle Mountain Basalt Member.

Samples: CR461-464

Location: N 46.4287°, W 117.1660°

K: 6.86

FM: 40.4

Strike: 023

Dip: 67

Site 79: Fine-grained, slightly vesicular basalt. Grande Ronde Basalt Member.

Samples: CR465-468

Location: N 49.5130°, W 117.2352°

K: 7.67

FM: 4.3

Site 80: Fine-grained, non-vesicular basalt. Outcrop on side of Wawawai-Pullman Road. Wanapum Basalt Member.

Samples: CR469-472

Location: N 46.6424°, W 117.2686°

K: 1.77

FM: 11.5

Site 81: Massive, fine-grained, non-vesicular basalt. Grande Ronde Basalt Member.

Samples: CR473-476

Location: N 46.5217°, W 117.8140°

K: 7.02

FM: 13.9

Site 82: Non-vesicular, fine-grained basalt. Grande Ronde Basalt Member.

Samples: CR477-480

Location: N 46.5228°, W 117.8178°

K: 9.36

FM: 33.4

Site 83: Massive, non-vesicular, fine-grained basalt. Slender columns overlying thicker ones at base. Saddle Mountain Basalt Member.

Samples: CR481-484

Location: N 46.5176°, W 117.7944°

K: 8.07

FM: 16.8

Site 84: Very friable, fine-grained basalt. Saddle Mountain Basalt Member.

Samples: CR485-488

Location: N 46.5155°, W 117.7901°

K: 4.09

FM: 28.9

Site 85: Slightly vesicular, medium-grained basalt. Friable at top, massive on bottom. Near survey marker. Saddle Mountain Basalt Member.

Samples: CR489-492

Location: N 46.4643°, W 117.7034°

K: 14.8

FM: 28.6

Site 86: Slightly vesicular, fine-grained basalt. Friable at top, massive at bottom. Grande Ronde Basalt Member.

Samples: CR493-496

Location: N 46.5241°, W 117.8194°

K: 5.77

FM: -0.5

Site 87: Non-vesicular, fine-grained basaltic columns. Grande Ronde Basalt Member.

Samples: CR497-500

Location: N 46.5232°, W 117.8173°

K: 2.36

FM: 27.6

Site 88: Fine-grained, friable basalt. Flow above this site but inaccessible. Grande Ronde Basalt Member.

Samples: CR501-504

Location: N 46.5255°, W 117.8043°

K: 4.75

FM: 35.9

Site 89: Fine-grained, very friable basalt, with some flattened vesicles. Slender columns and thicker undulating columns at bottom. Wanapum Basalt Member.

Samples: CR505-508

Location: N 46.5255°, W 117.7985°

K: 2.49

FM: 35.3

Site 90: Fine-grained, somewhat vesicular, slightly weathered basalt. Soil forming on top. Wanapum Basalt Member.

Samples: CR509-512

Location: N 46.5440°, W 117.7749°

K: 9.34

FM: 26.6

Site 91: Friable, fine-grained basalt. Wanapum Basalt Member.

Samples: CR513-516

Location: N 46.5591°, W 117.7715°

K: 2.18

FM: 32.9

Site 92: Medium-grained, somewhat vesicular basalt. Slender columns on top and thick columns at base sampled. Grande Ronde Basalt Member.

Samples: CR517-520

Location: N 46.5633°, W 117.7754°

K: 0.15

FM: 26.9

Site 93: Fine-grained, friable basalt. Wanapum Basalt Member.

Samples: CR521-524

Location: N 46.5652°, W 117.7775°

K: 5.74

FM: 44.2

Site 94: Fine-grained, friable, somewhat vesicular basalt. Large columns visible. Grande Ronde Basalt Member.

Samples: CR525-528

Location: N 46.5899°, W 117.7839°

K: 3.08

FM: 17.60

Site 95: Slightly vesicular, friable, fine-grained basalt. Grande Ronde Basalt Member.

Samples: CR529-532

Location: N 46.5936°, W 117.7821°

K: 16.6

FM: -15.1

Site 96: Fine-grained, friable, non-vesicular basalt. Non-vesicular on sampled basebut vesicular on top. Saddle Mountain Basalt Member.

Samples: CR533-536

Location: N 46.5989°, W 117.7850°

K: 2.49

FM: -24.4

Site 97: Friable, fine-grained basalt. Flattened vesicles. Outcrop on Lower Deadman Road. Grande Ronde Basalt Member.

Samples: CR537-540

Location: N 46.6170°, W 117.7898°

K: 7.48

FM: 13.6

Site 98: Friable, slightly vesicular, fine-grained basalt. Slender columns can be seen above thicker columns sampled. Grande Ronde Basalt Member.

Samples: CR541-544

Location: N 46.6489°, W 117.8079°

K: 18.1

FM: 12.1

Site 99: Fine-grained, non-vesicular, basalt; mostly massive with some friability. Grande Ronde Basalt Member.

Samples: CR545-548

Location: N 46.6563°, W 117.8055°

K: 8.85

FM: 14.2

Site 100: Fine-grained, massive basalt, with vesicular section on top. Grande Ronde Basalt Member.

Samples: CR 549-552

Location: N 46.6598°, W 117.8021°

K: 5.58

FM: -15.9

Site 101: Fine-grained, friable and massive basalt. On Lower Deadman Road. Grande Ronde Basalt Member.

Samples: CR553-556

Location: N 46.6160°, W 117.7674°

K: 15.6

FM: 27.3

Site 102: Fine-grained basalt; massive section. Grande Ronde Basalt Member.

Samples: CR557-560

Location: N 46.6275°, W 117.7207°

K: 9.16

FM: -2.2

Site 103: Vesicular, fine-grained basalt. Massive at sampled bottom and friable at top. Grande Ronde Basalt Member.

Samples: CR561-564

Location: N 46.6224°, W 117.6321°

K: 28.4

FM: 23.4

Site 104: Fine-grained basalt. Minimal vesicularity. Friable at top, massive at bottom. Grande Ronde Basalt Member.

Samples: CR565-568

Location: N 46.5983°, W 117.6033°

K: 9.57

FM: -14.2

Site 105: Fine-grained basalt. Massive and non-vesicular at base, friable and vesicular at top. Grande Ronde Basalt Member.

Samples: CR569-572

Location: N 46.5888°, W 117.5794°

K: 13.3

FM: 21.6

Strike: 260

Dip: 19

Site 106: Fine-grained, non-vesicular basalt. Friable at top, massive at base. Grande Ronde Basalt Member.

Samples: CR573-576

Location: N 46.5765°, W 117.5707

K: 9.19

FM: 45.5

Site 107: Fine-grained basalt. Friable soil overlying massive basalt. Slightly vesicular. Grande Ronde Basalt Member.

Samples: CR577-580

Location: N 46.5628°, W 117.5628°

K: 12.3

FM: 8.1

Site 108: Mostly non-vesicular, fine-grained basalt. Friable at top, massive at bottom. Wanapum Basalt Member.

Sampled: CR581-584

Location: N 46.5432°, W 117.5681°

K: 3.85

FM: 11.8

Site 109: Fine-grained, friable basalt. Soil on top. Saddle Mountain Basalt Member.

Samples: CR585-588

Location: N 46.5377°, W 117.5602°

K: 13.1

FM: 17.3

Site 110: Fine-grained, non-vesicular, very friable basalt. Grande Ronde Basalt Member.

Samples: CR589-592

Location: N 46.5323°, W 117.5593°

K: 12.0

FM: 35.0

Site 111: Non-vesicular, friable, fine-grained basalt. Grande Ronde Basalt Member.

Samples: CR593-596

Location: N 46.5076°, W 117.5659°

K: 12.6

FM: 15.8

Site 112: Friable, fine-grained basalt. Wanapum Basalt Member.

Samples: CR597-600

Location: N 46.4796°, W 117.5757°

K: 17.3

FM: -0.6

Site 113: Outcrop on Ping Gulf. Fine-grained, non-vesicular; massive at base, more friable toward top. Wanapum Basalt Member.

Samples: CR601-606

Location: N 46.6465°, W 117.7230°

K: 7.77

FM: -8.3

Site 114: Outcrop on Hastings Hill Road. Fine-grained basalt. Long, thick, massive columns. Barely vesicular. Grande Ronde Basalt Member.

Samples: CR607-612

Location: N 46.6396°, W 117.7605°

K: 15.8

FM: 16.8

Site 115: On Hastings Hill Road. Fine-grained basalt, non-vesicular. Previously drilled. Saddle Mountain Basalt Member.

Samples: CR613-618

Location: N 46.4774°, W 117.7675°

K: 3.95

FM: 18.9

Strike: 019

Dip: 48

Site 116: Fine-grained basalt. Vesicular at top, non-vesicular at bottom. Massive. One flow above this site but inaccessible. Wanapum Basalt Member.

Samples: CR619-624

Location: N 46.5724°, W 117.7384°

K: 21.7

FM: 24.5

Site 117: Fine-grained, massive and non-vesicular basalt. Grande Ronde Basalt Member.

Samples: CR625-630

Location: N 46.5509°, W 117.6769°

K: 13.4

FM: 29.9

Site 118: Massive, fine-grained basalt overlain by soil. Saddle Mountain Basalt Member.

Samples: CR631-636

Location: N 46.5246°, W 117.5820°

K: 9.82

FM: 10.9